Fast-timescale Control Strategies for Demand Response in Power Systems

by

Ian Burkley Beil

A dissertation submitted in partial fulfillment
of the requirements for the degree of
Doctor of Philosophy
(Electrical Engineering-Systems)
in The University of Michigan
2015

Doctoral Committee:

Professor Ian Hiskens, Chair
Scott Backhaus, Los Alamos National Laboratory
Associate Professor Heath Hofmann
Professor Jerome P. Lynch
Assistant Professor Johanna Mathieu

For my grandparents, Sam and Marilyn, with lots of love

ACKNOWLEDGEMENTS

This document represents four years of research and hard work, but more importantly, it represents the help of a lot of people and a lot of encouragement along the way.

First and foremost I'd like to thank my advisor, Professor Ian Hiskens, for teaching me the nature of research and giving me a world-class education in power systems engineering. Professor Hiskens is patient and perceptive, and his advising has been a great asset over the past four years. He has helped guide me through many tough intellectual challenges, and has participated in quite a few last-minute paper editing sessions. I really appreciate all the help; it's been fun being the other "Ian" in the group.

I also owe a big thanks to my entire committee - Dr. Scott Backhaus, Professor Heath Hofmann, Professor Johanna Mathieu, and Professor Jerome Lynch. During my visits to Los Alamos National Lab, and afterwards, Dr. Backhaus has been like a second advisor to me. His physics background has made for a very different and helpful perspective on things, and the testbed building that he set up was the foundation for much of the research presented in this dissertation. Professor Hofmann has been a steady source of encouragement over the years, and is one of the best engineering teachers I have ever had. Much of my research on demand response in buildings overlapped with previous work by Professor Mathieu, and her insightful comments and knowledge of the literature are much appreciated. And of course, I probably would not be here without Professor Lynch, who gave me my first research job as a sophomore in college, encouraged me to pursue graduate school, and even introduced me to Professor Hiskens.

Thanks also to Professors Juan Rivas and James Freudenberg, both of whom taught a large part of my graduate education, and believed in me during the Ph.D. qualification process. And a big thanks to Carrie Morton, who helped convince me to come to Michigan and did an outstanding job as the CERC-CVC coordinator.

My family has been a huge source of support during the last four years (despite being Buckeyes). To my parents, I cannot thank you enough for all the encouragement

you have given me. Thanks to my mom, Dana, for teaching me to write, and to my dad, Rick, for teaching me to approach everyday with a positive attitude (and for teaching me how to fish). Thanks to my brother Carter, my sister Addie, and my soon to be sister-in-law Tes for being cooler and funnier than me, and for letting me hang out with them anyway. And a very special thanks to my girlfriend Sarah Lucas, for keeping me grounded and for being willing to go on all kinds of adventures.

I owe more than I can say to my friends in EE:S. To the older guys - Mads Almassalkhi, Soumya Kundu, and Abdi Zenyu - thanks for encouraging me to come to Michigan and for showing me how successful graduate students conduct themselves. To the power and energy students - Aaron Stein, Dave Reed, Jenny Marley, Jon Martin, Max Markov, Jonas Kersulis, Steph Crocker, and Greg Ledva - thanks for pushing me to get better. Thanks for all of the homework help and the quals practice; thanks for sharing your ideas and for the honest, helpful feedback. And as for the signal processing folks - Nick Asendorf, Matt Prelee, Matt Muckley, Madison McGaffin, Mai Le and Greg Handy - I don't really understand what you do, but it's been great being friends.

A big shout out to the Electrical and Computer Engineering Graduate Student Council, which has been a great outlet for building a community outside of the office. A special thanks to Mads for recommending me for the gig, and to Nick and to Gopal Nataraj for their tireless (and underappreciated) leadership. Also, thanks to all the ECE sports teams! I was always proud of our heart and hustle, and we had some great playoff runs in there too.

And of course, GO BLUE!

TABLE OF CONTENTS

LIST OF FIGURES

Figure

LIST OF TABLES

Table

ABSTRACT

Fast-timescale Control Strategies for Demand Response in Power Systems
by
Ian Beil

Chair: Ian Hiskens

Power system operators are tasked with providing reliable electricity to their customers, and maintaining a continuous balance between generation and load is crucial to this objective. As electricity consumption has trended upward around the globe, the gap between capacity and peak demand continues to shrink, forcing grids closer to their operational limits. Traditionally, this trend has been mitigated by corresponding increases in generation capacity. However, concerns over carbon emissions from fossil fuel plants have lead to increased penetration of non-dispatchable renewable generation into the grid such as wind and solar, making the balancing of generation and load more difficult. For these reasons, demand-side strategies, which modulate load in a controllable manner, have been proposed as a way to add flexibility to the grid.

Resources with innate flexibility in their load profile are particularly suited to demand response (DR) applications. This dissertation examines two such loads: heating, ventilation, and air conditioning (HVAC) systems, and plug-in electric vehicle (PEV) fleets. HVAC systems operate throughout the day, and can vary the timing of when they draw power due to the thermal inertia inherent to their associated building(s). Meanwhile, PEVs typically only draw power for a fraction of the day, but offer very fast response times and, in aggregate, may in the future represent a significant (and flexible) load on the network.

The HVAC portion of this dissertation places emphasis on sub-hourly DR strategies, which is the timescale at which power system ancillary services typically operate. It explore the efficacy of using commercial HVAC for DR applications by employing an experimental testbed incorporating a 30,000 m^2 office building. The quality of

performance, in terms of accuracy in perturbing the load in a desired manner, as well as the efficiency of this process, and the profitability of such an endeavor, are analyzed in detail.

The PEV portion of this dissertation examines ways to control aggregate PEV power consumption in an environment in which communication resources are limited. Initial research examines how to mitigate the total load on distribution transformers with attached PEVs, in order to prevent overheating. The scope then expands to examine how a group of vehicles can be controlled to track a reference signal. It also utilizes optimal control strategies for modulating PEV load while limiting the number of potential control actions.

Overall, this dissertation provides new and useful ways to modulate load in order to integrate demand-side resources. These advances contribute to the growing paradigm of increased control in the electric grid, providing more flexibility to accommodate renewable resources, more efficient use of available generation assets, and ultimately, a grid that uses less fossil fuels and emits less carbon into the environment.

CHAPTER I

Introduction

Electrical power systems are often considered the largest machines in the world. They provide one of the essential resources of all modern economies, serve billions of customers, and operate at very high reliability factors. However, as the scientific evidence for human-driven climate change has mounted [112, 115, 129], policymakers have turned their attention to ways in which carbon dioxide emissions can be curbed. In the U.S. regulatory environment, this has resulted in stricter regulations on fossil fuel power plant emissions [30] as well as state-mandated minimum levels of renewable power, termed renewable portfolio standards [106, 131]. These factors have spurred an increase in the amount of wind and solar power generation on the grid.

While these resources are far less carbon intensive than fossil fuel plants, the physical phenomena that they rely on - wind and sunlight - are highly stochastic, making their generated power much less controllable. Thus, accommodating a generation portfolio with a large percentage of renewable resources requires a paradigm shift away from the traditional generation dispatch model.

1.1 Traditional Power System Operation

Power system operation lies at the confluence of engineering, economics, and public policy, and the regulatory framework that governs how grids are operated varies from country to country and state to state. In the discussion that follows, the details refer specifically to deregulated US electricity markets, although many of the core concepts are shared both by vertically integrated utilities in the US, and by international markets.

At the most basic level, power system operators seek to match generated power to the (traditionally uncontrolled) load, while ensuring that engineering constraints on the grid, such as generator real and reactive power capabilities, generator ramp

rates, and transmission line current limits, are not violated. Imbalances between generation and load are physically expressed through the frequency of alternating current (AC) power in the grid - nominally 60 Hz in the US - such that a surplus of generation causes the frequency to rise, and a deficit of generation causes the frequency to drop. Due to the relatively limited storage capabilities of existing power systems, any imbalance requires swift control actions so that the power system can remain in a stable operating region.

This balance is achieved through a hierarchical control structure. The different levels of control, listed from slowest to fastest timescale, are as follows:

- **Unit Commitment** determines which generators should be activated in the near future, typically 24-48 hours in advance. Relies on general forecasts of the next day's load based on historical data, anticipated weather, etc.

- **Economic Dispatch** uses market signals to dispatch power to participating generators while adhering to grid constraints. Often features several timescales such as as one-hour ahead and real-time.

- **Automatic Generation Control** (AGC) is used both to correct system frequency and account for tie-line imbalances between portions of the power system at faster (10 s - 10 min) timescales [132].

- **Governor action** takes places automatically through the governors that control synchronous machine generators. Small deviations in the frequency are corrected by adjusting the power output of the generators at fast timescales, with the speed of response determined by the generator fuel type and corresponding governor design.

1.1.1 Market Operation

In deregulated utility environments, markets are used to influence generator behavior in order to ensure smooth and continuous operation of the power system. Typically, markets are operated by neutral organizations, which in the U.S. are referred to as Regional Transmission Operators (RTO) and Independent System Operators (ISO).

There are several types of markets used in power system operations. Energy markets are used to assign power setpoints to participating generators in order to match the demand on the network. Capacity markets provide incentive to build new

generation resources by compensating generators for the total power they are capable of providing (even if this full quantity is not utilized).

Beyond these markets, generators can also (and are sometimes required to) participate in ancillary services markets, which include secondary services such as black start capabilities (the ability to self start a generator without external grid support) and reserve power. The service most germane to this dissertation is frequency regulation, which determines the pool of generators that provide AGC in a given area. Synchronous generators within a control area initially respond to a deviation in system frequency with governor action. When a disturbance becomes large enough, an area control error (ACE) develops[1] within a balancing authority, and this ACE signal is broadcast to the generators participating in frequency regulation. These generators then adjust their governor setpoints to account for the ACE signal, eventually restoring the frequency to nominal [47].

Ancillary service markets operate using mechanisms similar to energy markets. They typically feature a bid-based auction-style market design, where all participants are compensated at the clearing price of the market. In the case of frequency regulation markets, the bid process may be broken down further. Participating generators submit several bid components that take into account the capacity of power they provide as well as the cost to the generator of adjusting its output, which changes the heating dynamics and therefore the marginal cost of providing power (see for example [35], which discusses these details within the PJM Interconnect).

1.2 Demand Response

Demand response (DR) is one way to manage reduced flexibility and increased variability on the generation side. At its most basic, DR is the process of adjusting load to help maintain generation/load balance. Under this definition, DR procedures have existed for decades. Load shedding, in which utilities cut power to portions of the grid during sudden generation shortfalls [4, 89, 121], is perhaps the most extreme and rudimentary example. Since the 1970's, utilities have also experimented with a variety of demand-side programs [9], including direct control of customer equipment [49, 53, 56, 98], as well as pricing mechanisms to influence consumer behavior [51, 109, 110].

Traditionally, these demand-side strategies operated on multi-hour timescales, a rate far slower than the power dynamics inherent to wind and solar generators. However, in recent years power system communication equipment has become cheaper and

[1] An ACE signal can also result from tie-line imbalances between balancing authorities [132]

more ubiquitous. These advances have encouraged researchers to explore the use of DR control for the purpose of accommodating renewable generator power variation.

The possibility of fast-timescale DR control has also spurred regulatory action. In 2011, the Federal Energy Regulatory Commision (FERC) issued two key rulings. FERC Order 745[2] stipulates that DR resources can bid reductions in load into capacity markets in the same manner (and with the same compensation) that generators bid in their capacity [33]. Similarly, FERC Order 755 prohibits DR resources from being discriminated against in frequency regulation markets, and also requires fair compensation for these resources [34].

These decisions have led transmission operators to redesign their market structures in order to accommodate DR resources. The pace of market change has varied regionally within the U.S. [64, 84], and one of the more mature markets that currently accommodates DR resources is the Pennsylvania-New Jersey-Maryland Interconnection (PJM). Several of the chapters that follow use test signals and historical data taken from the PJM Regulation Market, because this market has operated successfully for several years, and because the rules governing this market are transparent and readily available [35, 36]. Although this dissertation uses PJM as an example, it is believed that the nascent DR markets in other ISO/RTOs will soon become more established and robust, and that the analysis herein will apply more generally to a variety of transmission operator environments.

1.3 Scope of the dissertation

This work examines demand-side strategies for modulating loads at faster timescales than has typically been attempted in industry, and at which compensation for renewable generator variability becomes viable. Specifically, the dissertation addresses two potential DR sources: heating, ventilation, and air conditioning (HVAC) systems in commercial buildings, and plug-in electric vehicles (PEVs). While the dynamics, prevalence, and control capabilities of these two types of loads differ significantly, both resources are capable of providing flexibility in their power demand, and both experience challenges when operated at fast timescales.

[2] As of publication, FERC Order 745 had been vacated by the U.S. Court of Appeals for the District of Columbia Circuit, although this decision has been staid until the case appears before the U.S. Supreme Count in October 2015 [114]

1.3.1 Commercial heating, ventilation, and air conditioning systems

HVAC systems are responsible for maintaining a certain climate within a building, in order to maintain occupant comfort, provide necessary ventilation, and protect equipment such as heat-sensitive servers. This dissertation focuses on commercial HVAC systems, in contrast to residential units. Residential HVAC systems usually employ a simple hysteresis controller to achieve climate control[3], whereas commercial HVAC systems are typically controlled in a hierarchical structure, with several interrelated control loops driving the thermal and electrical dynamics of the system.

In 2014, commercial building accounted for 18.7% of total U.S. electricity consumption [126], and thus these buildings represent a significant load on the grid. Furthermore, the thermal envelope inherent to large buildings effectively creates a low-pass filter that smooths out short term changes in heating and cooling levels. This buffering effect should in theory allow building HVAC systems to adjust their thermal output (and therefore manipulate building electricity consumption) on the short-term without significantly affecting occupant comfort.

In practice, these DR ideas have mostly been carried out in trials over multi-hour timescales [41, 63, 102] in which the focus was communication between some central entity and the commercial buildings. At these timescales, the transient dynamics of the HVAC system are less critical, because the building only spends a fraction of time in this condition before reaching a new steady-state operating point. However, as the speed of DR control increases, these transient dynamics tend to dominate the system response, making it more difficult to control HVAC electricity consumption.

Several studies [52, 74, 85, 142] have attempted to quantify this transient response both theoretically and experimentally, and to design controllers that can regulate HVAC power consumption at these fast timescales. The work presented in this dissertation adds the following contributions:

- **Chapter II** reviews the recent studies on fast-timescale DR control in commercial HVAC systems, and places these various control methodologies in context. Then, it presents experimental results collected from a 30,000 m^2 office building, in which a control methodology that had not been previously tested for fast timescale DR control - termed thermostat set-point offset - is used to adjust fan power within the building. Standardized benchmarking criteria from the PJM interconnect are used to compare the results of these tests to the performance

[3]Note that an aggregated population of residential HVAC units can create its own set of complex dynamics which can be used for DR control [66, 69, 99]

metrics of the other methods. Finally, the chapter discusses the merits and drawbacks of each of the potential control methodologies.

- **Chapter III** examines the control penalty of an HVAC system providing DR control, in terms of the reduction to system efficiency. Using a set of experiments designed to push the limits of the HVAC system transient response, it is determined that the energy penalty can be significant compared to the magnitude of DR power being provided. This is shown to be the case when considering solely the fan power consumption, as well as the combined consumption of both the fans and chillers.

The main new contributions to the literature from the HVAC portion of the dissertation are as follows:

- A summary of the potential control inputs that can be used to achieve HVAC DR in a commercial building, as well as a summary of the performance of various previous studies and the studies presented herein.
- The first experimentally-derived performance metrics for the temperature off-set method in a commercial building providing DR.
- Identification of excess energy expenditures that occur when the testbed building is exposed to DR input signals.
- Confirmation that this excess expenditure of energy occurs even when accounting for the effects of chiller power consumption within the building.

1.3.2 Plug-in Electric Vehicle loads

A PEV is any vehicle incorporating onboard battery storage that must charge these batteries from the terrestrial power system. Compared to commercial HVAC systems, PEVs currently represent a very small load on the grid. As of May 2015, an estimated 43,065 PEVs had been sold in the U.S. since their introduction in December 2010, out of a total of 6.79 million vehicles sold in that timeframe - a market penetration of only 0.64% [29]. Projections of future market penetration for PEVs vary significantly [28, 91, 125]; however, studies agree that PEV sales will likely continue their upward trend over the next several decades, suggesting that steps should be taken now to ensure that this additional load will be managed adequately in the future.

Individually, a PEV has a battery capacity on the order of 10-100 kWh[4]. The electric vehicle supply equipment (EVSE) that provides electricity to the battery is standardized to provide power at as high as 240 V, 80 A, 19.2 kW [123], although the EVSE for smaller battery cars tends to lie more in the 240 V, 15-30 A, 3.3-6.6 kW range.

At these power levels, a large population of PEVs could have a significant effect on power system dynamics. An uncontrolled PEV fleet could lead to problems both at the transmission level, where PEV loads have the potential to exacerbate capacity issues at peak load times [39, 83], and at the distribution level, where the additional load could cause overheating of substation and distribution transformer loads [44, 57] as well as distort voltage profiles and increase network losses [25, 60, 76]. Even moderate gains in PEV sales will therefore necessitate some form of charging control, in order to mitigate these issues.

A controllable PEV fleet, in addition to avoiding detrimental grid effects, also has the potential to provide DR services to the grid. Given that vehicles are often parked for a longer period of time than is necessary to fully recharge their batteries, there is an inherent flexibility in the PEV load. Furthermore, power electronics in the EVSE are capable of adjusting power at very fast timescales, meaning that a well-regulated PEV fleet has the capability to adjust its load at a rate similar to the variability of wind and solar generation.

A major challenge in regulating a fleet of PEVs lies in the lack of existing control and communication architecture. Vehicles connect with the electrical grid at the distribution level. Due to the large and dispersed nature of distribution grids, utilities prioritize cost when designing these systems. Therefore there is a limited number of sensors and actuators available for observation and control. In this environment, care must be taken when designing PEV fleet control algorithms to ensure that they take into account communication and computation constraints.

While there have been many studies on PEV fleet control, few focus on the limited communication environment present at the distribution level. This dissertation adds the following contributions to the field:

- **Chapter IV** investigates the effects of PEV load on a distribution transformer. A distributed control algorithm with minimal communication requirements is employed to regulate the thermal load on a transformer. The chapter also explores the voltage profile and power dynamics that result when this algorithm

[4]For example, the first generation Chevrolet Volt was equipped with a 16 kWh battery [90], while the 2015 Telsa Model S P85D features an 85 kWh battery pack [122].

is implemented on a standardized test distribution network. Finally, this chapter identifies scenarios in which the control algorithm can experience non-ideal performance.

- **Chapter V** develops a hierarchical control structure in order to regulate PEV power consumption for reference tracking purposes, while still adhering to distribution transformer constraints. The performance of this algorithm is quantified in the presence of communication delay. The limitations of the algorithm and its effects on the battery state-of-charge are discussed in detail.

- **Chapter VI** uses an optimal control approach to solve the PEV reference tracking problem. In this design, the controller uses a limited-bandwidth constraint to reformulate the problem in a way that takes into account the communication architecture. A model predictive controller is employed to adjust PEV load to track a signal without anticipatory knowledge of future signal data points. The performance of this method is compared to the previously suggested control schemes.

The main new contributions to the literature from the PEV portion of the dissertation are as follows:

- A validation of the AIMD algorithm for use on radial distribution systems in the presence of high PEV concentration.

- The development of an optimal controller that utilizes the constrained communication method for controlling PEV charging.

- The ability to provide temperature-based transformer overload protection in both cases.

CHAPTER II

Demand Response using Heating, Ventilation, and Air Conditioning (HVAC) Systems

2.1 Introduction

The proportion of wind and solar resources on the grid is rapidly increasing in response to energy policies that are encouraging less carbon-intensive generation portfolios. A heightened reliance on non-dispatchable resources results in less available generation-side control, increasing the difficulty of operating power systems. To counter this trend, more emphasis is being placed on demand-side strategies to balance generation and consumption through adjustment of load from its nominal value.

Demand Response (DR) is a broad class of demand-side control strategies that span wide timescales and magnitude and accuracy of response. Real-time pricing may be used to achieve DR [3,11,50,111]; however, regulators have so far been reluctant to continuously expose retail customers to the volatility of wholesale electricity rates [108]. Instead, DR has typically been implemented using direct load control such as emergency load shedding [4,121] or via long-term contracts that provide low energy prices for the right to curtail load [1,10,53,97]. Voluntary sustained DR is encouraged by fixed, time-of-use pricing or infrequent price increases during extreme system events, e.g. critical peak pricing [97].

Ancillary services (AS) markets are emerging as an alternative method to engage DR in power system control and as an additional source of compensation for customers capable of providing DR functionality. In particular, frequency regulation markets have opened up to non-traditional resources [58,64,83,84]. The rules governing these nascent markets are still in flux, but to qualify for participation, DR resources must pass performance benchmark tests and maintain acceptable performance scores over the full time interval of participation [36].

Heating, ventilation, and air conditioning (HVAC) systems within commercial buildings are an attractive source of DR. As a significant portion of commercial building electricity consumption, they could create a considerable resource when aggregated across a sufficient number of buildings. Furthermore, a building's thermal mass buffers short-term fluctuations in net thermal load, enabling DR to perturb HVAC operation and its electrical consumption around nominal conditions with limited impact on occupant comfort.

This chapter discusses different control strategies for providing frequency regulation DR from commercial HVAC systems and components, and compares performance results from the presented experiments and from experiments and simulations of other researchers. In particular, it considers the physical variables used to provide this control—direct control of fan speed or indirect control through manipulation of air mass flow rates, supply air pressure, or thermostat set-points—and the trade-offs between open-loop and closed-loop DR control. To illustrate these ideas, it presents experimental data from a $\sim$30,000 m^2 commercial office building where the HVAC electrical demand is modulated to track PJM qualification and historical frequency regulation signals. Performance of the HVAC system DR control is compared against standardized metrics [35].

The remainder of the chapter is organized as follows. Section 2.2 provides an introduction to market-based frequency regulation from DR resources. Section 2.3 reviews typical commercial HVAC system architecture and the properties of several control methodologies for providing frequency regulation from commercial HVAC systems. Section 2.4 reviews and compares experimental and simulation results from other researchers and from new experiments performed by the authors. Section 3.2 presents experimental results on the energy costs incurred while providing frequency regulation from the experimental testbed. Finally, Section 3.7 offers a conclusion and suggestions for future work.

2.2 An Emerging Demand Response Market

As discussed in Section 1.2, in the US, the Federal Energy Regulatory Commission (FERC) mandates Independent System Operators (ISO) and Regional Transmission Organizations (RTO) to provide several ancillary services (AS) to ensure power system operability, including maintaining the system frequency at its nominal value. For significant frequency deviations, generating units respond locally through individual governor action [132], i.e. primary frequency regulation. Currently, primary frequency

regulation is not compensated. Governor droop characteristics cannot completely restore nominal frequency, and centrally-controlled secondary frequency regulation [59, 132] is used for this purpose. Participating resources adjust their active-power set-point according to a system-wide signal and are compensated through market mechanisms that exist in several electrical grids.

Secondary frequency regulation is typically provided by synchronous generators, but recent changes, most notably FERC Order 745 [33], have promoted demand-side resource participation. Order 745 requires that DR resources be fairly compensated in frequency regulation markets using performance-based metrics. Economic studies [17, 65] suggest that DR from the industrial and commercial sectors may soon be competitive with current AS market clearing prices, although the situation varies significantly from market to market. For a survey of the DR policy environment within various ISO/RTOs, see [64] and [84]. In one example, the Pennsylvania-New Jersey-Maryland (PJM) Interconnection has moved to accommodate increased DR into its frequency regulation market by providing a near-real-time market structure and allowing aggregation of a customer's demand assets [84].

However, as initially detailed in Section 1.3.1, participation in the PJM Demand Response Frequency Regulation Market [35,36] (and similar markets) requires control actions on much shorter timescales and with higher tracking accuracy than previous DR applications. To enter and remain in these markets, participants must pass performance tests against standard benchmarks and maintain acceptable metric-based operational performance. Section 2.4 provides further details on these benchmarks and metrics and examines the performance capabilities of a commercial HVAC system.

2.3 Demand Response Control in Commercial HVAC Applications

Buildings contain multiple electricity-consuming systems including lighting, computing loads, and security systems, as well as HVAC equipment. The last is uniquely qualified for DR participation because perturbations of an HVAC system (when well-designed) have a minimum impact on occupant comfort. Modulation of HVAC operation causes corresponding changes in the temperature of the occupied spaces, but the thermal mass of the building tends to buffer these effects, such that the temperature changes may be imperceptibly small (ex. 1-2°C) to the building occupants. On the contrary, lighting systems provide a load that is adjustable at faster timescales and

higher accuracies, but the flickering and outright darkness that would result make DR participation for lighting systems practically impossible.

Commercial and residential HVAC DR both have unique challenges. Residential HVAC units are controlled individually by simple hysteresis controllers that regulate building temperature within a specified deadband. The challenge occurs when controlling large aggregations of these individually small thermostatically-controlled loads (TCLs). Recent research has used simple first-order thermal models to describe this aggregate behavior and develop model-based control techniques [15,66,68,69,81].

In contrast, individual commercial HVAC systems (the focus of this manuscript) can provide a much larger controllable load than individual residential units. However, commercial HVAC systems have complex integrated subsystems, often featuring a variety of electricity-consuming equipment and interdependent control loops that create self-correcting behavior. Consequently, perturbing the electrical load of a commercial HVAC system to track a frequency regulation reference signal is a challenging task.

Previous experimental DR work using commercial HVAC systems focused on peak shaving applications and typically consisted of infrequent reductions in load sustained over multi-hour timescales. For example, [102] demonstrated hour-long load shedding across geographically disparate commercial buildings under dynamic electrical pricing, and [92] utilized critical peak electricity pricing. The experiments in [117] (multi-day timescales) and [94] (one-hour intervals) examined energy use in European commercial buildings, which often have different HVAC architectures than our own testbed building (specifically, they lack variable air volume units, discussed in Subsection 2.3.1).

The relatively infrequent but time-extended DR (load reductions only) discussed above can be accomplished by shutting down HVAC equipment or otherwise curtailing HVAC operations. DR participation in non-spinning reserve markets was investigated in [62], in which the relevant buildings met a 10-minute response time criterion required for market participation, and maintained service for 2-hour intervals. However, a frequency regulation service operates continuously at a sub-hourly timescale with both increases and decreases in load, and market performance metrics require a more accurate response than load curtailment. A better understanding of HVAC system architecture is needed to design a frequency regulation control system for commercial HVAC DR.

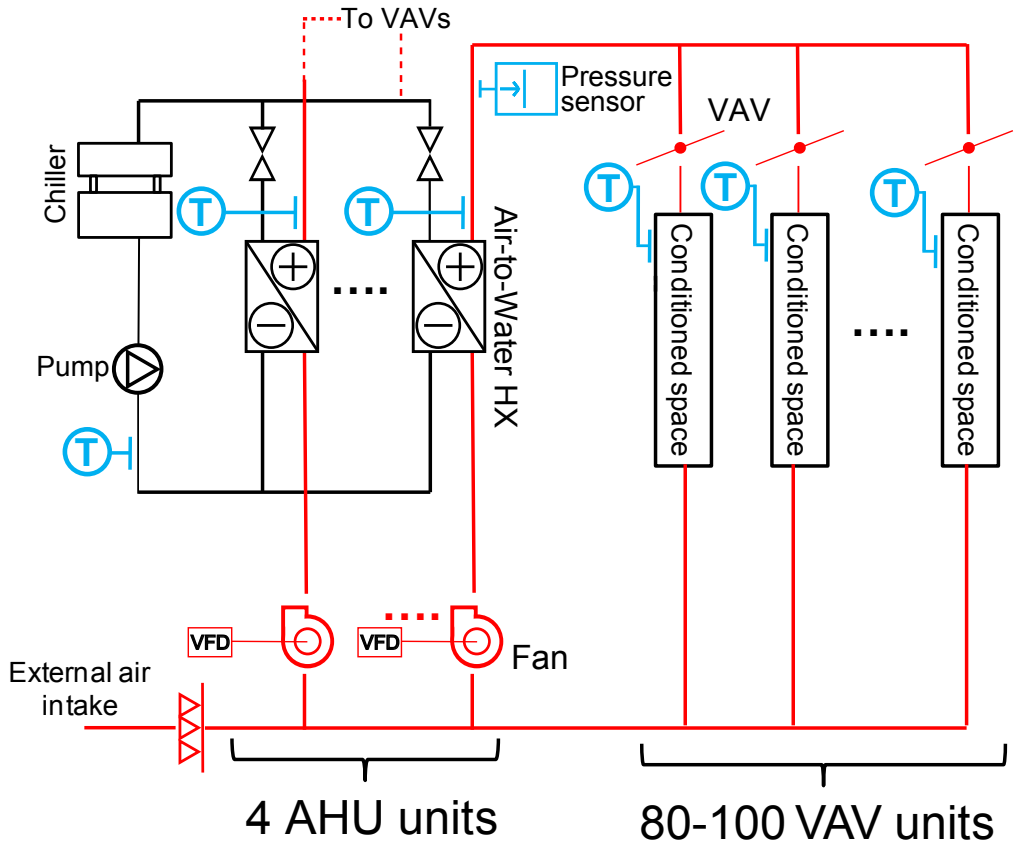

Figure 2.1: A generalized HVAC system layout representative of the testbed used in previous experiments [43] as well as the work presented in Chapters II and III. It is composed of two main loops. The first is a water loop that circulates water between the chiller plant and air-to-water heat exchangers, where the water loop interfaces with the air loop. In the air loop, fans in the Air Handling Units (AHUs) force warm return air from the conditioned spaces through the air-to-water heat exchangers where it is cooled and then delivered as supply air to the inlets of variable air volume (VAV) units. Thermostats (**T**) in the conditioned spaces regulate VAV damper positions to control the amount of cooled air entering a conditioned space. Another thermostat on the chilled water loop regulates the chilled water flow to control the temperature of the cooled air supplied to the VAVs. A pressure sensor at the outlet of the AHUs regulates the fan speed to maintain a constant pressure for the supply air.

2.3.1 Typical Commercial HVAC Architecture

Commercial building HVAC systems come in a variety of architectures, with larger systems often being custom designed. However, HVAC systems often share many properties; for instance, the architecture used in the experiments presented in Chapters II and III (see Fig. 2.1) is functionally similar to the experiments [43, 74, 85] and simulations [74, 142] of other researchers. The HVAC system of interest consists of a central chiller plant that distributes chilled water to heat exchangers in several independent air handling units (AHU). Each AHU contains a fan that circulates warm return air through the heat exchangers to supply cold air to the conditioned spaces. The flow of cold air into each space is regulated by a damper valve in a variable air volume (VAV) unit. Physically collocated VAVs are grouped together and connected via ductwork to a common AHU supply point (see Fig. 2.1). The testbed building contains four AHUs, each serving ∼100 VAVs. The supply air fan and associated variable frequency drive (VFD) in each AHU is controlled to generate a constant air pressure at the supply point.

Unlike the discrete, hysteretic control in residential HVAC units, the error signal from the conditioned-space thermostats is the input to a local proportional-integral-derivative (PID) controller that continuously varies the VAV damper valve opening between 100% (fully open) to about 20-30% open [93]. The lower limit ensures the conditioned space always receives the required minimum level of ventilation. The local PID controller and the mechanical response time of the damper valve determine the rate at which the air flow responds to changes in the thermostat error signal. Typical response times are ∼1 minute in addition to any communication latency.

The heat removed from the warm return air is absorbed by the chilled water, which is circulated back to the chiller plant. The chillers remove this heat and reject it to the ambient environment (see Fig. 2.1). There are two controls on the chilled water loop. First, water valves regulate the supply of chilled water to each air-to-water heat exchanger to control the AHU supply air temperature. A second controller regulates the chilled water outlet temperature by adjusting the number of chiller compressor units that are engaged. Both of these controls operate on a timescale of ∼10-15 minutes making them relatively slow compared to the VAV and supply air pressure controls.

The Building Automation System (BAS) provides communication and supervisory control for the entire HVAC system. Based on data gathered from a building's sensors and actuators, the BAS optimizes the operating set-points for several key system parameters, including supply air pressure, supply air temperature, and chilled

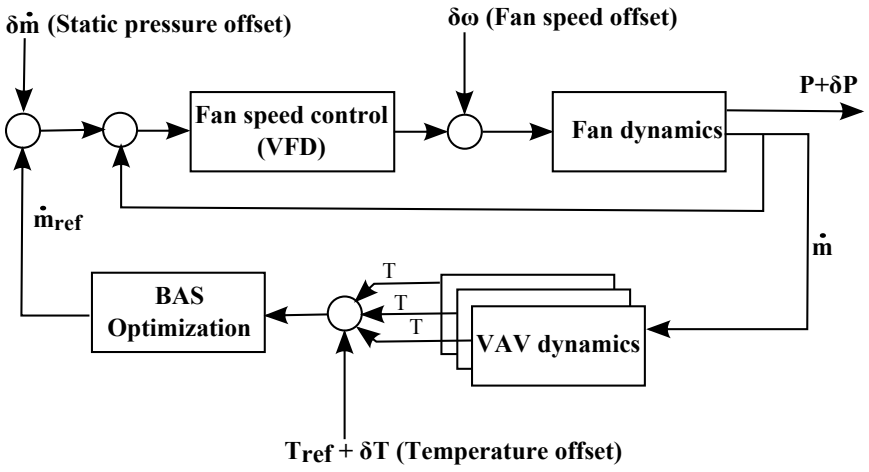

Figure 2.2: A simplified HVAC control diagram and the various control inputs that can be used to influence fan power consumption. Adapted from Fig. 4 in [74].

water supply temperature. The BAS updates these set-points on a timescale of ∼15-30 minutes, i.e. much slower than the VAV and AHU fan response times.

2.3.2 Commercial HVAC DR Control Methods

Modulating HVAC electrical load to track a DR reference signal over multiple timescales while maintaining occupant comfort is challenging due to the interdependent control loops within an HVAC architecture [6]. However, the focus on faster DR applications like frequency regulation narrows the potential control options. For example, infrequent chiller control for peak shaving has been thoroughly examined [12,70,78], but their slow response and potentially high on/off cycling make them inappropriate for frequency regulation. The remainder of this section focuses on leveraging the faster responding AHU fans for frequency regulation.

Fig. 2.2 schematically shows the multiple control loops that affect fan power. These loops can be modified in several ways to influence fan electrical load. This analysis focuses on three methods:

- **Fan speed offset** - Directly adjusting fan speed through control of the VFD, e.g., by adding a fan speed offset signal $\delta\omega$.
- **Supply pressure/Mass flow set-point offset** - Adjusting supply mass flow (or supply pressure) set-point by adding an offset $\delta\dot{m}$ (or δp) which then modifies fan speed via a local control loop that regulates supply pressure or mass flow.

- **Thermostat set-point offset** - Adjusting the thermostat set-points to modify the VAV opening via the local PID controller with subsequent impact on air flow and fan speed via cascading effects through the supply pressure control loop or mass flow control loop.

Each of these may be implemented in an open-loop or closed-loop configuration. Section 2.5.2 makes comparisons between different control methods based on technical performance. The following is a brief description of the stated control methods as well as some comment on their qualitative features. The reader is encouraged to the original references for detailed descriptions.

2.3.2.1 Fan Speed Offset

The fan speed offset method is the most direct way to influence fan power consumption and has been implemented in open-loop [85] and closed-loop [74] configurations. Both implementations require some level of system identification, either an experimentally-determined transfer function [74] or a trained predictive model for power changes [85]. In either case, an offset is added to the motor speed signal to modulate the fan motor's power consumption. The number of supply fans in a commercial HVAC system is typically small, creating some advantages. First, it limits communications and associated latency. Second, the VAVs are not directly involved in the control which avoids their mechanical latency. Finally, the control input is as close to the power consuming load as possible, reducing the complexity and uncertainties and likely improving DR reference signal tracking. In fact, this form of control has been used to mitigate photovoltaic generation variations [86] which are faster than the frequency regulation signals considered here.

There are however some drawbacks to supply fan speed offsets. It may require retrofits to legacy VFD hardware adding cost and complexity. Also, downstream control loops regulating supply pressure or mass flow or VAVs controlling conditioned space temperature will compensate for changes to supply fan speed, limiting the ability to track reference signals with timescales longer than approximately one minute [74]. Motor speed ramp-rate limiters in the VFD likely limit the highest response frequency. When controlling fans that supply many VAVs, e.g. $\sim$100 as in [43], this method lacks the ability to customize DR control for specific occupants or conditioned spaces that may be particulary sensitive to HVAC variability.

2.3.2.2 Supply Pressure Or Mass Flow Set-Point Offset

In many respects, supply pressure or mass flow set-point offsets are very similar to supply fan speed offsets. Whether supply pressure or mass flow is used depends more on the design of the HVAC control system and is not really a choice of the DR control designer. This method has been implemented in closed-loop form in [74], and the open-loop form has been studied in simulation [142]. In either case, the set-point offset to the respective control loop forces that loop to modify its input to the motor VFD, which ultimately changes the fan motor speed and power consumption. The advantages of this method are similar to the supply fan speed offset method; i.e., low latency from a small number of end-points and no purposeful involvement of VAVs. The complexity is still relatively low, but somewhat higher than supply fan speed offset because of the involvement of the physics of the supply duct work and the response of the pressure or mass flow controller. However, the physics of the flow in the duct can be explicitly incorporated [142], enabling accurate DR reference tracking. Finally, only software changes are anticipated because the supply pressure or mass flow set-points can generally be modified via the BAS.

Drawbacks to this method are also similar to supply fan speed offsets. To maintain conditioned space temperature, the downstream VAVs will compensate for the imposed set-point changes limiting the ability to track DR reference signals with longer timescales [142]. The response of the local pressure or mass flow control loop will likely limit the highest response frequency. When controlling the supply pressure or mass flow in an AHU that supplies many VAVs, e.g. $\sim$100 as in [43], this method has the same limitations as mentioned for fan speed offset.

2.3.2.3 Thermostat Set-Point Offset

Thermostat set-point offsets (also termed global thermostat reset–GTR) are the least direct control method discussed in this manuscript. This method has been demonstrated experimentally in closed-loop form for non-spinning reserve markets [62]. It has also been implemented in open-loop form in [43] and in the work presented in this chapter, and has also been simulated in [142]. As of publication, the author is unaware of an implementation or simulation study for frequency regulation using a closed-loop form. If the thermostats in a group of VAVs are adjusted to a cooler set-point, local PID controllers on the VAVs open their damper valves to increase air flow. The subsequent drop in upstream supply air pressure forces the supply pressure control loop (discussed above) to increase supply fan speed (via the VFD) resulting in

higher electrical power consumption. Similarly, a decrease in electrical power occurs when thermostats are adjusted to a warmer set-point.

Advantages and disadvantages of thermostat set-point offsets are mostly reversed relative to the previous two methods. Communicating with every VAV in a large building can create significant latency (∼one minute for the testbed used [43]) and the direct involvement of the VAVs in the control adds their mechanical latency [43, 142] (∼30 seconds). The control is now quite complex as it relies on the behavior of a large number of VAVs, conditioned spaces and occupants, all of which are subject to many disturbances and not easily or accurately modeled. Statistical models have been developed to predict this behavior, but their accuracy in experiments is limited [43]. Simplified thermal-hydraulic models of the building and HVAC system have been used in simulation [142], but these were not subjected to significant disturbances or changes in nominal conditions.

This control method also has some significant advantages. Only software modifications are needed because remote control of the thermostat set-points is possible through many BASs. This also enables tailoring the participation to individual VAVs with the ability to exclude particularly sensitive conditioned spaces or occupants from DR control. Note that this method enables simple (and easily verified) guarantees on occupant comfort through limiting the range of thermostat offsets. Although the initial response is slow because of latency, thermostat set-point offsets are least susceptible to HVAC control system self-correcting effects and can track DR reference signals with longer timescales. In [43], tracking of square-wave reference signals with thirty-minute steps was achieved with no significant roll off of the response.

2.4 Performance Metrics

FERC Order 755 [34] stipulates that DR resources must be compensated for the quality of service they supply to the electrical grid, with the specifics of the quality assessment left to each ISO/RTO. To improve the assessment of quality, the PJM Demand Response Frequency Regulation Market divides the frequency regulation burden into two components: traditional regulation (termed RegA) and dynamic regulation (RegD) [35]. RegA is a low-pass filtered ACE signal[1] designed for ramp-limited DR resources that cannot adjust their demand quickly. RegD is a high-pass filtered ACE signal for fast ramping resources that are capacity-limited; e.g., flywheels

[1]The ACE signal for a balancing authority (control area) is a weighted sum of the mismatch between nominal and actual system frequency together with the mismatch between scheduled and actual power flows on tie-lines to adjacent balancing authorities [59, 132].

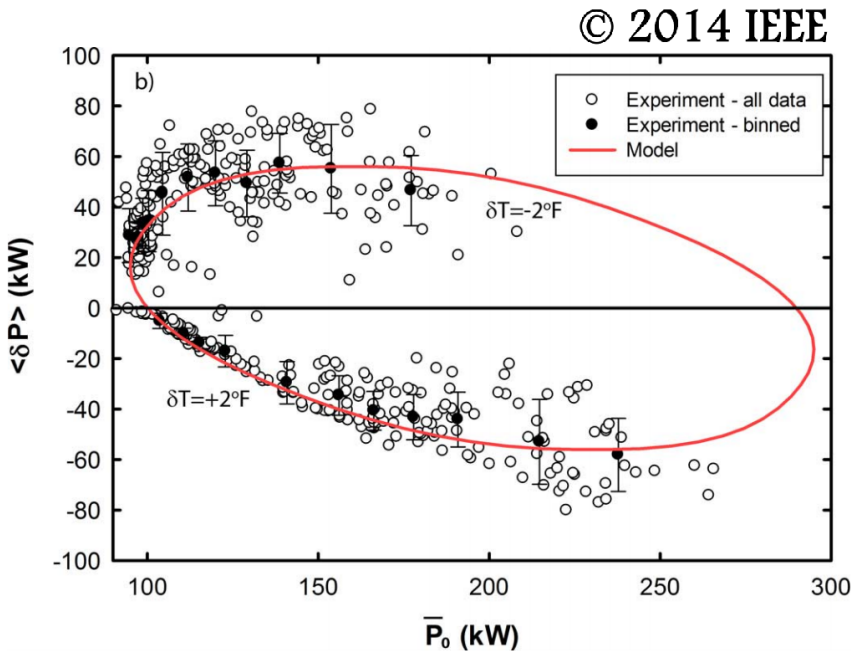

Figure 2.3: A reprint of Figure 4 from [43], which displays a reduced-order model (the red ellipse) that relates initial fan load and the resulting change in fan power when both +2°F and -2°F thermostat off-sets are applied. The authors in [43] use this model to develop a mapping from a desired change in fan power to a thermostat off-set temperature, and this mapping is employed in the experimental studies discussed Section 2.5 (the same testbed building is used both in [43] and the studies in this chapter). *The IEEE does not require individuals working on a thesis to obtain a formal reuse license, however, you may print out this statement to be used as a permission grant.*

and batteries. A more thorough discussion of the PJM market, and RegA versus RegD, is given in [142]. Resources bidding into the PJM regulation market specify the total up and down regulation that they can provide; e.g., ±120 kW. PJM calls upon these resources by broadcasting a signal in the range $[-1, 1]$ which the resources locally scale to their cleared capacity.

Before a DR resource can participate in the PJM market, it must demonstrate adequate performance against a standard 40-minute qualification reference signal that commands the DR resource to adjust its load over its full capacity range, as shown in Fig. 2.4. Performance scores for both RegA and RegD participants are generated based on three criteria [36]:

- **Delay** - the time delay (rounded to the nearest 10 seconds) that provides the maximum correlation between the reference signal and the DR power deviations.

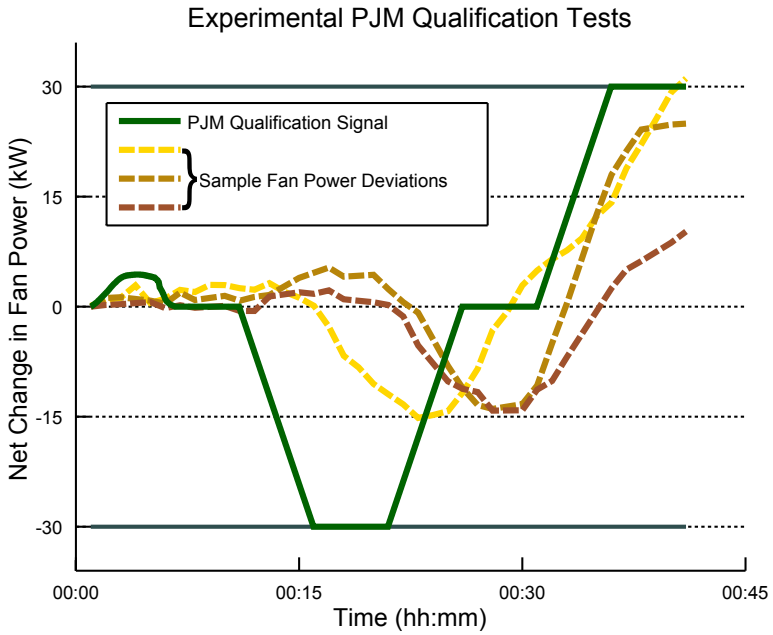

Figure 2.4: Experimental results from our 30,000 m^2 test building. The 40-minute PJM RegA qualification test (solid green line) is broadcast to the BAS. Using the control method developed in [43], the HVAC system uses the thermostat set-point offset method to adjust fan power to track the reference signal. Sample deviations in fan power from nominal are shown as dashed lines.

The score linearly decreases with delay, where a 10-second delay nets a perfect 1.0, and a delay of 5 minutes 10 seconds or more scores a 0.

- **Accuracy** - the maximum correlation between the reference signal and the DR power deviations with the measurements time shifted to remove the delay calculated above.

- **Precision** - the integral of the absolute value of the error between signal and response, without correcting for the delay.

The aggregate score is the average of these three components. To qualify, DR resources must pass three Qualifying Tests with an aggregate score of 0.75 or better, and must maintain a 100-hour rolling average aggregate score of 0.40 or better to remain in the market.

2.5 Experimental Tests

Qualitative advantages and disadvantages of the different control methods were discussed in Subsection 2.3.2. This section presents details on the experiments carried out on the LANL testbed building using PJM RegA qualification test signals, and compares these results to experimental and simulation studies utilizing different control methods. This section then examines the behavior of the testbed building when introduced to historical RegA market signals, which are less aggressive than the RegA qualification test.

The DR control in the testbed building uses an open-loop, thermostat set-point offset method where the open-loop control law was determined experimentally in [43] (using the same LANL testbed building). Figure 2.3 illustrates the mapping developed in [43], where the horizontal axis specifies the aggregate fan power when a thermostat off-set command was initiated, and the vertical axis denotes the corresponding change in fan power, for both +2°F and -2°F thermostat offsets. The experimental results were then binned, and a reduced-order model (shown as an ellipse in the figure) was used to describe the relationship between a fixed temperature offset and the corresponding change in fan power. Using this information, [43] then derives the inverse relationship, i.e. a mapping from a desired change in fan power to the corresponding thermostat off-set temperature. The experiments presented in the next section attempt to track the PJM qualification test signal using the mapping detailed in [43].

2.5.1 RegA Qualification Test

The qualification test experiments were conducted over several weeks in the summer and early fall of 2014, when HVAC load is at its peak. Six two-hour tests ran from 07:00 to 19:00 each day consisting of a 40-minute period in which thermostat set-points were adjusted to track the PJM RegA Qualification Test reference signal, followed by an 80-minute period in which control was released so that the system could return to nominal operation. The regulation signal was scaled to ±30 kW, which is not large enough to meet the 100 kW minimum for participation[2], but is

[2]PJM requires the total capacity of a resource to be ≥100 kW. The testbed building has a maximum nameplate fan load of 295 kW, although it typically operates closer to the minimum fan power of 120 kW (determined by ventilation requirements). At this lower power rating, a ±30 kW change already represents a ±25% change in fan power, and hence a 100 kW adjustment is infeasible for the individual building. Aggregating several building loads would be one way to achieve the necessary DR capacity.

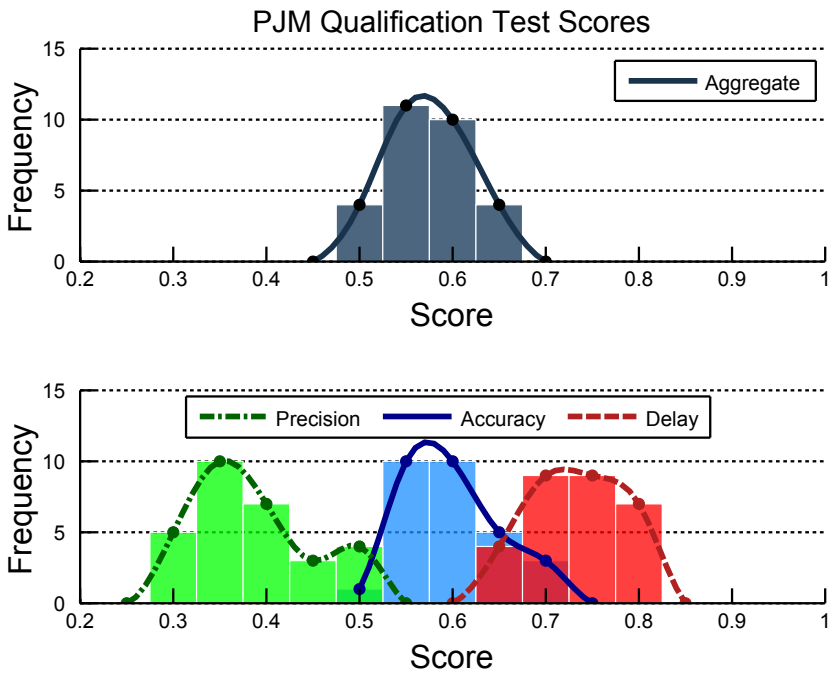

Figure 2.5: Histograms of the PJM performance scores for the tests using the 40-minute PJM RegA Qualification Test signal. Upper plot–Aggregate scores. Lower plot–Delay (red), Accuracy (blue) and Precision (green) scores.

sufficient to induce observable non-linear behavior in the HVAC system. Three examples of the experimental fan response are shown in Fig. 2.4, and a histogram of all the qualification test scores is presented in Fig. 2.5.

The observed aggregate scores for this building and control system are in the 0.5-0.65 range and fall short of the 0.75 score required for qualification. Each component score can be analyzed in light of limitations of the control methodology, communications and the particular HVAC equipment involved. The average Delay score of $\sim$0.75 implies a time delay of about 1.5 minutes, which is consistent with the typical combined communications latency ($\sim$1 minute) and VAV response time ($\sim$30 seconds) for this testbed. The Delay score could be improved in several ways. Other BASs use communications protocols with lower latency than the serial protocol used in the testbed and so should perform better. However, modifying existing BAS communications just to improve DR control for frequency regulation is not likely to be cost effective. A BAS with slow communications might be better suited for direct fan control or supply pressure/mass flow set-point offset control schemes. It is also possible to design controllers that account for communication delay. For instance,

in [71] the authors use model predicative control and state estimation to improve DR tracking performance of residential HVAC systems connected by a constrained communication network.

The Accuracy scores of 0.55-0.60 are likely limited by the complexity and open-loop nature of the thermostat set-point offset control methodology. Although this control methodology provides for easy customization to individual building occupants (e.g. it excludes ∼10% of the VAVs based on perceived sensitivity) and simple power baseline tracking, it is probably the least accurate in tracking a frequency regulation reference signal. It cannot correct for uncertainties and exogenous disturbances to the HVAC system caused by ambient environment changes, occupant level variability or other disturbances. However, it is possible that on-line identification techniques [77] could be used to regularly update the control law and potentially improve the Accuracy score.

The low Precision scores (0.30-0.50) are caused by both time delays and inaccuracies in the open-loop scheme. The relatively fast ramping of the RegA Qualification Test signal compared to the communication latency creates control errors during ramping that are somewhat compensated by the time shift in the Accuracy metric, but create significant penalties in the Precision score.

2.5.2 Comparison of Control Methods

The experimental results from Subsection 2.5.1 are listed in Table 2.1 (the final entry in the table, labeled "LANL"), along with available experimental and simulation studies[3], to compare the DR control methods based on their expected technical performance. We restrict the range of studies to those focused on providing frequency regulation and that have used reasonably similar test procedures, i.e. the use of PJM metrics [36].

However, the comparison is still difficult because the studies use different reference signals. The experiments conducted in Subsection 2.5.1 use RegA qualification test signals. Filtered ACE signals are used in [74], but this filtering is matched to the HVAC DR control system under test and not defined by the market or ISO/RTO. In [142], RegD reference signals are used in simulations.

Differences also exist between the experimental DR control systems and their representation in simulations. The simulations in [142] do not include any effects of com-

[3]The entries in the footnotes of Table 2.1 refer to the original references and specify the source of the results, the name or acronym for the control method, whether the control is open- or closed-loop, and the control reference signal that was used.

Table 2.1: Summary of PJM Performance Scores.

Control Method	Test	Agg	Acc	Del	Pre	Source
Fan speed	Sim	0.89	-	-	-	[74][1]
	Exp	0.77	0.83	1.00	0.49	[74][2]
	Exp	-	~ 0.90	-	-	[85]
Supply pressure/	Sim	0.77	0.87	1.0	0.44	[142][3]
Mass flow rate	Sim	0.82	-	-	-	[74][4]
	Exp	0.81	0.98	0.95	0.50	[74][5]
T-stat set-point	Sim	0.82	0.92	0.99	0.54	[142][6]
	Exp	0.57	0.60	0.73	0.38	LANL[7]

[1]Table I, ASHFS (True output), Closed-loop, Reference=Fast ACE
[2]Table IV, ASHFS, Closed-loop, Reference=Fast ACE
[3]Figure 5, Open-loop, Reference=RegD
[4]Table I, ASLAF (True output), Closed-loop, Reference=Slow ACE
[5]Table IV, ASLAF, Closed-loop, Reference=Slow ACE
[6]Figure 8, Open-loop, Reference=RegD
[7]Current work (Figure 4), Open-loop Reference=RegA

munications latency. This omission likely has minimal effect on supply pressure/mass flow set-point offset control in [142] because the number of control end-points is small (a few AHUs) and the VAV dampers are not directly involved. The close comparison between the simulations of [142] and the experiments of [74] for "supply pressure/mass flow" in Table 2.1 provides some evidence for this conclusion. However, the high scores in [142] for the thermostat set-point offset control (listed under "T-stat set-point" in Table 2.1) are questionable. In a large building, these control signals are sent to a large number of thermostat end-points potentially creating significant latency. These effects lead to a lower Delay score for the current work versus [142], 0.73 versus 0.99. As was argued earlier, this delay leads to lower Precision and Accuracy scores and likely accounts for some of the difference between these scores for the current work and in [142], 0.38 versus 0.54 and 0.60 and 0.92, respectively.

There are also significant differences between the experimental testbeds. The building that forms the testbed in [74] includes three AHU's, but the DR control is implemented on a single motor-fan unit that serves a single large auditorium through a single VAV. Also, the tests were carried out over a relatively short time period. Taken together, these two observations imply the HVAC system was not subject to significant exogenous disturbances that could degrade the DR control performance.

In contrast, the studies conducted in this chapter were carried out on all four main AHUs serving nearly all the floor space of a 30,000 m^2 office building through nearly 500 VAVs. In addition, these experiments were carried out over 12 hours, from a few hours after the morning start up to the beginning of the night setback. Because of this testbed configuration and test protocol, the system is subject to numerous exogenous disturbances, primary among these are highly-variable occupancy, opening and closing of external air dampers for economizer operation, and the typical diurnal heat load cycle. These real-world processes likely act to decrease the Accuracy and Precision performance scores for the "LANL" experiments in Table 2.1, but illuminate the practical difficulties involved in qualifying a commercial HVAC system for DR participation.

In spite of the differences in the testbeds, test protocols and simulation fidelity, some general conclusions can still be drawn from the results in Table 2.1. First, even if the BAS communication protocol is not particularly fast, the smaller number of control end-points for the direct fan speed control or the supply pressure/mass flow control minimizes the effect of communication latency. In addition, by not involving VAV dampers, these control methods avoid this extra mechanical latency. These design choices are the likely reasons for the higher Delay scores for the experiments in [74] as compared to the current work.

Closed-loop DR control is expected to perform better than open-loop control; however, the differences in Table 2.1 are not very large. The DR control in [142] is open-loop, and although only studied in simulation, it shows tracking performance similar to the closed-loop control in [74]. The algorithm in [142] is based on a physics model of the duct system and fans. The quality of the tracking is a function of the accuracy of this model, which can be made quite detailed to capture the important effects. A similar conclusion can be made regarding the Accuracy score of the open-loop fan speed control in [85] versus [74]. However, as the open-loop control actuation moves closer to the end-points, in particular the thermostats and VAVs in the thermostat set-point offset controls, control performance suffers because accurate models are no longer feasible. Because the experiments presented in this chapter relied on the reduced-order, data-driven statistical models developed in [43] (which, by their nature, cannot capture all of the system detail), the reduced model accuracy may be reflected in Table 2.1 by the lower Accuracy and Precision scores of the "LANL" entry versus [74] and [142].

Throughout this analysis, it must be emphasized that the primary goal of the HVAC system is to maintain occupant comfort. The DR control system should allow

the HVAC system to track, on average, its baseline power consumption curve over the day. Each of the DR controllers discussed above achieves this in a slightly different way. The closed-loop controls in [74] apply a bandpass filter to the incoming frequency regulation signal to eliminate the zero and low frequency components. The existing HVAC control is then still able to track the low frequency daily evolution of load. However, long-term testing was not carried out in the experiments of [74]. The open-loop supply pressure control in [142] does not directly control the VAVs. On longer timescales, the VAVs would be free to compensate for the changes in supply pressure, but the simulations in [142] where only carried out for one hour and the nominal heat load on the HVAC system was constant over this time. The open-loop thermostat set-point control method used in the LANL testbed never allows the thermostat set-point adjustments to deviate more than $\pm 2^{\circ}$F. This approach naturally allows the HVAC system to track its baseline load over the entire day and was demonstrated over entire days in [43] and in the experiments presented in this chapter.

2.5.3 Historical RegA Signal Tests

To assess performance under typical operating conditions, the same building and open-loop thermostat set-point offset control system was tested using historical RegA signals from the PJM Demand Response Regulation Market. The test protocol is the same as for the RegA Qualification Test, except the duration of the historical RegA signal is 60 minutes instead of 40 minutes. A sample experiment is shown in Fig. 2.6. The distributions of Delay, Accuracy, Precision and Aggregate performance scores are presented in Fig. 2.7. Compared to the RegA Qualification Test, the historical RegA signals display lower ramp rates. The Delay scores are primarily a function of communication latency, and are mostly unaffected by the lower ramp rates. However, the lower ramp rates result in smaller control errors during the ramps and improvements in both the Accuracy and Precision scores. The Aggregate score is improved to $\sim$0.65, which is better than the minimum Aggregate score of 0.40 required for continued participation in the PJM market.

2.6 Conclusion

Growth in renewable generation is challenging operational strategies that have traditionally maintained the balance between generation and load. Flexible demand-side resources may help alleviate this issue. Ancillary services markets such as PJM's Frequency Regulation Market are expanding to allow these resources to participate,

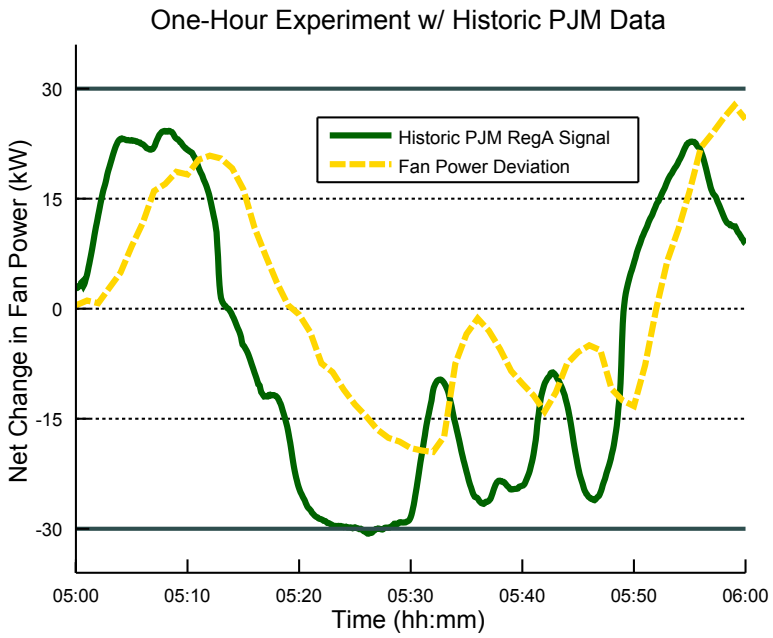

Figure 2.6: An experiment using input from a one-hour sample of the PJM RegA signal recorded on May 5, 2014 (solid green line) and the response of the HVAC system fan power consumption (dashed yellow line). The less aggressive ramp rates of actual RegA market data compared to the RegA qualification test results in better tracking performance in the testbed building.

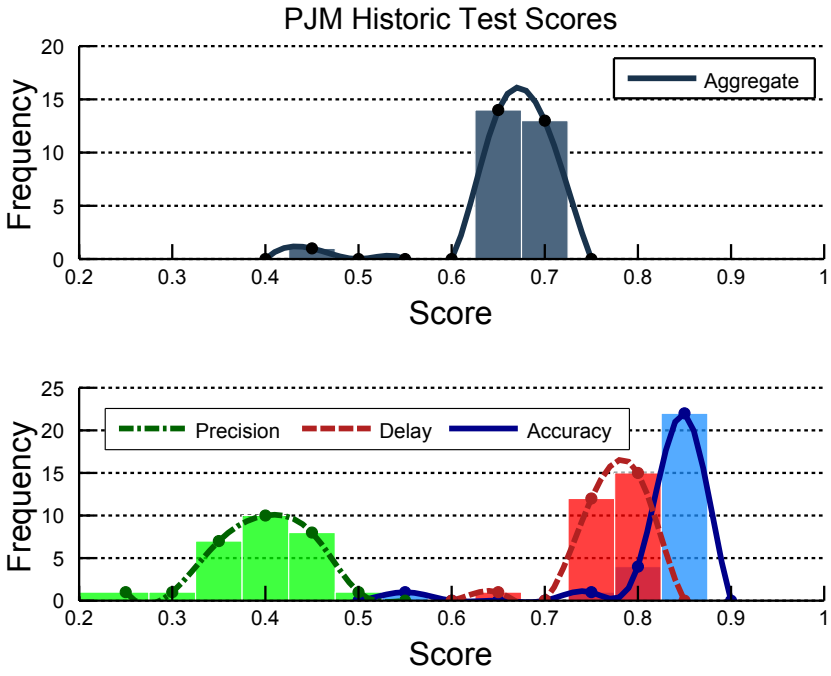

Figure 2.7: Histograms of the PJM performance scores for the tests using historical RegA signals from the PJM market. Upper plot–Aggregate scores. Lower plot–Delay (red), Accuracy (blue) and Precision (green) scores.

provided they can pass minimum performance tests. This new application of demand response (DR) requires controlling these resources on faster timescales, far more frequently, and more accurately than is the case in traditional DR applications.

This chapter reviews experimental and simulation studies [43, 74, 85, 142], and presents new experimental work investigating the ability of a commercial HVAC system to provide frequency regulation services. The studies are used to compare different DR control methodologies (open- versus closed-loop) and different DR control inputs (direct fan speed offset, supply pressure/mass flow offset, and thermostat set-point offset). The small number of studies reported to date have been undertaken under very different conditions, including bench top experimental tests of single components in [85], in-building experimental test and simulation of small sections of a HVAC system in [74], numerical simulation of representative portions of a building in [142], and full-scale experimental tests on an entire building in [43] and in the experiments presented in this chapter. Table 2.1 provides a summary of these studies.

Although these projects demonstrate wide diversity, some general conclusions can still be drawn. Firstly, in-building communication latency and mechanical latency can significantly impact the performance of fast DR controls. Comparing the current experimental results with those in [142] shows that, if these latencies are not considered, DR control performance may be significantly overestimated. Secondly, the choice of control inputs can impact the degree to which these latencies affect performance, from minimal effect for direct fan speed control [74, 85] or supply pressure/mass flow set-point offsets [74,142] to a significant effect for thermostat set-point offsets in [43] and the studies presented in this chapter. However, the choices that offer reduced latency come at a cost of not being able to customize the DR participation for individual conditioned spaces or occupants. Thirdly, as expected, closed-loop DR controls [74] generally perform better than the open-loop DR controls in [43, 85, 142] and the present work. However, as the control input is moved closer to the HVAC fan (e.g. direct fan control in [85] or supply pressure/mass flow set-point offsets in [142]), open-loop performance appears to approach that of closed-loop control. Note again, though, that this improvement in performance comes at the cost of not being able to customize the DR participation for individual conditioned spaces or occupants, as can be achieved with the methods presented in the current experimental studies.

CHAPTER III

The Control Penalty of HVAC Load Modulation

3.1 Introduction

As discussed in the previous chapters, the intent of DR load control is to adjust the time at which energy is consumed in order to assist with the management of generation-load balance. DR is already used in many electrical grids to provide ancillary services, with the majority of these uses being called on relatively infrequently. The impact to the interrupted load is primarily disruption of the end use. Other forms of DR, such as frequency regulation service [142], will require much more frequent and continual modification of load behavior, which may have performance implications beyond just a disruption of the end use.

The assumption by many DR research efforts [32, 80, 142, 143] is that disruption of the load by DR has little or no effect on the total energy consumption or that the effect is insignificant compared to the value of the DR service. For loads that are simply deferred, for example dish washing and clothes drying, or for grid services that only require a few load adjustments per day, this assumption is likely quite good. However, if DR requires that load consumption be modulated about a mean level on sub-hourly timescales, this assumption may not hold and additional energy consumption may be required to serve the disturbed load. Some experimental [50] and simulation [23] work has demonstrated an increase in average total energy consumption due to the relatively slow preheating or precooling of homes driven by time variable energy pricing. However, insufficient attention has been given to possible energy losses incurred because of DR control, especially DR conducted at fast timescales.

Large commercial heating, ventilation, and air conditioning (HVAC) systems are attractive loads for DR applications because they already include relatively sophisticated control and communications architectures, reducing the expected incremental capital cost of adding DR capability. In contrast, a population of small residential

loads may provide a well-understood and repeatable demand profile [15], but the capital cost of the enabling control and communication infrastructure is significant. The operational or control cost of AC-based DR is typically discussed in terms of occupant discomfort—a very important metric because a DR control that exceeds comfort levels too often could be discontinued. Occupant discomfort depends upon the DR control system and how it weights discomfort versus other objectives, e.g. accuracy in tracking load power reference signals. However, there may exist additional operating costs. If the building controls for a large commercial HVAC system are operating in a quasi-steady state, perturbing these operations will likely increase the time-averaged energy consumption, thereby creating additional operating costs for the asset owner who is providing the DR service. This chapter focuses on characterizing these additional energy costs for one type of large commercial building HVAC at timescales comparable to those in frequency regulation service.

This chapter reexamines the experiments from Chapter II and also presents a new set of experiments that provide a methodology for measuring this extra energy consumption. The new DR experiments are primarily carried out at the 15-minute time scale, a speed appropriate for mitigating fluctuations due to wind and PV variations, and approaching the control speeds needed for participation in frequency regulation markets [103]. The HVAC-based DR is characterized in terms of a round-trip efficiency so that it can be directly compared to other forms of energy storage; e.g., the round-trip energy losses incurred when charging and discharging a battery.

The remainder of this chapter is organized as follows. Section 3.2 reviews the energy usage patterns of the experiments presented in Chapter II. Section 3.3 introduces an analogy to round-trip efficiency of battery charging/discharging that will be useful in the discussion of the experiments. Section 3.4 describes the experimental protocol used for determining AC-based DR round-trip efficiency—a method that is reasonably applicable to most large commercial HVAC systems and large aggregates of residential HVAC units. Section 3.5 presents the results of the measurements and a comparison with additional analysis of data from related experiments [50] and simulations [23]. Section 3.6 provides a discussion of the results in terms of an economic model for the DR service and some potential implications for advanced load control. Finally, Section 3.7 presents the conclusions and a discussion of potential future work.

3.2 Cost of Control—Previous Experiments

Demand response may have several costs—capital costs to install the controls and communications and operating cost (e.g. maintenance), but also potential operating costs related to increased energy consumption due to less efficient load operation. Estimates of the capital costs are beyond the scope of the current work. Instead, this chapter focuses on a different question–*if the capital cost can be sufficiently reduced, how will the profitability of demand response be affected by reduced load efficiency?* Specifically, it considers the impact of DR on the time-average efficiency of commercial HVAC operations and the cost of the additional energy required to operate the HVAC system while being controlled for DR. Note that the impact of infrequent DR control (time-of-use tariffs, peak shaving, etc) on time-average load efficiency and energy costs are expected to be small compared to the high value of these operations [24, 50]. However, the frequency regulation considered here is expected to operate frequently and even relatively minor changes in efficiency could significantly increase energy costs compared to the expected frequency regulation revenue.

The importance of the impact of frequency regulation on HVAC efficiency can be understood by considering a traditional generator providing the same service. A traditional generator dispatched to a constant power output P_0 will consume fuel at a constant heat rate H_0. If that same generator is also used for frequency regulation with capacity ΔP, its output P will continually vary between $P_0 - \Delta P$ and $P_0 + \Delta P$, but its time-average power output will still be the same, i.e. $\overline{P} = P_0$ (assuming a balanced regulation signal). However, the continual ramping of the generator reduces its efficiency and increases its time-average heat rate, i.e. $\overline{H} > H_0$. The higher heat rate increases the generator operating cost, and this increase is factored into the generator's bid [36] into the frequency regulation market.

The author proposes that a similar phenomenon occurs when commercial HVAC loads attempt to provide DR capabilities. To introduce this concept, consider Figure 3.1, which presents the total fan energy consumption during the PJM Qualification Test and Historic Test from Chapter II. The experiments took place during the 07:00 to 19:00 time window, for days when control was applied and during days when no testing was performed. The calculated data only consider non-holiday weekdays to compare days with similar load profiles. Each day's total fan energy versus the average daily temperature (also computed between 07:00 and 19:00) is a reasonable proxy for the total HVAC energy consumption. The figure shows a linear fit to the data for each type of reference signal.

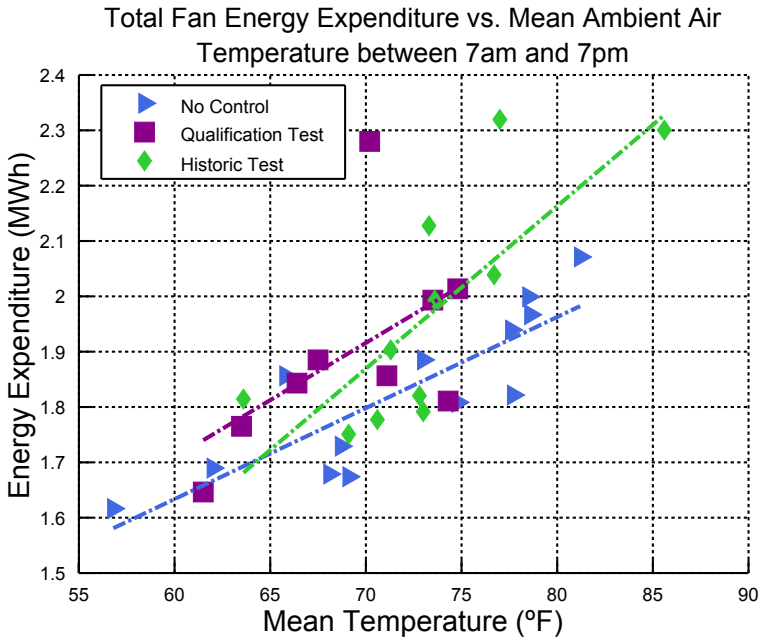

Figure 3.1: Total fan energy consumption versus average daily temperature, both computed between 07:00 and 19:00. The data are sorted into days with no DR control, Qualification Test signal days, and historic signal days. Days where DR control was performed display higher energy consumption than when no DR control was performed.

Although there is considerable scatter in the data, Fig. 3.1 displays a clear trend, in that the energy consumption for Qualification and Historical Test days is higher than when no DR control is performed. At an average ambient temperature of 75°F, the extra energy is ∼100 kW-hrs, corresponding to $10 for a tariff of $0.10/kW-hr. During the tests with the historical RegA signal, the building provided 30 kW of frequency regulation capacity for six hours. Based only on the cost of the extra energy, the operating cost to provide this frequency regulation service is ∼$55/MW/hr, which is higher than typical PJM clearing prices [104]. While it must be emphasized that these results are for a single commercial HVAC system using one type of DR control (open-loop thermostat set-point offests), the results are nonetheless significant and warrant further investigation. Additional work is needed to categorize the general trends in the costs of additional energy consumption and to explore means for reducing this additional cost.

3.3 Battery Analogy

When discussing the energy efficiency of HVAC-based DR ancillary service experiments, it is convenient to make an analogy to the *losses* in a battery and the *round-trip efficiency* of battery charging/discharging. Fig. 3.2 plots the grid power exchange and state-of-charge (SOC) for a hypothetical charge-discharge cycle for a lossy battery. In control period 1, the battery is charged with a constant power P drawn from the grid. Because of charging losses, the power delivered to the battery is less than P. The battery SOC increases but at a rate lower than P. During the control period 2 (the same duration as period 1), the battery is discharged with a constant power P delivered to the grid. Because of discharge losses, the battery discharges at a rate higher than P, and the battery SOC decreases at a rate faster than P.

At the end of control period 2, the net energy exchange *with the grid* is zero, however, the internal state of the battery (i.e. the SOC) is lower than at the beginning of this process. To restore the internal state requires an additional charging period (control period 3) to replace the energy dissipated in the first two periods. After restoring the SOC to its initial value, the battery has taken more energy from the grid (E_{in}) than it has delivered to the grid (E_{out}). The round-trip efficiency for this battery can now be defined as

$$\eta_{RT} = E_{out}/E_{in}. \tag{3.1}$$

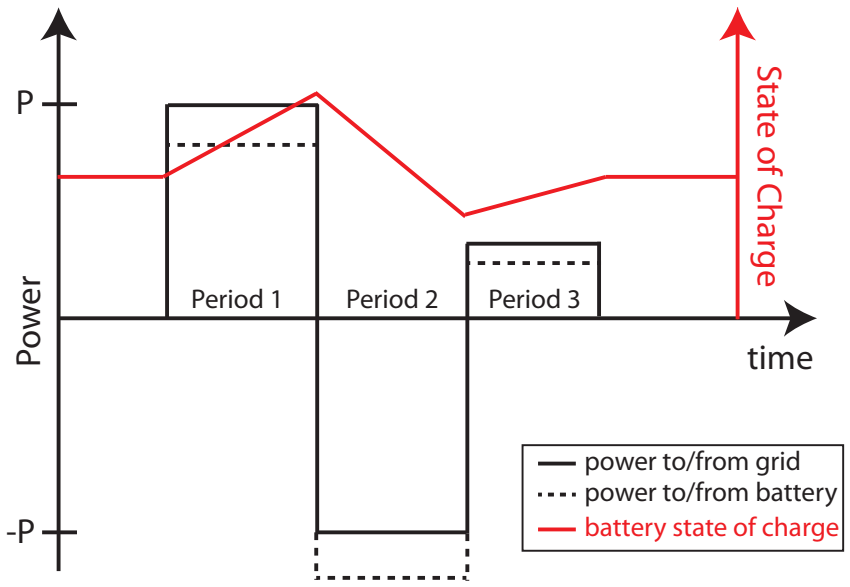

Figure 3.2: Prototypical charge/discharge cycle of a lossy battery. During the first period, the battery charges by drawing power P from the grid (solid black line), however, the losses reduce the power delivered to the battery (dashed black line) and the battery state of charge (SOC) (red line) increases at a reduced rate. During the second control period, the battery discharges with power P delivered to the grid. Losses result in the battery discharging at a rate larger than P and the SOC decreases at an accelerated rate. This charge/discharge cycle results in the SOC being lower than at the start of the process. A third period of charging is required to restore the SOC to the starting value.

The same definition works equally well for more complicated charge/discharge processes, e.g. the charge and discharge periods need not be the same length or exchange the same power with the grid. The only requirement is that the battery SOC is the same at the beginning and end of the process, and E_{in} and E_{out} account for all of the energy extracted from or delivered to the grid, respectively.

3.4 Experimental Protocol

To control the building power consumption in this chapter, the experiments leverage the same open-loop DR control algorithm developed for the building in previous work [43], and also utilized in Chapter II. The algorithm converts an input electrical power (kW) change command into a Global Thermostat Reset (GTR) that simultaneously shifts nearly all of the ∼500 thermostats in the building to approximate the desired electrical power change from the fans in the AHUs (see Fig. 2.1). The extreme reduction in dimensionality of the control model limits the accuracy of the algorithm [43], but it is sufficient for the experiments carried out in this chapter.

The BAS is programmed to perform a repetitive set of DR experiments throughout the day. A single-day sample of the HVAC fan power recordings is presented in Figure 3.3. The Control Input trace indicates the DR signal implemented by the BAS. It consists of a 15-minute period where the HVAC fan power is increased by 15 kW above the baseline, followed by a 15-minute period where the HVAC fan power is decreased by 15 kW below the baseline. This near zero-energy exchange with the grid is followed by a 90-minute period where the DR control is set to zero to allow the building to return to its baseline operation before the next DR experiment is initiated.

These experiments are repeated throughout the day for approximately 15 days. To check for hysteresis effects, the experiment is run with both polarities of the DR control pulse. The amplitude of the DR control pulse is 30 kW in the majority of these experiments. To determine an accurate baseline, the HVAC fan power data is interpolated between a short time window that immediately precedes the DR control pulse and a second short time window immediately prior to the next DR control pulse. Subtracting the baseline from the recorded fan power yields the DR power provided to the grid (see Fig. 3.3).

To assess the effect of baseline accuracy on the results for round trip efficiency, this same linear interpolation was performed over two hour time periods on seven days in which control actions were not taken; i.e., the HVAC system was unperturbed.

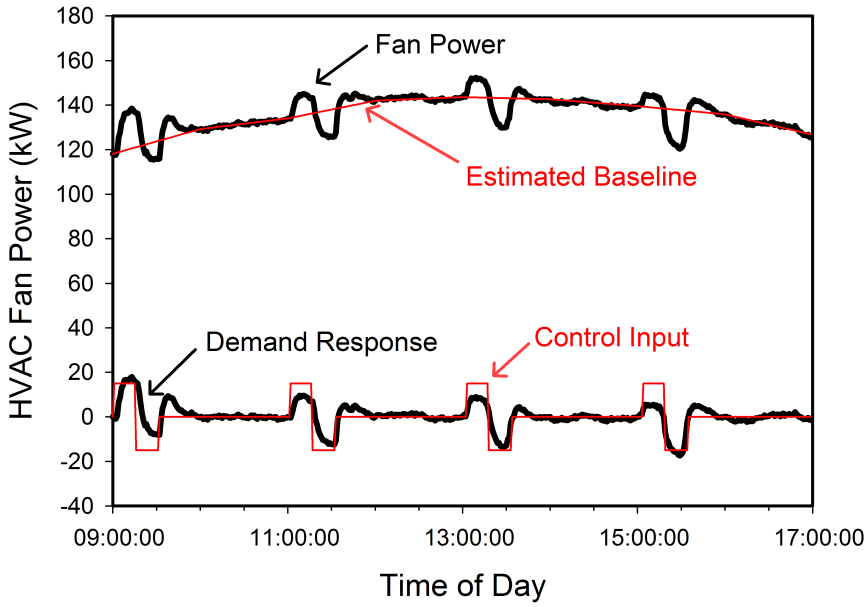

Figure 3.3: Full-day recording of the DR control input signal, the HVAC fan power data, linearly interpolated baseline load, and resulting demand response (DR) profile. Each control period consists of a 15-minute interval where an open-loop control [43] is used to increase the HVAC fan power above the baseline by 15 kW followed by a second 15-minute period where the HVAC fan power is decreased below the baseline by 15 kW. Following this near zero-energy exchange with the grid, the DR control is set to zero for 90 minutes to allow the building to return to its baseline operation before the next DR experiment is initiated. DR experiments are not performed between 5pm and 9am because night setback and morning cool down of the building take precedence.

The same linear interpolation (at two hour intervals) was used to determine an estimated counterfactual baseline. Because these were days when no testing was being undertaken, the recorded fan power served as the actual baseline. When comparing the actual baseline to the estimated counterfactual waveform, the tests revealed an average energy over the counterfactual baseline of 0.724 kWh per two hour control period, and an average energy under the counterfactual baseline of 0.532 kWh for the same time frame. Our experiments use control pulses of $30\text{kW} * 0.25\text{hours} = 7.5\text{kWh}$ giving a conservative estimate of the error in round trip efficiency on the order of $\sim$10%. (For a more in-depth examination of variability in baseline HVAC load estimation, see e.g. [88]).

Figure 3.4 shows a magnified view of the HVAC fan power over a single control period (from a different experiment than shown in Fig. 3.3). The experiment is initiated at 11:00 using a 30 kW amplitude DR control signal with the same two 15-minute control periods, as discussed above. During the first control period, the extra power consumption is converted into extra cooling power in excess of the internal heat generation and the heat leak into the building. This excess cooling power is absorbed by cooling the building thermal mass. The control is not perfect, and the peak change in fan power consumption approaches $\sim$35 kW. At 11:15, the control algorithm is instructed to decrease fan power consumption by 60 kW for another 15 minutes; i.e., 30 kW below the baseline at 11:00 am. The AC cooling power is lowered below the internal heat generation and heat leak into the building. During this time, the heat leak and internal heat generation are absorbed by the building thermal mass. At 11:30, the open-loop DR control is released; i.e., all thermostat set-points are returned to their nominal values prior to 11:00.

If the processes described above were reversible, the amount of heat extracted from and injected into the building thermal mass during the two control periods would be the same and the building state at 11:30 would be identical to the building state at 11:00. However, the fan power remains elevated for approximately 60 minutes following the release of the DR control. In effect, the apparently zero-net electrical DR control during the first two control periods between 11:00 and 11:30 has driven the building away from its quasi-steady equilibrium. Additional cooling power (and therefore electrical energy) is required to restore this equilibrium after 11:30.

The behavior of the building and AC-based DR in Fig. 3.4 is qualitatively similar to the lossy battery charge/discharge analogy discussed in Sec. 3.3 and shown in Fig. 3.2. The thermal energy stored in the building mass is the internal state variable that plays the analogous role to the battery SOC, and variations in the HVAC fan

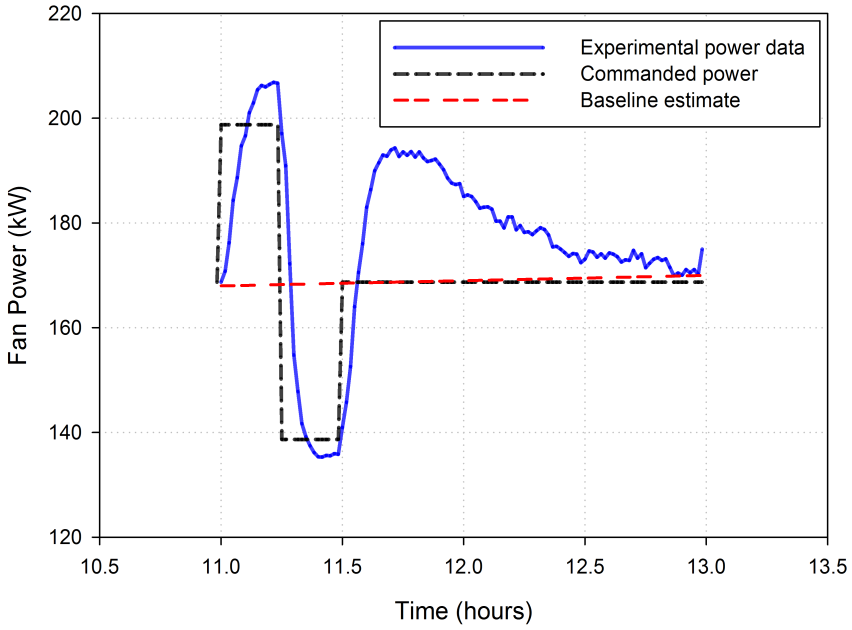

Figure 3.4: A typical DR control transient. The black dashed line is the DR control signal implemented by the Building Automation System (BAS) which translates it to a global thermostat shift using the controller developed in [43]. The control signal is zero for 90 minutes prior to 11:00 (not shown), i.e. the control is requesting no change relative to the fan power baseline and the building HVACis running as though no demand response is requested. After the positive and negative cycles of DR, the control is released, i.e. no DR is requested and the building is allowed to return to its baseline operation. The solid blue trace is the measured fan power response. The fan power tracks the DR control signal reasonably well with a few minutes of time delay. After 11:30, the measured fan power remains high, i.e. above its baseline power, to return the building to its state prior to the initiation of the DR control at 11:00 hours. The dashed red line is the baseline fan power estimated by linear interpolation between short windows of data immediately preceding the control period (just prior to 11:00) and just before the next control period (just before 13:00).

power around the baseline play the role of battery charge/discharge power. During the first period of increased electricity consumption, the HVAC system is asked to remove heat from the building at a rate higher than the baseline. During the second control period of decreased electricity consumption, the HVAC system is asked to remove heat from the building at a rate lower than the baseline. Electrical, hydrodynamic and thermodynamic losses associated with disturbing the system from its quasi steady state subsequently force additional electricity consumption to restore the building's "SOC". Using this analogy, the round-trip efficiency of each of the DR experiments is computed from the measured data in a similar way as for the battery, i.e.

$$\eta_{RT} = E_{out}/E_{in}, \tag{3.2}$$

where

$$E_{out} = \text{the total energy below the baseline}$$
$$E_{in} = \text{the total energy above the baseline,}$$

with the energy totals computed over the entire two-hour span of each measurement (see Figs. 3.3 and 3.4)

3.5 Results

3.5.1 Round Trip Efficiency—Current Study

Our experiments consist of repetitions of the DR control pulses shown in Fig. 3.3 over many days to sample the building performance over a range of conditions. The HVAC fan power depends on many variables including the outside air temperature, which changes throughout the day. As a result, many of the baselines are not flat but instead slope upwards in the morning hours and downwards in the evenings. For each DR pulse, the round-trip efficiency η_{RT} is computed using (3.2). The distribution of all the η_{RT} samples is plotted in Fig. 3.5 (filled circles). The samples of η_{RT} display significant scatter, with a few rare samples giving values greater than one. The variability in η_{RT} is likely because of the variability in the building and AC system conditions that are beyond control. Averaging over all of the samples results in $\langle\eta_{RT}\rangle$=0.46 which is a rather low round-trip efficiency compared to most battery storage systems [103] (although it should be noted that capital costs of retrofitting HVAC systems for DR are likely much lower than the costs of procuring an equivalent

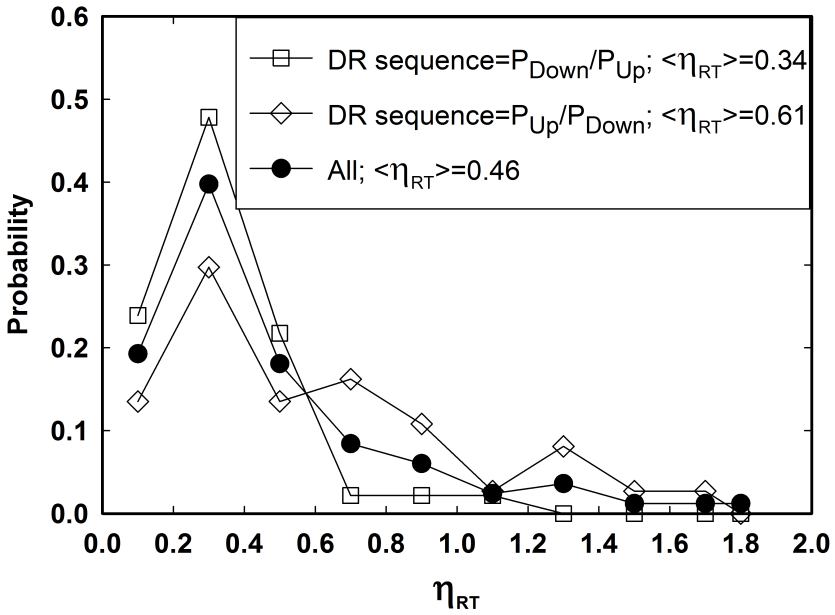

Figure 3.5: Probability of observing a round-trip efficiency of η_{RT} for a 30 kW-amplitude DR pulse as shown in Fig. 3.4. The term $< \eta_{RT} >$ refers to the mean round-trip efficiency for a given set of data. The filled circles show the results for all 83 measurement samples. The open squares show the results for the measurement samples when the HVAC power was first decreased and then increased (46 samples). The open diamonds display the results for samples when the HVAC power was first increased and then decreased (37 samples). The measurements are binned in this way because, under the majority of conditions tested in this work, an initial 30-kW decrement in fan power is expected to cause many of the VAV dampers to saturate at their minimum opening causing an asymmetry in the fan power response. An initial increase in fan power is not expected to encounter this initial saturation [43].

capacity of battery storage).

As noted earlier, a VAV must provide a minimum ventilation flow to the conditioned space it serves and is restricted in the amount that it is allowed to close. This saturation will affect the AC fan power and may potentially bias measurements of the round-trip efficiency. To test whether the experiments are subject to such bias, DR control pulses of both polarities are used so that the potential VAV saturation is experienced in the first or second control period. The data samples are partitioned into two sets according to the polarity of the pulses. The DR pulses that initially open the damper valves, i.e. increase the fan power, show $\langle \eta_{RT} \rangle$=0.61 and a larger spread in the measured values as compared to the DR pulses that initially close the

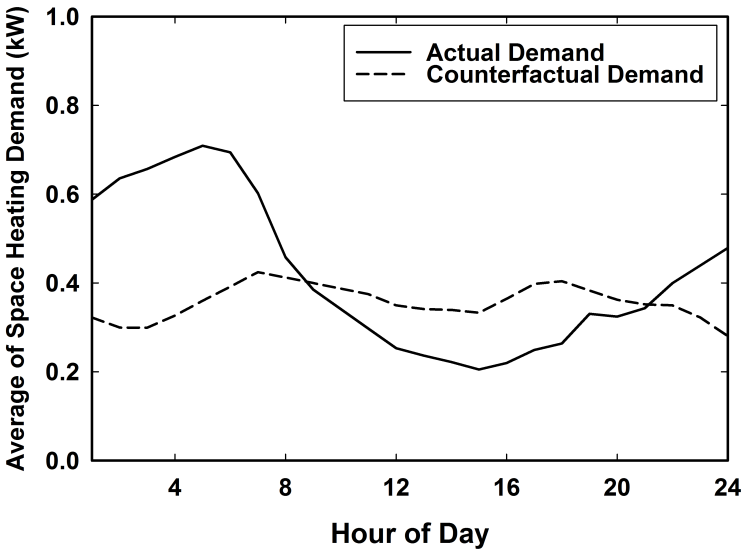

Figure 3.6: Adapted from Figure 7.10a) of [50], shows energy expenditures over 24-hour window in previous experiments. Average space conditioning electrical demand for a range of residences participating in transactive control in a double auction market with five-minute clearing. Both the measured demand (solid line) and counterfactual demand (dashed line) are given. The deviations of the actual around the counterfactual is interpreted as a grid service similar to experimental data in Fig. 3.5. The round-trip efficiency of this service is estimated to be η_{RT}=0.42.

damper valves ($\langle\eta_{RT}\rangle$=0.34). However, this difference does not materially change the discussion in the remainder of this chapter.

3.5.2 Round Trip Efficiency—Previous Studies

An average round-trip efficiency of 0.46 may appear to be rather low for the HVAC system used in this work, however, additional analysis of other experiments and simulations reveal similar round-trip efficiencies for space conditioning applications. For example, experiments in [50] utilized a transactive control scheme to control the demand of several types of home appliances including electric space heating and cooling. In contrast to the more complex AC system studied in this work, the residential heating and cooling systems in [50] were far simpler with on/off hysteresis control. Figure 3.6 is an estimate of the data from Fig. 7.10a) of [50] that displays the measured average space-conditioning electrical demand versus the time of day and the counterfactual estimate, i.e. an estimate of what the demand would have been if there had been no load control. Lower prices during the nighttime encouraged higher

electrical demand for precooling/preheating of the space followed by lower electrical demand during daytime hours when prices were generally higher. Taking the counterfactual as the baseline in Fig. 3.6, the average energy "delivered to the grid" between the hours 9 and 21 is calculated to be 1.1 kW-hr and the energy "taken from the grid" between the hours of 0 and 9 and 21 and 24 is 2.6 kW-hr. Assuming that the conditioned spaces end up on average in the same state in hour 24 as they began at hour 0, the round-trip efficiency is 0.42—a result that is surprisingly close to the η_{RT}=0.46 measured in this work. Similar observations have been made in simulations of residential HVAC systems operated so as to reduce on-peak energy usage [23]. Figure 10 of [23] shows that moving ∼4.2 kW-hr of energy consumption away from a four-hour-long peak period caused an additional energy consumption of ∼3.9 kW-hr above the baseline. Using these results in (3.2), we obtain η_{RT}=4.2/(4.2+3.9)= 0.52. Although the round-trip efficiencies in these two cases are similar to that obtained from the measurements in this chapter, the time scale of the control is significantly longer than for the experiments presented in this section.

3.5.3 Effects of Chiller–Current Study

Fan power is only one portion of HVAC electricity consumption. It is important to consider the impact of other power consumptions, e.g. the chillers, on the measurements of round trip efficiency. The experiments in Section 3.5.1 were reanalyzed to include both fan and chiller power consumption. The example presented in Figure 3.7 demonstrates that, similar to the fans, the chiller experiences a post-control period of heightened electricity consumption. Using the same baseline estimation techniques and definition of efficiency as in Section 3.5.1 yields an aggregate average round trip efficiency of $\langle\eta_{RT}\rangle$=0.42 indicating that chillers also incur a similar energy penalty while providing DR control.

3.5.4 Effects of Perturbation Size on Efficiency

Although the preceding analysis only discusses perturbation of the fan load at a constant magnitude (specifically ±30kW), it is likely that the round-trip efficiency of the HVAC system is partially dependent on the size of these perturbations. The observed degradation in fan efficiency may be related to the non-linear fan affinity laws discussed earlier, which result in large increases in fan power for only modest increases in cooling capability. If this is the case, then more efficient operation may be obtainable by reducing the magnitude of fan power perturbations, especially in

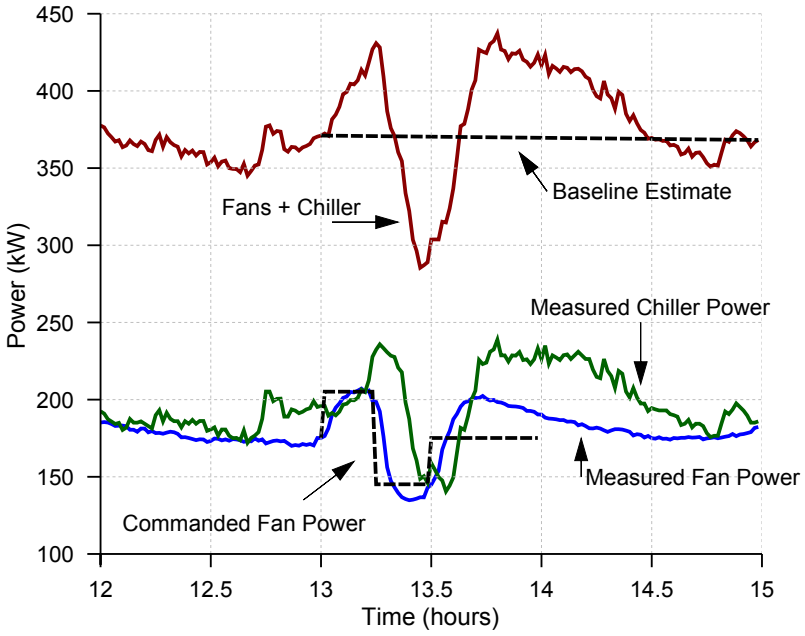

Figure 3.7: An experimental fan power trace with chiller power included as well. A square wave pulse is broadcast to the VAVs at 13:00, resulting in the measured fan power deviation shown. The fan power deviation is mirrored in the chiller power consumption, with a time delay induced by the dynamics between the warm return air and cooled water loop. The combined fan + chiller power consumption (the upper red trace) is used to determine efficiency of the overall system. Note the elevated post-control power consumption for the combined power, which is similar to the phenomenon observed when only considering fan power consumption (as in Figure 3.4).

proportion to baseline fan load, thereby keeping the fans closer to a linear operating region. These considerations would correspondingly effect the capacity bid that a participating building would submit to an FR market.

3.6 Discussion—Economic Analysis

The measurements presented above suggest that the participation of large commercial HVAC systems in fast DR ancillary services may increase total HVAC energy consumption. This section discusses the impact of this observation on the economics of fast DR ancillary services from large commercial HVAC systems, with an emphasis on frequency regulation services.

The frequency regulation market is a bid-based auction-style market in which the marginal unit sets the clearing price for all participants. To participate and compete in this market, resources should submit bids that reflect their cost of providing frequency regulation service. The PJM market [103, 142] requires a Cost-Based Regulation Offer that is split into a capability component and a performance component [103] whose definitions are tailored for fuel-consuming generators. Interpretation for a DR regulation resource are as follows:

1. Capability Component/Steady Operation Fuel Costs—For a fuel-fired resource, this is the steady-state increase in fuel costs associated with operating the resource at power output that is different from its optimal economic dispatch point. Our DR resource is not making a steady-state change in its operation and this cost is effectively zero.

2. Capability Component/Margin Adder—Up to \$12/MW of margin can be added to the Capability Component. The margin is included at the discretion of the resource owner and will not be considered in this analysis.

3. Performance Component/Variable Operation Fuel Costs—For a fuel-fired resource, this is the increase in fuel costs because of non-steady operation. This effect is directly tied to the results for round-trip efficiency in Section 3.5 and the associated increase in costs because of higher electricity consumption.

4. Performance Component/Variable Operation and Maintenance Costs—PJM defines a cap on these costs for different generating unit types. No cap is given for demand resources, and it is assumed this cap is zero.

From the description of the PJM frequency regulation market above, we conclude that the major component of the resource's DR bid into PJM's RegA market would be the increased electricity costs arising from variable HVAC operations. However, caution must be taken in comparing this cost with historical market data. The model of DR inefficiency described in Section 3.4 is based on energy exchanges with the electrical grid above or below baseline operations, while the PJM market assumes that the primary cost driver is an increase in fuel cost for making *changes* in generator output; i.e., regulation mileage [103]. PJM publishes average regulation mileage data, but it does not provide data on the regulation energy exchanges above and below the generator set-points.

Historical data for the PJM RegA signal from December 18, 2012 to January 18, 2014 show that, on average, a 1-MW capacity RegA resource "injects" 0.14 MW-hrs of energy into the grid and "absorbs" 0.35 MW-hrs of energy from the grid each hour. Here, the energy "injected" is computed using only times when the RegA signal is positive, and "absorbed" is computed using only times when the RegA signal is negative. The bias toward a negative RegA signal is persistent throughout the data investigated and may reflect a bias in the PJM market or reliability operations.

To simplify the market analysis of the DR resource, the zero of the RegA signal is shifted to balance the energy exchanges so that, on average, energy $E_{ex} \sim 0.25$ MW-hrs is injected and absorbed during one hour of frequency regulation service. Under these conditions, the extra energy consumption E_{lost} because of round-trip losses can be computed from (3.2) as

$$E_{lost} = \frac{1 - \langle \eta_{RT} \rangle}{\langle \eta_{RT} \rangle} E_{ex}. \tag{3.3}$$

The additional energy required for a DR with $\langle \eta_{RT} \rangle$=0.46 is 0.29 MW-hrs for each MW and each hour of frequency regulation service. The cost of this additional energy can vary widely depending on the tariff structure of the utility provider. For an energy tariff of \$0.10/kW-hr the cost of providing this DR service is \$29/MW/hr which is typically near the marginal cost for this service in the PJM market [104]. However, this cost does not include any profit for the owner ("margin adder") of the asset providing the DR service.

3.7 Conclusions and Future Work

This chapter develops a methodology for measuring the round-trip efficiency of large commercial air conditioning loads controlled for fast demand response (DR).

This methodology is applied to a large commercial air conditioning system that is controlled on the 15-minute time scale—a speed that is approaching that needed for participating in many frequency regulation markets. For the large commercial air conditioning load studied in this work, the calculated round-trip efficiency is approximately 0.46 when only considering fan power, and an efficiency of 0.42 when analyzing the combined power of the chiller and fans. These rather low results are very similar to the round-trip efficiencies 0.42 and 0.52 estimated from data in other experimental [50] and simulation work [23], respectively. Although the timescales in this other work are quite different, the similarity of the results suggests that the loss mechanisms may be related. It is therefore possible that this low round-trip efficiency may carry over to other space conditioning loads.

The experiments presented in Chapters II and III also point to an issue that may have significant impact on the economic viability of fast, continuously operated DR control like the frequency regulation service explored here. A commercial HVAC system that is continually perturbed from nominal operation, and that is rapidly ramped between these very different operating states, will display a lower average efficiency than when operated in a steady manner. The lower efficiency translates into increased average energy consumption. The effect is similar to that experienced by a traditional fossil fired generator whose efficiency suffers when ramped up and down to provide frequency regulation service. Much like a traditional generator, the increased cost of serving the HVAC load should be incorporated into the cost of providing the frequency regulation service. For the building and control system investigated here, the calculated cost is rather high ($\sim$\$55/MW/hr). In contrast, for relatively infrequent DR control like spinning reserves or peak shaving, the impact of these effects on long-run efficiency and DR economics is minimal.

CHAPTER IV

Transformer Overload Mitigation using Plug-In Electric Vehicles (PEVs)

4.1 Introduction

Concerns over global climate change have led policy makers to adopt regulations that reduce the consumption of fossil fuels. Along these lines, plug-in electric vehicles (PEVs), which derive a portion of their energy from onboard batteries charged from an external source, have become an increasingly popular way to reduce demand for petroleum. However, care must be taken when coupling the transportation sector's energy consumption to the terrestrial power grid, so that the increased load does not damage power system equipment or disrupt electrical service.

The electric vehicle supply equipment (EVSE) that provides electricity to vehicle batteries is standardized to provide power at up to 19.2 kW [123]. At these power levels, a large population of PEVs could have a significant effect on power system dynamics. An uncontrolled PEV fleet could lead to problems both at the transmission level, where PEV loads have the potential to exacerbate capacity issues at peak load times [39, 83], and at the distribution level, where the additional load could cause overheating of substation and distribution transformers [44, 57, 87] as well as distort voltage profiles and increase network losses [25, 60, 76, 101]. While projections for the future market penetration of PEVs vary significantly [28, 91, 125], even moderate gains in PEV sales will likely necessitate some form of charging control in order to mitigate these issues.

Recent research on charging algorithms has focused on mitigating undesirable effects at the distribution level, with several papers combining analysis of charging scheme effectiveness from a controls perspective with simulations of the resulting power dynamics. Work in [38] applied a utility function method to prevent voltage

dips and line overloading on realistic low-voltage networks. Other researchers have used queuing formulations [73] to dispatch PEV charging while maintaining grid stability. Another approach detailed in [118] proposes utilizing vehicle chargers for reactive power balance in order to bolster voltage sags in high PEV penetration networks. On-line linear programming techniques have also been applied [107].

This chapter extends previous work by examining a low-voltage test circuit, the IEEE 34-node network, in conjunction with a fleet of electric vehicles under additive-increase multiplicative-decrease (AIMD) control. Unlike similar charging schemes, AIMD has the ability to provide decentralized, coordinated control with a minimal investment in computational and communication equipment. While others [75] have focused on power regulation at the substation level, the emphasis of this work is on preventing thermal overload of individual distribution transformers using temperature-based AIMD control, and the distribution-level power system dynamics that result when PEVs are charged in this manner.

The remainder of the chapter is organized as follows. Section 4.2 discusses the theory behind the AIMD algorithm and its application to the PEV charging problem. Section 4.3 explains the parameters used in simulations. Section 4.4 examines simulation results including voltage quality and transformer temperature. Section 4.5 looks at the conditions under which thermal overload can arise, and Section 4.6 concludes the chapter.

4.2 Additive-Increase Multiplicative-Decrease Control

The AIMD algorithm was first proposed by Chiu and Jain [21] as a means of maximizing throughput while managing congestion in constrained networks, originally applied to communication links. The implementation is as follows. A group of participants shares a common, constrained network resource. At each time-step, participants increase their rate of use of the global resource by a fixed additive amount α. This process continues unabated until the common resource exceeds its maximum limit. At this time a congestion event signal is broadcast out, and each participant decreases its consumption rate by a multiplicative factor β. This process is illustrated in Figure 4.1.

The AIMD algorithm is appealing for several reasons. Through adjustment of the parameters α and β, trade-offs can be made between fairness (the equitable sharing of resources among participants) and efficiency (the fraction of the total available throughput that is being utilized), as well as between responsiveness (the time it takes

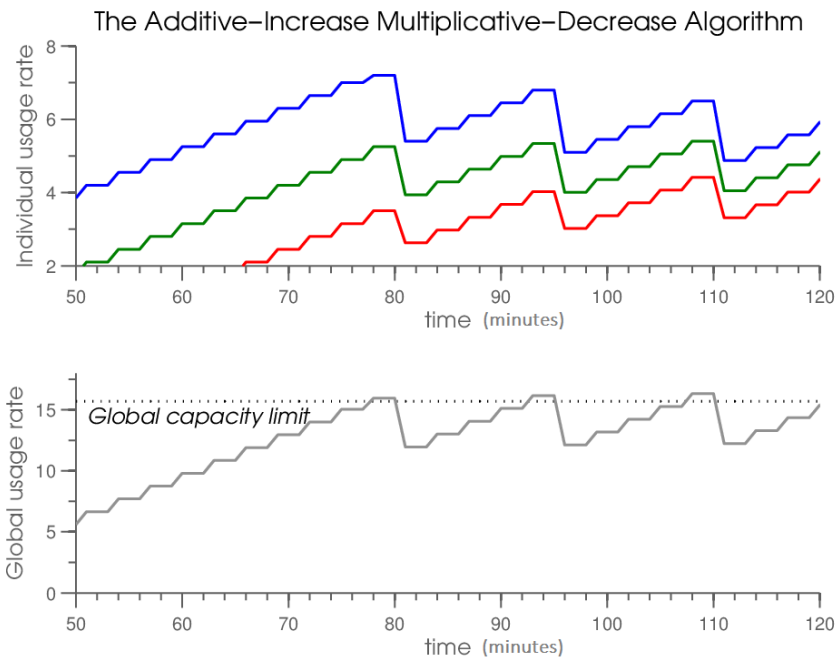

Figure 4.1: Example AIMD algorithm progression. As participants join the network, their rate of use evolves additively until a global limit is reach, at which point a capacity event is triggered, reducing the usage rate of all participants multiplicatively. In perpetuity, all participants converge to the same utilization pattern.

the system to achieve equilibrium) and smoothness (the size of the oscillations that develop in steady state). Given the simple implementation and adaptable operation, AIMD control has long been used for regulating packet congestion on TCP/IP links.

More recently, investigators [116] proposed using AIMD as a novel means of controlling PEV charging on a power constrained network. Under this scheme, vehicles start charging at a low rate when first plugged into the power grid. The vehicles on a particular feeder increase their individual charging rates until they reach a local constraint dictated by the EVSE, or a global power constraint on the substation feeder is reached, at which point the vehicles decrease their power multiplicatively. The advantage of an AIMD implementation is the reduced communication and computation requirements, as the feeder can simply monitor its power locally. The only information broadcast to the participating PEVs is the occurrence of a capacity event.

This work focuses on distribution level effects of AIMD charging; specifically, the adjustment of PEV charging rates to limit aging in distribution transformers, which experience rapid degradation when hot-spot temperatures exceed rated values. Vehicles on a particular transformer increase their charging rate additively until the

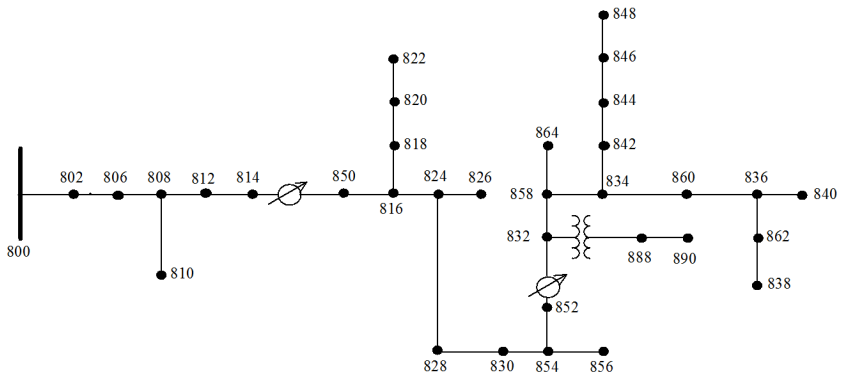

Figure 4.2: The IEEE 34-node test feeder.

transformer's temperature reaches a set limit, at which point PEVs are commanded to decrease charging in a multiplicative fashion. The choice of additive and multiplicative parameters affects coordinated charging performance, as discussed in Section V.

4.3 Simulation Specifications

All simulations were undertaken using the IEEE 34-node distribution test feeder, which represents a realistic rural distribution circuit [61]. This feeder layout is shown in Figure 4.2. Current and voltage dynamics were calculated using the three-phase radial power flow method developed in [20], which uses a forward/backward iterative technique. This method incorporates full three-phase dynamics, including inductive coupling between lines and the existence of single-phase branching feeders that extend from the main feeder.

In order to streamline the simulation, the distributed loads on the test feeder were converted to spot loads by dividing the real and reactive power requirements equally between the two ends of a given line. Capacitor banks were modeled as a shunt capacitance at the relevant nodes. The two voltage regulators present in the IEEE 34-node system are programmed to step tap positions to regulate voltages. It is quite plausible that the voltage variations induced by load control schemes may interact with such voltage regulators, possibly resulting in excessive tapping. However, to better understand the influence of charger controls, it has been found helpful to decouple regulator effects by holding tap positions constant for fifteen minute intervals. Further work is required to determine a tap update strategy that achieves good voltage regulation yet prevents excessive tap-change operations.

The electric vehicles on the network represent a fleet of heterogeneous medium-range plug-in hybrids similar to the Chevy Volt. Though the Volt has a listed battery

capacity of 16 kWh [100], the effective portion that can be repeatedly charged and discharged is only about half this total. As a result, the simulations use battery sizes that vary randomly between 6 and 10 kWh. For the remained of the chapter, effective state-of-charge (SoC) refers to the capacity of the portion of the battery which can be charged/discharged, and can vary from 0-100%. Vehicles arrive for nighttime charging with between 1-25% effective SoC. Existing Level II charging capabilities for the EVSE servicing the car are a 240 V, 15 A connection for a rated maximum power of 7.2 kW, with an efficiency of $\eta = 90\%$.

Table 4.1: Electric Vehicle Charging Specifications.

Battery size	Between 6 and 10 kWh
Initial state-of-charge	1-25%
Maximum charging rate	7.2 kW
Charging efficiency (η)	90%
Power factor	1.0 (unity)

These simulations investigate an overnight charging scenario. The specified background (non-PEV) load on the system wanes overnight, with load values scaled proportional to a sample Midwest ISO demand curve. The given IEEE 34-node values for system load were matched to the peak of the demand curve, and nighttime values were adjusted accordingly. Electric vehicles were assumed to arrive randomly with a uniform distribution between 9pm and 12am. In order to capture the full overnight charging profile of the PEVs, the total simulation runs in 1 minute time-steps for the ten hour period from 9pm to 7am to reflect typical charging patterns.

The total IEEE-34 load is divided by an assumed mean peak household load of 1.75 kW, for a total of 1294 individual residences. PEV penetration levels listed for some of the simulations are based off of this figure; e.g., 25% PEV penetration corresponds to 323 vehicles on the network.

Each node has a number of 25 kVA single-phase transformers apportioned appropriately to meet normal daytime demand. For instance, a node with 60 kVA aggregate load on its A-phase would be assigned three 25 kVA transformers, and each would serve a background load of 20 kVA. The amount of spare capacity on each transformer for PEV charging therefore varies randomly from node to node. The total vehicle population was then assigned randomly to the transformers on the network, with a fixed maximum number of PEVs per transformer to avoid unrealistic buildup on a single piece of equipment.

The temperature dynamics are derived using a first-order differential equation model of a thermal mass, where the transformer is heated by i^2R losses and cooled by the ambient temperature, as in [55]. Thermal dynamics are specified in Kelvin, and the AIMD algorithm engages whenever the total current through the transformer would result in a steady-state temperature above 120°C (or 393°K).

The IEEE 34-node network is long and lightly loaded, which can on occasion lead to convergence issues with some power flow solvers, although this concern did not arise during the loading scenarios studied.

4.4 Simulation Results

4.4.1 Sample Case

The main goal of temperature-based AIMD control is to keep the 25 kVA transformers that service residential loads from exceeding their hot-spot temperature, while providing as much power as possible to the connected electric vehicles in a fair and efficient manner. Simulations were undertaken to assess control performance, with these objectives met in most cases. As an example, Figures 4.3 and 4.4 show respectively the charging profile of all PEVs attached to Transformer #1 at node 860 and the temperature of this transformer. Initially, only one PEV is connected to the transformer, and even though it charges at the maximum rate of 7.2 kW, the transformer temperature actually drops due to the significant nighttime drop-off in background load. However, as more PEVs begin to charge, increasing the current through the transformer, its temperature begins to increase towards its specified maximum. AIMD control sends out the first congestion event at the 68th minute to reduce the charging rate of all attached vehicles.

The average charging rate of each PEV continues to decrease until all vehicles have arrived. Shortly after this point the charging rates converge to a common pattern and enter a period of regular, repeated oscillations. This persists until vehicles begin to complete charging. As the PEVs disconnect, the average charging rate per vehicle increases, causing the remaining cars to finish even faster. Eventually, so few vehicles are connected that they can all charge at full power once again, and the temperature of the transformer begins to drop. The final result is a group of fully charged vehicles and reduced thermal stress on the distribution transformer.

In this example, all the vehicles achieve unity state-of-charge well before the given deadline. However, situations can arise where this is not feasible. The initial background load for the A-phase of node 860 is 51 kVA, which is split equally among

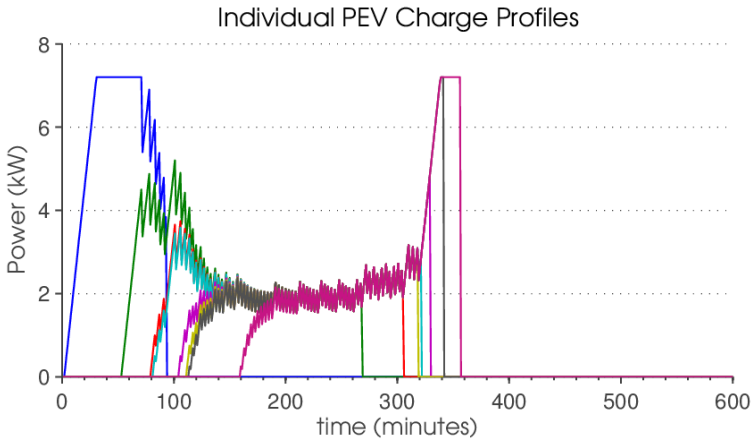

Figure 4.3: Charging rates of each electric vehicle attached to Transformer #1 on node 860 A-phase. Vehicles arrive at randomly determined times and draw power until their batteries are fully charged. The AIMD algorithm engages whenever the current through Transformer #1 exceeds rated value.

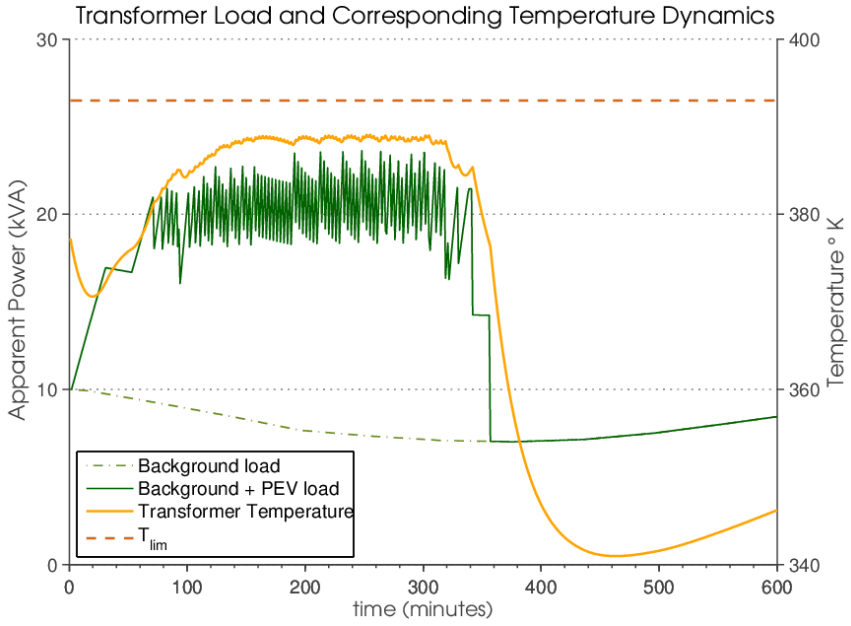

Figure 4.4: Load and temperature data for Transformer #1 temperature at node 860 A-phase. Total load (solid line) includes background demand (dash-dot line) and the sum of the charging profiles from Figure 4.3. Temperature dynamics are derived from this load and the equations in [55]. The AIMD algorithm succeeds in maintaining transformer temperature below the imposed thermal limit.

three 25 kVA transformers at 17 kVA each, leaving 8 kVA of available charging capacity. Available capacity increases further as the nighttime background demand wanes. However, if background peak demand at this node was slightly below 50 kVA, for instance, and only two transformers were assigned to service the load, then the power available to charge the electric vehicles could be inadequate for the given charging-time constraint. In such cases, no form of control could charge all of the vehicles in time without violating transformer hot-spot temperature limits. The distribution utility would have no option other than to install a new transformer. In these situations, AIMD gives priority to distribution transformer health, but still provides a way to maximize throughput to the vehicle loads within this constraint.

4.4.2 Voltage Dynamics

In addition to the car charging dynamics, it is important to ensure that AIMD-induced variations in power levels do not cause unacceptable voltage oscillations. AIMD control is designed to synchronize vehicle charging rates in a pattern of slow increases in power (the additive stage) followed by a rapid decrease (the multiplicative stage), and these dynamics have corresponding effects on voltage levels, which in a radial distribution network may already be close to their limits.

A sample voltage profile for node 860 is shown in Figure 4.5, which displays the three phase voltages over the entirety of nighttime charging. Since control occurs in one minute intervals, voltage oscillations vary on the same time scale. In this example, there are a total of 24 vehicles charging on the transformers attached to the three phases of node 860, and with a PEV penetration level of 15%, 194 total cars on the network. Despite the size of the vehicle population, the amplitude of the resulting voltage variations is minimal. Ignoring tap changes, the largest minute-to-minute voltage variation in this simulation is less than 0.005 per unit. Moreover, there is no discernible pattern in the variations, as the minute-to-minute voltage profile fluctuates arbitrarily. Over hour long timescales, there is a general upward trend in voltage due to decreasing background load, but this phenomena occurs regardless of coordinated vehicle charging.

The lack of more problematic voltage variations is due to several factors. First, although all of the vehicles on one transformer eventually synchronize in a shared pattern of charging, the other transformers on the network have different available power capacities, randomized vehicle arrival times, and charging requirements. The variations in load capability along with the heterogeneous vehicle fleet lead to different charging patterns at each transformer, and the net effect is a canceling out of much

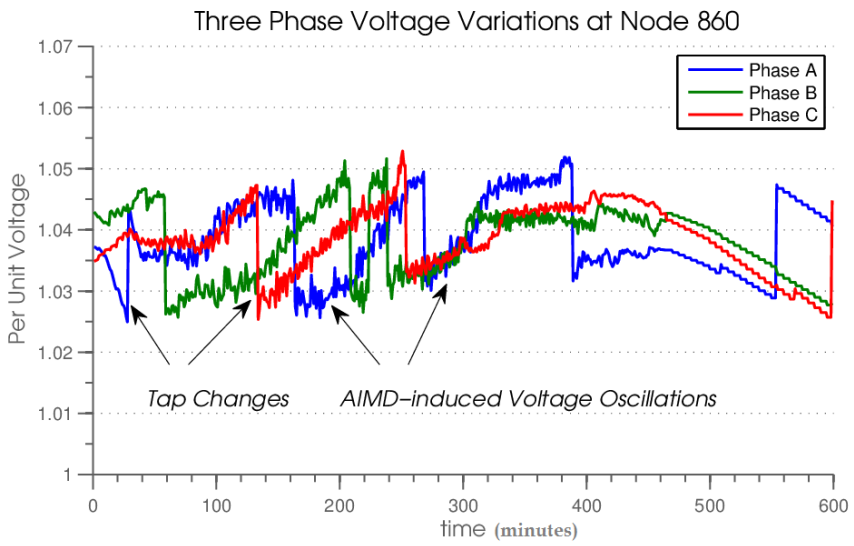

Figure 4.5: Voltage oscillations under AIMD regulation with a 15% PEV penetration level. Tap changes occur as nighttime demand falls, independent of vehicle loading.

of the variations in power (and corresponding changes in voltage) from one time step to the next.

Furthermore, each transformer has only a fixed amount of available power for vehicle charging, and although this capacity increases somewhat as the nighttime background load decreases, this nonetheless limits the amount of power that can oscillate on the system. Consequently, charging variations have less of an effect than might be expected, especially at lower vehicle population levels.

To illustrate this point, a series of simulations was run to determine the largest difference in voltage between two successive steps at any node (excluding tap change events). The results are shown in Table 4.2, which records the worst-case voltage fluctuations after 100 simulations for several PEV penetration levels.

Table 4.2: Maximum nodal voltage variations for randomized PEV populations over 100 simulations.

PEV %	Average worst-case	Absolute worst-case	Node
10	0.0083 p.u.	0.0145 p.u.	846, Aϕ
25	0.0089 p.u.	0.0163 p.u.	840, Aϕ
40	0.0109 p.u.	0.0167 p.u.	840, Aϕ
55	0.0133 p.u.	0.0230 p.u.	840, Aϕ

This sensitivity analysis shows that as the PEV population increases, both aver-

age and absolute worst-case voltage variations tend to increase in magnitude, likely because there are more cars per transformer and correspondingly larger multiplicative power drops (and voltage rises). Furthermore, voltage deviations become increasingly acute as vehicle penetrations levels rise. This non-linear relationship is due to the presence of background demand. At low vehicle populations, the continually-varying PEV charging load represents a small proportion of aggregate system demand, and variability is minimal. However, larger vehicle populations result in a significant proportion of load being adjustable, leading to a more erratic voltage profile.

4.5 Detrimental variations leading to thermal overload

Using AIMD-based control allows electric vehicles to receive their required energy while allocating the load in such a manner that the transformers servicing the vehicles are prevented from overheating. However, under certain conditions, the transformer temperature can actually rise past the specified hot-spot limit. This section examines the causes of thermal overload and possible solutions to mitigate this phenomenon.

For simplicity, assume that background demand on a particular transformer is constant and thus the total power available for PEV charging is also constant. In this situation, every additional vehicle that plugs into the network lowers the average power delivered to each individual charger.

Given n vehicles charging on one transformer and a maximum charge rate P, the total increase in power during each additive step is $n \times \alpha$, and the amplitude of the subsequent multiplicative drop in power is $P \times (1 - \beta)$. Eventually, if enough vehicles charge simultaneously, the aggregate power increase during the additive stage of load control exceeds the decrease during the multiplicative stage. For a given P, α, and β, this occurs when the number of vehicles exceeds the constraint

$$n > P(1 - \beta)/\alpha$$

An example of this charging situation is shown in Figure 4.6, in which twelve PEVs charge on Transformer #2 at node 820 A-phase. The corresponding transformer temperature profile is shown in Figure 4.7. Using $\alpha = 0.25$ kW and $\beta = 0.7$, and given that Transformer #2 has 8 kW of spare capacity, the equipment is only capable of handling nine cars before thermal overload will occur. As can be seen from the detailed inset, once all of the vehicles charge simultaneously, the power increase from a single additive step surpasses the power decrease made during the multiplicative step,

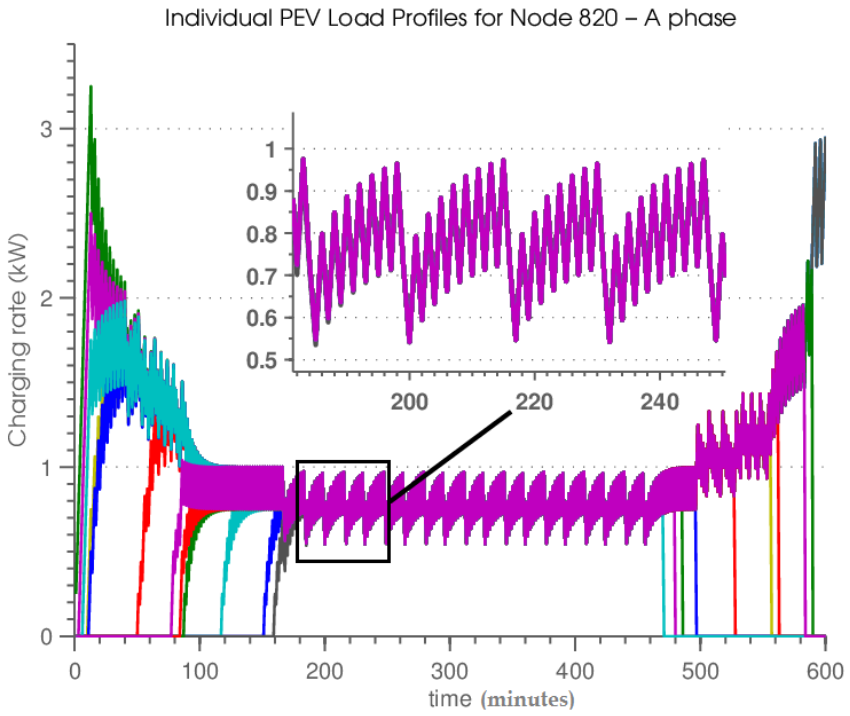

Figure 4.6: Individual transformer overload charging profile. With enough electric vehicles on transformer #2 of node 820 A-phase, the additive increase step exceeds the magnitude of the corresponding multiplicative decrease step, leading to an average aggregate PEV charging level that exceeds the transformer rating.

and eventually two multiplicative steps are called in a row to keep the power below its limit. When this occurs, the average power delivered to the transformer is greater than its rated kVA limit, and the transformer overheats as a result. Additionally, given the thermal inertia of the transformer, even once the power drops below its rated capacity the transformer temperature will take an extended period to fall to an acceptable level. Therefore it is important to prevent excessive power draw over the entire time frame.

There are several possibilities to address this issue. First, one could simply limit the number of vehicles charging on any one transformer. However, the limit may be relatively small. Consider the transformers attached to node 820 A-phase. Each has a spare capacity of 8 kW. If the AIMD parameters $\alpha = 0.25$ kW and $\beta = 0.9$ are used, then no more than three vehicles could charge at this transformer. This method would vastly under-utilize the charging capabilities of individual transformers.

A second approach would be to adjust the AIMD parameters in real-time in accordance with the number of vehicles connected to a transformer. Decreasing the β

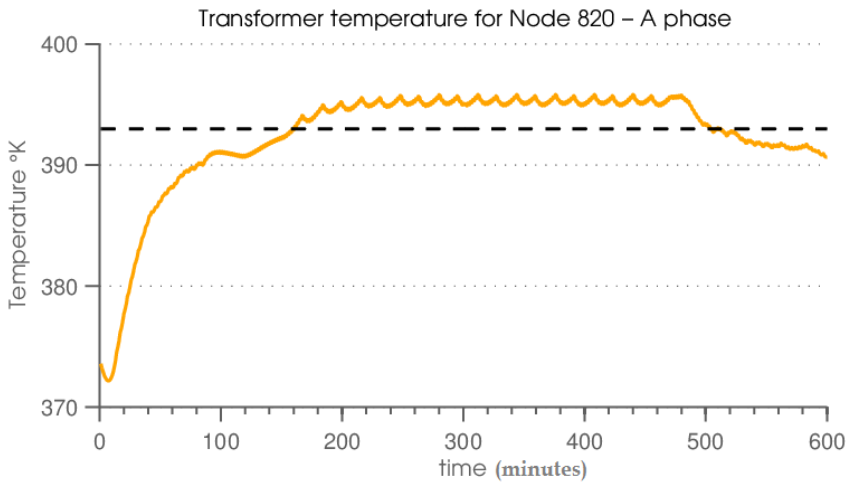

Figure 4.7: An example of incorrectly chosen AIMD parameters leading to transformer overload. Due to thermal inertia, this elevated temperature persists until several cars complete charging around 475 minutes into the simulation.

parameter allows more vehicles to plug in, but decreases the overall throughput of power delivered to the cars. On the other hand, decreasing the α parameter also accommodates more vehicles without affecting overall throughput, but increases the time needed for PEVs to initially reach full charging rate, and increases the time taken for multiple cars to reach fair, synchronized charging. Given that thermal overload conditions only occur during synchronized charging, it makes sense to adjust the additive parameter according to the number of vehicles on a transformer.

This method would require additional communication and computational infrastructure to assess the number of PEVs at a particular transformer. Solving the optimization algorithm could be accomplished off-line and then implemented as a simple lookup table, where values of α and β were stored for a particular number of vehicles and available power. This would ensure that all the vehicles use the largest percentage of available power possible without danger of violating transformer thermal limits.

4.6 Conclusion

Plug-in electric vehicles (PEVs) represent a sizeable additional load on power distribution systems. Due to the radial structure of these networks, this additional load could potentially lead to voltage quality issues. Also, overloaded distribution transformers will be vulnerable to thermal damage. It is therefore imperative that large-scale PEV charging be accompanied by some form of coordinated control. The

additive-increase multiplicative-decrease (AIMD) algorithm has been proposed as a possible method of regulating charging due to its minimal computational and communication requirements.

This chapter illustrates that AIMD control can be used to limit the temperature of distribution transformers, thereby protecting the health of these expensive devices. This control method induces oscillations in the power consumption of PEV chargers and hence in nodal voltages. It was therefore important to assess the amplitude of those variations. This was considered through simulation of a fleet of PEV charges connected to the IEEE 34-node network during a nighttime loading scenario.

Given randomized vehicle arrival times and initial battery state-of-charge, the AIMD control algorithm was generally capable of charging vehicles by their scheduled completion times. The exception was when a transformer had very little spare capacity due to excessive background load. It should be noted though that in such cases no form of control would have accomplished full charging without overheating the transformer. Under certain circumstances, transformer temperature limits were exceeded when a large number of vehicles charged with poorly adjusted AIMD control parameters. Modifying these parameters to account for the number of vehicles guarantees that thermal constraints are never violated.

CHAPTER V

Consensus Algorithms for Demand Response Control of PEVs

5.1 Introduction

As discussed in the previous chapter, it is conceivable that in the future, a large population of PEVs could detrimentally alter grid dynamics by adversely affecting distribution transformers, among other equipment. While Chapter IV discusses ways to coordinate PEV charging in order to avoid such a situation, Chapters V and VI extend the demand response concept by additionally using the PEV fleet to provide a source of functional services to power system operators.

One service that PEV fleets could potentially provide is frequency regulation (FR), in which participating resources perturb their active-power setpoints to match a broadcast signal. This signal reflects the deviation of the current power system AC frequency from nominal, as well as any tie-line imbalances between neighboring system operators [132]. FR is usually provided by synchronous generators, but recent legislation, most notably FERC Orders 745 and 755 [33,34], has encouraged demand-side resource participation; i.e., loads that can adjust their power consumption levels, such as aggregations of PEVs.

Resources are compensated for participation in FR markets. Traditional generation units, which tend to track FR signals with a high degree of accuracy, are reimbursed based on the magnitude of power flexibility provided. On the other hand, demand-side resources tend to be less accurate in responding to commanded power perturbations, and thus the market mechanisms used to determine their payments are more complex. In fact, such resources must pass qualifying benchmarks on the accuracy and latency of their response to specified FR signals in order to participate in the market [35,36]. This chapter focuses on the FR performance scores achievable

by a PEV fleet under coordinated charging control.

The literature proposes many types of controllers to regulate PEV power levels, and these can broadly be divided into two categories: centralized schemes [25, 134], where a single entity computes charging trajectories and dispatches decisions to the individual PEVs, and distributed schemes [39, 46, 82], in which multiple lower level controllers cooperate to achieve a desired global result. Distributed schemes offer the advantage of reduced computational burden by dividing control responsibilities among the participants. The disadvantage is that distributed controllers also necessitate heightened communication capabilities, because at least some peer-to-peer communication is required.

Average consensus [96] is a distributed, graph theory-based control algorithm in which participants communicate iteratively to converge on a particular value. While convergence is guaranteed in the infinite time case under certain assumptions [96], finite-time approximations are often implemented in practice [14, 127], although this adds the challenge of determining when approximate convergence has been achieved [136].

The average consensus approach has been proposed as a means of regulating flexible demand-side resources in a distributed fashion [27], and this methodology has been extended to residential loads [19] as well as PEVs [5, 26, 40, 54, 141], with control objectives varying from study to study. For instance, [26] considers a quadratic cost function that reflects the desired PEV charging trajectory. Using the Lagrange dual of this formulation, the study divides the solution in a distributed manner to be solved by each local PEV. In [54], the authors use consensus-based control to manage PEV battery consumption while the vehicle is operating, in consideration of concurrent power system dynamics. Another study [5] formulates a nonlinear optimization problem to maximize eventual vehicle state-of-charge (SoC), and uses the consensus algorithm to approximate the best charging trajectories.

Schemes in which simultaneous communication between PEVs is not possible have also been considered. For example, [141] implements an incremental cost consensus methodology to achieve asynchronous control. Different forms of control signals have been used to influence PEV power consumption, such as in [40] which uses pricing signals that must be carefully chosen to avoid selfish charging behavior.

This chapter examines the use of PEVs for FR services. In this case, the control objective is to track a reference signal as accurately as possible. In previous related work [138], the controller design focused mainly on grid frequency measurement using consensus-based sensing via the PEVs. This frequency information was then used to

determine the proper active-power setpoint adjustments undertaken by each vehicle. In contrast, the current work ignores frequency measurements and instead bases charging trajectory calculations on a broadcast FR signal. There are two reasons for this approach:

1) Grid frequency is uniform across an interconnect, and frequency deviations only become significant with MW-scale power swings. Small aggregations of PEVs would have a minimal impact on grid frequency alone. Proportional-based feedback controllers could not eliminate steady-state error, and integral-based feedback could introduce hunting and saturation issues. Furthermore, the fluctuating number of controllable resources would necessitate changes in the controller gains, complicating operation.

2) Typical FR signals account not only for frequency deviations, but also tie-line imbalances, which cannot be detected with frequency measurements alone. Absent of this information, participating resources could exacerbate power imbalances between regulated areas, detrimentally affecting the grid.

Therefore this chapter advocates an average consensus-based reference tracking algorithm, where PEVs track an FR signal supplied by grid operators. The chapter focuses on the design trade-offs of this distributed control approach, especially when considering the time-delay effects induced by the underlying communication network. It should be noted that, for the suggested algorithm, the distributed control properties extend only to the distribution transformer network. The overall control structure proposed is a hierarchial approach, in which transformers adapt their loads through the consensus algorithm, but some form of direct communication between the transformers and the individual PEVs is required to determine the individual loads (the constrained communication algorithm proposed in Chapter VI is one candidate to achieve this process).

The rest of the chapter is organized as follows. Section 5.2 formulates the distributed PEV charging control problem. Section 5.3 discusses the effects of time delay, and proposes an optimized reference tracking controller for this environment. Section 5.4 examines the performance scores that the proposed control methodology could achieve, and Section 5.5 summarizes the chapter and proposes several extensions.

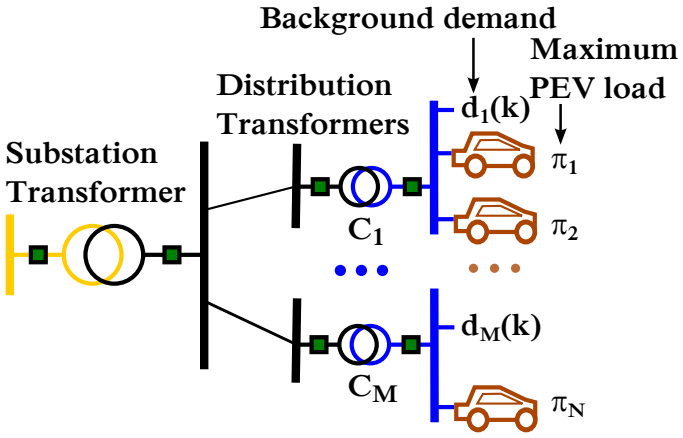

Figure 5.1: A schematic of the electric vehicle charging infrastructure. Distribution transformers provide low-voltage power to their attached loads, including PEVs. The transformer $T_1 ... T_M$ use consensus algorithm protocol to divide the requested FR power amongst themselves, based on the power capacity of their respective pools of attached PEVs.

5.2 Problem formulation

PEVs typically connect to the power system through the low-voltage distribution networks that serve commercial and residential loads. This chapter assumes a two-level controller, as shown in Figure 5.1. At the higher level, distribution transformers communicate using the consensus algorithm and arrive at a power dispatch for each transformer based on available capacity and PEV load capability. At the lower level, each distribution transformer allocates charging amongst individual PEVs based on current battery SoC and final charge deadlines. This bi-level structure reduces the communications burden by eliminating the need for PEVs to communicate independently.

The average consensus approach at the higher level builds on graph theory concepts. Consider a graph $\mathcal{G} = \{\mathcal{V}, \mathcal{E}\}$. The vertex set $\mathcal{V} = \{1, 2, ..., M\}$ corresponds to the distribution transformers, and the edges $\mathcal{E} \subseteq \mathcal{V} \times \mathcal{V}$ correspond to the communication links between transformers, with $(m_1, m_2) \in \mathcal{E}$ if transformer m_1 can receive communication from transformer m_2. Assume an undirected graph: $(m_1, m_2) \in \mathcal{E} \iff (m_2, m_1) \in \mathcal{E}$, or in other words that the existence of a communication link from transformer m_1 to m_2 implies the reverse is also true.

Distribution transformers have a limit on the apparent power they can supply, based on the current carrying capacity of their windings. While it is possible to violate this limit over short time periods [44][1], here the assumption is a fixed limit

[1]Transformer overloading (i.e. the process of delivering more than the rated power through the

denoted C_m. Within this limit, the amount of active power available for control at each transformer is governed by the number and charging capability of its attached PEVs. These PEVs are denoted $i \in \mathcal{I} = \{1, 2, ..., N\}$, where I_m denotes the set of PEVs attached to transformer m and $|I_m|$ refers the number of vehicles attached to transformer m, and the maximum charging rate of each vehicle is denoted π_i. Therefore the maximum power $\bar{p}_m$ deliverable by transformer m is restricted by the total charging power of its attached PEVs and the spare capacity on the transformer, whichever is smaller

$$\bar{p}_m = min\Big(\sum_{i \in I_m} (\pi_i), C_m - d_m \Big) \tag{5.1}$$

where d_i is the background (non-PEV) load for transformer i.[2]

Average consensus is a distributed control algorithm in which each participant updates a local value based on a weighted average of the values of its neighboring nodes. The set $\mathcal{N}_m$ denotes all of the nodes that can communicate to transformer m, and the scalar $\mathcal{D}_m$ denotes the cardinality of the corresponding $\mathcal{N}_m$. Therefore $\mathcal{D}_m$ captures the number of other nodes that each transformer is in communication with. In order to implement a fair-splitting strategy such as the one developed in [95], the updated nodal value from one iteration to the next is given by,

$$x_m[k+1] = \frac{1}{1+\mathcal{D}_m} x_m[k] + \sum_{n \in \mathcal{N}_m} \frac{1}{1+\mathcal{D}_m} x_n[k] \tag{5.2}$$

Alternatively, this update can be expressed in matrix form as

$$x[k+1] = \Gamma x[k] \tag{5.3}$$

where $x[k] = \Big[x_1[k] \quad x_2[k] \quad ... \quad x_M[k] \Big]^\intercal$. The matrix Γ is doubly-stochastic, which implies that all rows and columns sum to unity.

Distribution transformer power allocation is achieved using the algorithm developed in [27], in which each distributed resource performs two parallel consensus cal-

transformer) increases heat losses within the copper windings, consequently damaging the transformer's insulation. While insulation aging is a stochastic process, this excess heating has been shown to accelerate distribution transformer failure rates, causing outages and costly equipment replacement.

[2]While both the number of PEVs attached to a transformer and the background demand on the transformer are time-varying, here we assume time-invariance of these quantities over the timescales required for approximate consensus algorithm convergence.

culations. The first, denoted

$$y[k] = \begin{bmatrix} y_1[k] & y_2[k] & ... & y_N[k] \end{bmatrix}^\intercal$$

determines the FR signal S broadcast to all units, while the second,

$$z[k] = \begin{bmatrix} z_1[k] & z_2[k] & ... & z_N[k] \end{bmatrix}^\intercal$$

determines the total available system power capacity. Power is then allocated proportionally to each transformer's available capacity $\bar{p}_m$. Analytically, this can be expressed as

$$y[k+1] = \Gamma y[k] \tag{5.4}$$

$$z[k+1] = \Gamma z[k] \tag{5.5}$$

where

$$y_0 = \begin{bmatrix} S & 0 & ... & 0 \end{bmatrix}^\intercal \tag{5.6}$$

$$z_0 = \begin{bmatrix} \bar{p}_1 & \bar{p}_2 & ... & \bar{p}_M \end{bmatrix}^\intercal \tag{5.7}$$

and

$$p_m = \lim_{k\to\infty} \frac{y_m[k]}{z_m[k]} \bar{p}_m. \tag{5.8}$$

Given an infinite convergence time, this approach guarantees that the aggregation of power among distribution transformers is equal to the broadcast FR signal: $\sum_{m=1}^{M} p_m = S$, while also ensuring fair allocation based on each transformer's available capacity. However, in practice, an approximate finite-time consensus algorithm [14, 127] will need to be implemented. This chapter examines the behavior of the algorithm for a fixed fixed number of iterations K, and explores how tracking performance is effected by variations in K.

5.3 Communication Delay Effects

Distributed control algorithms have several advantages in that they eliminate the need for a centralized control entity and enable agents to make decisions based on local information without requiring global knowledge. The communication infrastructure is similarly distributed, which often reduces the cost and complexity of these systems.

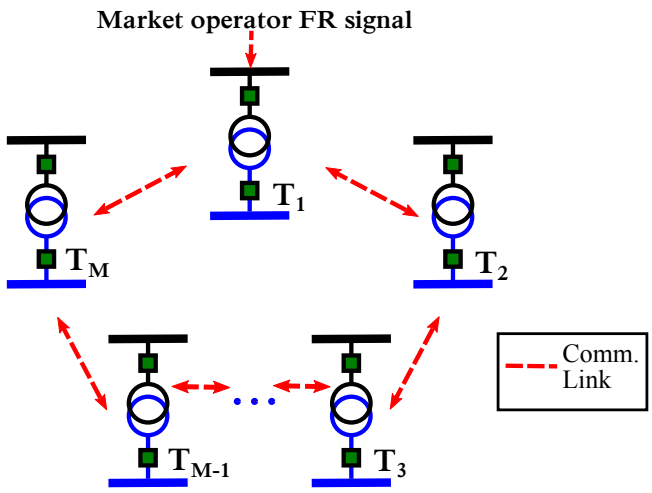

Figure 5.2: Proposed ring communication architecture

However, the iterative process involved in many distributed control algorithms means that time delays in the communication system may sometimes have detrimental effects on controller performance.

In typical power distribution systems, cost is the driving factor in system design. Thus, the communication network envisioned for this particular control application should minimize the number of necessary communication links. One way to accomplish this is a ring structure, such as that shown in Figure 5.2. This case provides two links to every distribution transformer node, with the initial FR reference signal provided only to Node #1. Since any number of link failures greater than one would isolate a portion of the communication network, this configuration would likely need to be robustified in practice. However, the slow convergence rate of this particular network structure serves as a test case for the effects of severe time-delays on FR performance.

The aforementioned effects occur when the FR reference signal varies on the same timescale as communication delays within the network. A typical FR signal updates at a 2-10s rate, while the physical communication infrastructure used for PEV control will vary based on a number of factors[3]. If there exists a time delay of δ between synchronized communication events that is of the same order of magnitude as the FR signal update time, then a distributed algorithm requiring many iterations to converge could potentially experience severe performance dropoffs.

To illustrate this phenomenon, consider a group of distribution transformers em-

[3]See [137], While investments in advanced metering infrastructure are curbing this trend [31], the existing grid lacks ideal communication capabilities.

ploying the consensus algorithm to allocate power among themselves while tracking a reference signal. As the number of iteration steps K increases, the allocated power tends to more accurately track the specified reference signal value. However, this effect is counterbalanced by the increase in the size of the enforceable sampling period, which adds discretization error to the system response. Furthermore, these delays directly add latency to the system, causing an increased lag between signal and response.

Thus, the number of iterations taken by the consensus algorithm for approximate convergence has a significant effect on the controller performance. The next section focuses on ways to quantify the trade-off between accuracy and latency of the system response.

5.4 PEV Fleet Performance

This section examines the achievable performance of a fleet of PEVs employing consensus-based control. In order to draw a fair comparison, the PJM Interconnect Demand Response Regulation Market is used as an example scoring criterion (for a thorough discussion of the PJM market, see Section 2.4, previous literature [142], or the original operational guidelines [35, 36]).

The FR market structure incentivizes participants to achieve the highest performance scores possible. Using the consensus-based controller defined in Section 5.2, deviations of aggregate PEV power from the reference signal (and therefore reductions in the performance scores) arise due to the communication delay effects identified in Section 5.3.

Conceptually, the performance of the consensus algorithm in the presence of communication delays involves a trade-off, because increasing the number of algorithm iterations K elicits a response that more accurately tracks the input values, but also causes larger delays between sampled values, decreasing the resolution of the resulting response. Quantitatively, the controller performance is dictated by the convergence rate of the consensus algorithm ρ, which is defined in [135] as

$$\rho = \sup_{x(0)\neq x^*} \lim_{t\to\infty} \left(\frac{||x(t) - x^*||_2}{||x(0) - x^*||_2} \right)^{1/t} \tag{5.9}$$

where $x^* = \lim_{t\to\infty} x(t)$. If the eigenvalues of the matrix Γ are ordered in magnitude $\{\lambda_1, ..., \lambda_N\}$, then a well-known result from [135] states that the convergence rate ρ is

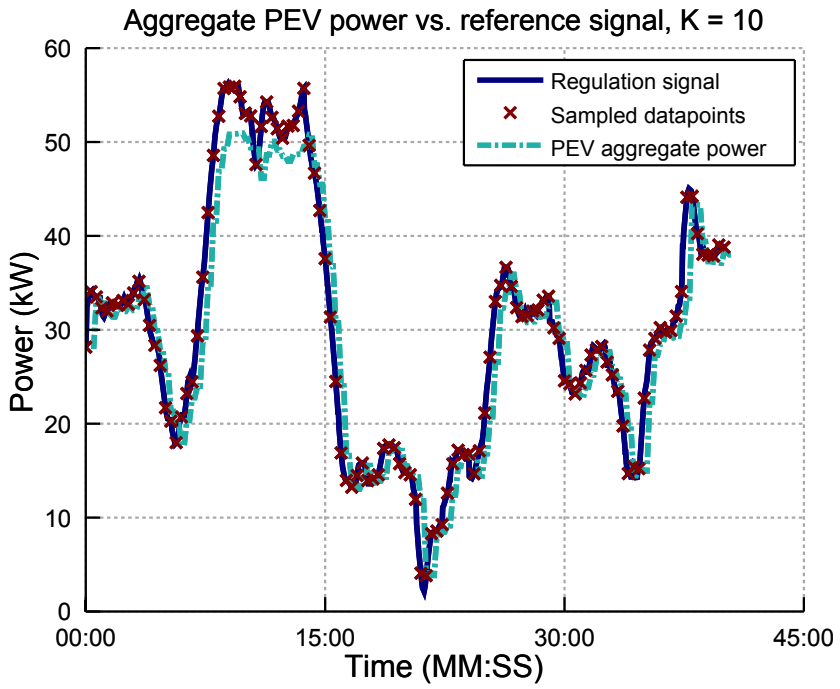

Figure 5.3: Results of the PJM RegD Qualification Test using $K = 10$ iterations of the consensus algorithm. The limited number of iteration means that the consensus algorithm approximates the correct value with some error, but this is counterbalanced by the low delay between input and response.

equal to the magnitude of the second largest eigenvalue[4], denoted λ_2. Thus, in the case of the proposed PEV charging setup, the rate of convergence of the consensus algorithm is related to the structure of the communication system connecting the distribution transformers.

For the ring communication topology shown in Figure 5.2, the eigenvalues of Γ depend only on the number of distribution transformers in the network N. As the number of nodes increases, λ_2 also increases, and the transformers take longer to arrive at the correct values of y_i and z_i (within a fixed error tolerance).

One way to test the performance capabilities of the proposed PEV charging algorithm is to simulate system behavior using a Monte Carlo approach. This provides an estimate of the achievable PJM Qualification Test scores. The simulation parameters are as follows. Consider a distribution system of $M = 8$ distribution transformers, each with $|I_m| \in [1, 5]$ PEVs per transformer. Each vehicle has a maximum charge rate of $\pi_i \in [1.5, 2.5]$ kW. The transformers communication topology is shown in Figure 5.2, in which distribution transformer #1 receives a FR signal from the market

[4]The formulation of Γ as a doubly-stochastic matrix implies that its largest positive eigenvalue λ_1 is equal to unity, and that all other eigenvalues are real with a magnitude strictly less than 1.

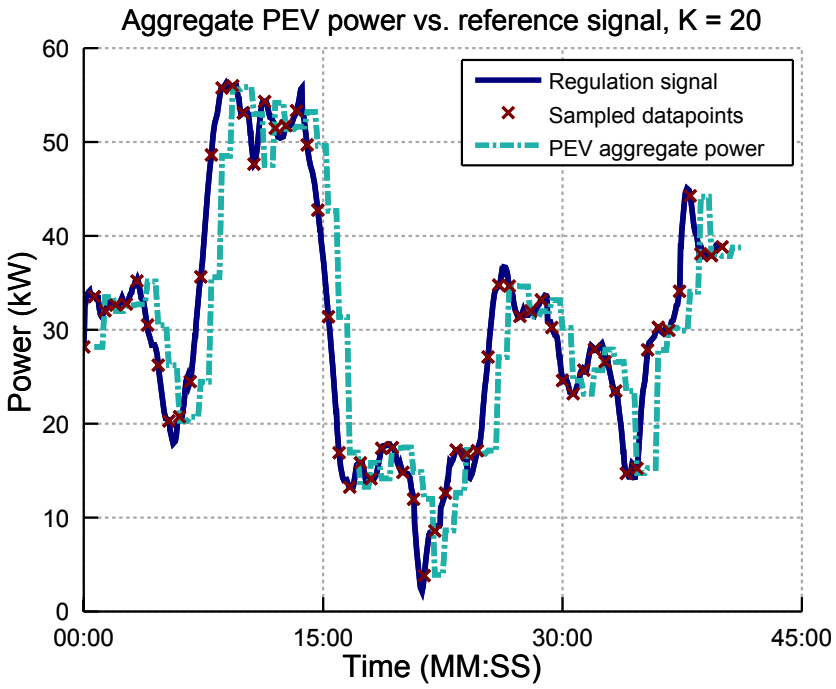

Figure 5.4: Another PJM RegD Qualification Test, this time with $K = 20$ iterations. The PEVs converge to a more accurate value of the assigned power, but do so with larger time delays.

operator, and all transformers are connected in a ring layout. For this particular set of simulations, the time delay between synchronized communication events is set at $\delta = 2$ seconds. While the exact time delay within a communication network will vary considerably depending on the chosen communication technology and the corresponding data transmission rate, scalability, device compatibility, etc. [48], this delay value represents the upper end of plausible time delays, and thus serves as a worst-case scenario for testing purposes.

Using the preceding parameters, a set of Monte Carlo simulations was conducted for various values of K, the maximum number of consensus algorithm iterations. Examples of the aggregate PEV load compared to the reference Qualification Test signal are shown in Figures 5.3 and 5.4. Using 100 simulations for each K value, the PJM Qualification Test scores are enumerated in Table 5.1.

There are several trends that can be identified in the data. Foremost, as expected, the Delay score directly correlates to the number of iterations K of the consensus algorithm. This score decreases as the number of iterations increases. Less obviously, the Accuracy score also decreases as the number of iterations increases. While using more iterations causes the assigned PEV aggregate power to more accurately approx-

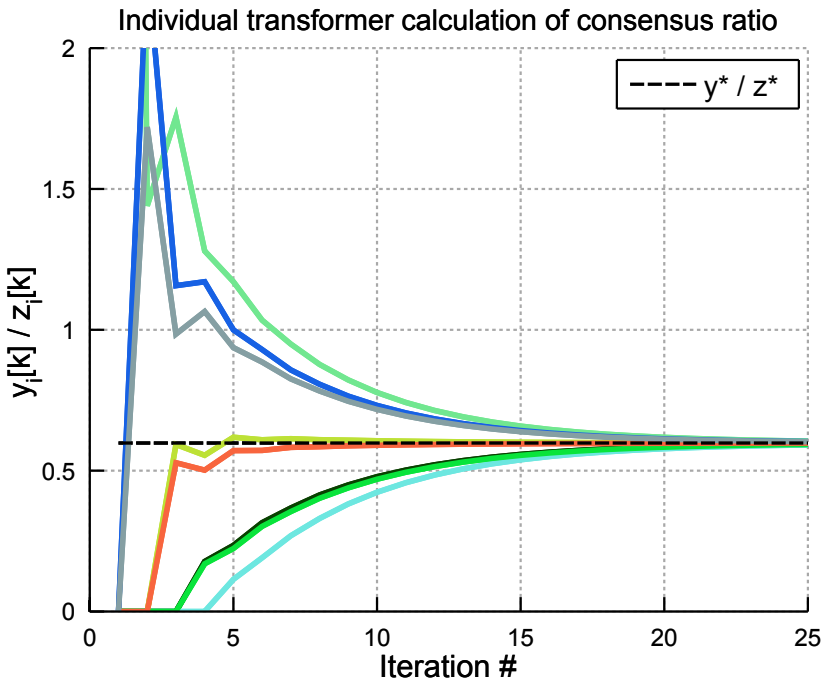

Figure 5.5: The evolution of the $y_m[k]/z_m[k]$ calculation at each transformer.

Table 5.1: Qualification Test scores

K	Accuracy	Delay	Precision	Aggregate
5	0.9879	0.9893	0.8183	0.9318
10	0.9649	0.9627	0.8042	0.9106
15	0.9422	0.9271	0.7133	0.8609
20	0.9308	0.8740	0.6091	0.8046

imate the sampled values of the reference signal, the reduced sampling rate enforced by the communication delay counteracts this benefit, leading to an overall decrease in the Accuracy metric. The Precision score also experiences a drop-off as the number of iterations increases, due to the corresponding increase in response delay and the errors between the reference and output signals that result.

5.4.1 Individual transformer analysis

Besides the ability of the aggregate PEV load to track a reference signal, it is also important that the individual transformers are assigned a power commensurate with the expected value given in (5.8). For instance, consider Figure 5.5. While the aggregate power quickly converges to the reference value, it takes considerably more iterations before the individual $y_m[k]/z_m[k]$ values match the final y^*/z^* quantity.

Table 5.2: Error summary (per transformer)

K	Average error per time-step	Total error
5	1.42 kW	3.36 kWh
10	0.57 kW	1.30 kWh
15	0.16 kW	0.74 kWh
20	0.04 kW	0.16 kWh

This phenomenon is due to the transformer communication topology. Nodes that are more closely connected to Transformer #1, which receives the broadcast signal s, tend to initially overestimate values of $y_m[k]$, while the more distantly connected nodes tend to underestimate this same value. This issue is exacerbated as the degree of the vertex set $\mathcal{V}$ increases, i.e. as more transformers join the network while maintaining the original ring communication topology.

These system dynamics imply that the proposed consensus-based approach may consistently under- or over-assign power to certain transformers if the number of consensus algorithm iterations is not sufficiently high. For example, consider Table 5.2, which summarizes the average error between the calculated value from the term $y_m[K]/z_m[K] \times \bar{p}_m$ and the exact solution $y^*/z^* \times \bar{p}_m$, using the data set from the Monte Carlo simulations discussed previously. The results are averaged across all distribution transformers in the system.

As expected, Table 5.2 displays a clear trend of decreasing error in individual transformer power assignment as the number of iterations K of the consensus algorithm increases. Since these errors are enforced by the communication topology, transformers have a consistent positive or negative bias in their calculations. If uncorrected, these errors would be passed on to the PEV fleet, where some vehicles would be undercharged at their given deadline, while other vehicles would complete charging faster than expected, removing them from the controllable pool and reducing FR capacity. Thus, while increasing the number of iterations of the consensus algorithm may negatively impact the achievable performance scores for a fleet of PEVs when communication delays are included, the counter effect is that it eliminates inaccuracies in the power assigned to specific transformers, ensuring a more appropriate distribution of the assigned power.

5.5 Conclusion

Plug-in electric vehicles represent a new source of potential flexibility for power system operators. However, in order to utilize these resources, care must be taken in the choice of the control algorithm used to regulate vehicle power. This chapter examines the use of the average consensus algorithm in a PEV charging setting, and presents a distributed control methodology that causes aggregate PEV power consumption to track a specified reference signal at the fast timescales (2-10s) typically required for frequency regulation support.

It was shown that there exist trade-offs between accuracy and latency of the resulting PEV response, specifically when considering the presence of communication delay in the system. It is also shown that the proposed control architecture achieves performance scores that would qualify the aggregate PEV fleet for participation in an existing frequency regulation market, although the performance tends to degrade as communication delays increase. The next chapter, therefore, will focus on a controller design that is less affected by the communication capabilities of the system.

CHAPTER VI

Signal Tracking Methods for a Plug-in Electric Vehicle Fleet in a Constrained Communication Environment

6.1 Introduction

Chapters IV and V both consider the process of coordinated electric vehicle charging. Chapter IV examines ways to prevent transformer overloading, and the grid level effects that this type of control imparts on the distribution system, in terms of power fluctuations and changes in voltage profiles. Chapter V broadens the scope of the PEV charge scheduling problem to include not only transformer overload mitigation, but also the ability to track a signal for frequency regulation purposes. Using a version of the average consensus algorithm, it was shown that a PEV fleet can be made to track a reference signal while adhering to grid constraints. However, it was also revealed that excessive communication needs can detrimentally affect the aggregate PEV fleet performance when the consensus algorithm is employed. Thus, consideration of the communication network limitations was shown to be crucial to achieving optimal controller performance.

This chapter introduces a novel framework for controlling a fleet of PEVs that considers communication limitations as a fundamental part of the controller design. Using an assumption of a limited-bandwidth environment, a discrete-time optimal controller is proposed that can regulate a fleet of electric vehicles to track a reference signal. In addition to reference tracking, the controller considers two additional objectives - the vehicle owners' desire to have a fully charged battery, and the system operator's goal of limiting transformer overloading. Then, using a mathematical formulation developed in [37], an additional constraint is introduced that models a bandwidth-limited communication channel. Finally, the controller is reformulated in

a model-predictive control (MPC) approach, in order to eliminate dependence on *a priori* knowledge of the reference signal.

6.1.1 Previous Literature

Past studies have investigated the use of PEV regulation to achieve a variety of control objectives (for an overview of the relevant literature, see [139]). At the transmission level, the goal is typically to shift PEV load to off-peak hours in order to avoid added congestion on the network. Load shaping techniques have been developed using Nash equilibrium concepts [39, 83], as well as using optimization tools such as sequential quadratic programming [140]. At the distribution level, researchers have designed control strategies to reduce system losses [22, 25, 113, 120], avoid voltage degradation [120], and prevent transformer overloading [55].

Given the sensitivity of the lithium-ion batteries used in PEVs to both over- and under-charging [79], as well as the cost of these components, battery health is of paramount concern to vehicle owners. Control algorithms that ignore battery degradation effects can significantly affect their longevity [128], and thus control objectives that minimize battery damage have also been considered [7, 119, 128].

The focus of this chapter lies on matching the aggregate power consumption of a group of electric vehicles to a reference signal, in order to provide DR capabilities. This generalized reference signal could represent the variability in power output of a wind or solar farm that contracts with the PEV fleet for balancing services. Alternatively, it could be a signal that is broadcast to PEVs providing ancillary services such as frequency regulation or spinning reserves. Regardless of the specific application, the control objective in this situation is to track the reference signal with as high a degree of accuracy as possible.

An overview of PEV reference tracking is discussed in [16]. Different controller topologies have been used to achieve the tracking objective. For example, [67] uses adjustments of a deadband around the desired PEV battery state-of-charge trajectory to influence aggregate charging behavior. In [133], the authors use a joint-optimization problem to determine both real and reactive PEV load setpoints. A hierarchical control structure is proposed in [72] to adapt PEV charging in a manner that buffers variability in wind farm generation. Optimal power flow formulations have also been employed [45] to control PEVs in a frequency regulation scenario by considering the additional storage potential of the vehicle batteries.

It is crucial that PEV controllers incorporate communication limitations into their designs. Previous studies have proposed several ways to accomplish this goal. Com-

munication capabilities for PEVs are discussed in [2], which also describes a charging algorithm based on quality-of-service principals that specifically adresses PEVs in a wireless communication setting. In [138], the authors use frequency measurements at local transformers to provide controller input while limiting external communication. The authors in [124] utilize a one-way communication scheme and use statistical methods and queuing theory to approximate the expected PEV power response. A communication hierarchy is proposed in [130] that reduces the necessary communication requirements, although the resulting optimization function is non-convex and must be solved using convex relaxation techniques.

6.1.2 Organization

The rest of the chapter is organized as follows. Section 6.2 rigorously defines the PEV reference tracking problem. Section 6.3 describes the optimal controller formulation and resultant cost function and constraints. Section 6.4 introduces the communication limitations of the distribution network. Section 6.5 develops the MPC formulation of the controller. Section 6.7 summarizes the findings and suggests future directions of research.

6.2 Reference Tracking Problem Setup

Consider a population of N plug-in electric vehicles connected to the distribution grid and supplied by a common substation transformer, as shown in Figure 6.1. A vehicle aggregator must dispatch the PEV loads in a manner such that the aggregate vehicle power consumption tracks a reference signal broadcast to the aggregator, while also adhering to vehicle battery charging requirements, as well as limitations on the distribution equipment providing power to the PEVs.

The tracking problem occurs over some time interval $k \in [1, K]$. The states of the system $x_i(k),\ i \in \mathcal{I} = \{1, 2, ..., N\}$ correspond to the normalized state-of-charge (SoC) of the i^{th} vehicle's battery at time k, with

$$x_i(k) \in [0, 1], \quad \forall k \in [1, K] \tag{6.1}$$

Let the inputs to the system

$$u_i(k) \in [0, 1], \quad \forall k \in [1, K] \tag{6.2}$$

be the normalized charging rates corresponding to vehicle i at time k. Note that the

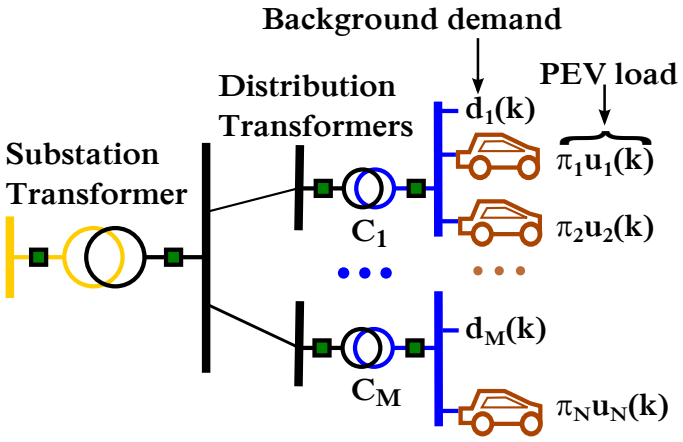

Figure 6.1: The power system topology for PEVs charging on the distribution grid. Each vehicle i connect to the grid through its EVSE, which is rated to a certain power level π_i. The inputs to the system is the normalized charging power $u_i(k)$ drawn by vehicle at time k. The distribution transformers that provide power to the vehicles have a fixed capacity C_m and a time-varying background demand $d_m(k)$. Note that this is the same charging setup utilized in Chapter V, Figure 5.1.

restriction on u_i as a non-negative quantity implies that vehicle-to-grid charging is prohibited.

The remaining vehicle parameters are as follows - π_i is the maximum charge rate of vehicle i (in kW), β_i denotes the size of battery of vehicle i (in kWh), and η_i is the charging efficiency of the EVSE supplying power to vehicle i. Finally, Δk is the interval between timesteps k, expressed in fractions of an hour.

6.2.1 State equations

Given the above notation, it is possible to formulate a state-space representation of the system as follows. The state equation describing how each vehicle battery's SoC evolves is given by

$$x_i(k+1) = x_i(k) + \gamma_i u_i(k) \tag{6.3}$$

with

$$\gamma_i = \frac{\pi_i \eta_i \Delta k}{\beta_i}$$

The state-space representation of this system is therefore

$$x(k+1) = Ax(k) + Bu(k) \tag{6.4}$$

Table 6.1: Notation

N	Number of vehicles
$\mathcal{I}$	The set of PEVs, cardinality N
$[1, K]$	Time horizon
$x_i(k)$	State-of-charge of vehicle i at time k (the states)
$u_i(k)$	Normalized charging rate of vehicle i at time k (the inputs)
π_i	Maximum charging rate of vehicle i (in kW)
β_i	Capacity of the battery pack of vehicle i (in kWh)
η_i	Efficiency of the EVSE supplying power to vehicle i
Δk	Interval between timesteps, expressed in fractions of an hour
M	Number of distribution transformers
$d_m(k)$	Background demand on transformer m at time k (in kW)
$D_m(k)$	Total demand on transformer m at time k (in kW)
C_m	Capacity of transformer m (in kW)

with

$$x(k) = \begin{bmatrix} x_1(k) & x_2(k) & ... & x_N(k) \end{bmatrix}^\intercal \tag{6.5}$$

$$u(k) = \begin{bmatrix} u_1(k) & u_2(k) & ... & u_N(k) \end{bmatrix}^\intercal \tag{6.6}$$

$$A = I_{N \times N} \tag{6.7}$$

$$B = \text{diag}\Big(\begin{bmatrix} \gamma_1 & \gamma_2 & ... & \gamma_N \end{bmatrix} \Big) \tag{6.8}$$

6.2.2 Desired charging trajectory

Each vehicle i enters the network with an initial SoC $x_{i,0} \in [0, 1)$. Upon arrival, each vehicle provides its desired final SoC at time K, denoted $x_{i,f} \in (x_{i,0}, 1]$. Assume that the average desired power $u_{i,d}$ required to achieve $x_{i,f}$ does not violate the capabilities of the vehicle's charging equipment, i.e.

$$u_{i,d} = \frac{(x_{i,f} - x_{i,0})\beta_i}{\eta_i K \Delta k} \leq \pi_i \tag{6.9}$$

Finally, define x_0 and x_f, the initial and final SoC vectors, respectfully, as

$$x_0 = \begin{bmatrix} x_{1,0} & x_{2,0} & ... & x_{N,0} \end{bmatrix}^\intercal \tag{6.10}$$

$$x_f = \begin{bmatrix} x_{1,f} & x_{2,f} & ... & x_{N,f} \end{bmatrix}^\intercal \tag{6.11}$$

6.2.3 Distribution transformers

The network consists of M distribution transformers that provide power to the PEVs (see Figure 6.1). Let $I_m \subseteq \mathcal{I}$ denotes the set of PEVs attached to transformer $m \in [1, M]$, with each vehicle assigned to a single transformer such that

$$I_{m_1} \cap I_{m_2} = \varnothing, \ \forall m_1 \neq m_2 \tag{6.12}$$

Each distribution transformer has a capacity of C_m (in kW), and a time-varying background demand denoted by $d_m(k)$. Defining the total load at transformer m as $D_m(k)$, and assuming that no transformer may be overloaded at any timestep leads to the following constraint

$$D_m(k) = \sum_{i \in I_m} \pi_i u_i(k) + d_m(k) \leq C_m, \quad \forall m, k \tag{6.13}$$

6.2.4 Demand response signal

Before the control period begins, the vehicle aggregator must specify two quantities:

- $\bar{S} > 0$ denotes the average load the the PEVs will draw during the time period [1,K]
- $\widetilde{S} > 0$ denotes the magnitude of (symmetrical) up/down regulation that the PEVs will provide

Both quantities are given in kW.

During the control period, the aggregator is supplied with a normalized signal, denoted $\sigma(k)$, which is bounded such that

$$\sigma(k) \in [-1, 1], \quad \forall k \in [1, K] \tag{6.14}$$

The vehicle aggregator then scales the normalized signal as follows

$$S(k) = \bar{S} + \widetilde{S}\sigma(k) \tag{6.15}$$

where $S(k)$ is the total load requested of the PEVs at timestep k, hereafter referred to as the reference signal (see Figure 6.2).

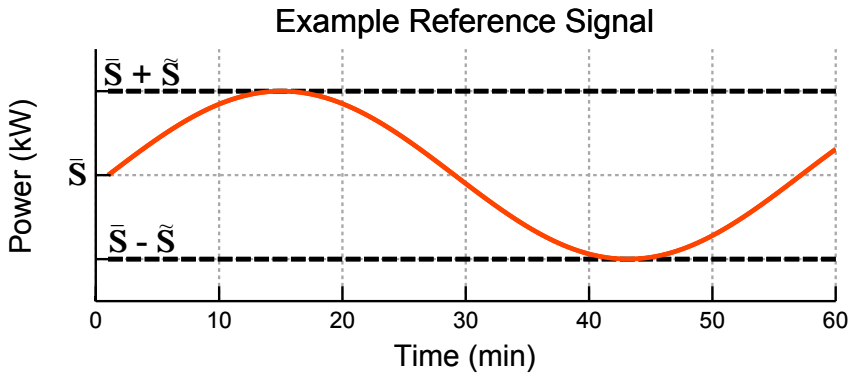

Figure 6.2: The reference signal $S(k)$ as described in Section 6.2.4. The normalized signal $\sigma(k)$ (in this case a sine wave) is scaled by a factor $\widetilde{S}$, after which an offset $\bar{S}$ is applied.

6.2.5 Control Objective

The PEV reference tracking problem, as defined in this section, is a threefold challenge. First, the aggregate vehicle load at timestep k, $\sum_{i\in\mathcal{I}} \pi_i u_i(k)$, must match the reference signal $S(k)$ as closely as possible. Second, the final SoC of each vehicle battery $x_i(K)$ must match the desired value $x_{i,f}$ as closely as possible. Third, the restriction on transformer overloading given by Equation (6.13) must be observed over the full time horizon.

Section 6.3 proposes a controller design that solves this problem without considering communication limitations. Section 6.4 then introduces additional constraints that model reduced-communication capabilities.

6.3 Optimal controller formulation

The initial controller formulation assumes that the vehicle aggregator possesses *a priori* knowledge of the reference signal $S(k)$ and the background demand $d_m(k)$ for all time $k \in [1, K]$ and all transformers $m \in [1, M]$.

6.3.1 Capacity Bid

As detailed in Section 6.2.4, the vehicle aggregator must specify both the expected average PEV load $\bar{S}$ and the flexibility in this load $\widetilde{S}$. Since the aggregator has access to the average desired power of each vehicle $u_{i,d}$, the calculation of $\bar{S}$ is straightforward.

$$\bar{S} = \sum_{i\in\mathcal{I}} u_{i,d} \tag{6.16}$$

The flexibility bid $\widetilde{S}$ represents the largest *symmetrical* change in load that the vehicle fleet can supply. Therefore this quantity is limited by either the up- or down- regulation capability of the fleet, whichever is smaller. The flexibility bid is determined by maximum charging rate of each vehicle's EVSE and its expected average charging rate.

$$\widetilde{S} = \min\Big(\sum_{i\in\mathcal{I}}(\pi_i - u_{i,d}),\ \sum_{i\in\mathcal{I}} u_{i,d}\Big) \tag{6.17}$$

6.3.2 Cost Function

A discrete-time optimal controller is used to determine the sequence of inputs $u = \begin{bmatrix} u(1)^\intercal & u(2)^\intercal & \dots & u(N)^\intercal \end{bmatrix}^\intercal$ that achieves the goals enumerated in Section 6.2.5. The cost function is given by

$$J = \sum_{k=1}^{K} \Big\{ \Big(\sum_{i\in\mathcal{I}} \pi_i u_i(k) - S(k) \Big)^\intercal \mathbf{R} \Big(\sum_{i\in\mathcal{I}} \pi_i u_i(k) - S(k) \Big) \Big\} + \Big(x(K) - x_f \Big)^\intercal \mathbf{Q} \Big(x(K) - x_f \Big) \tag{6.18}$$

The solution for u must adhere to the system dynamics described by Equation (6.4), as well as the limits on the states and inputs provided by Equation (6.1) and Equation (6.2) and the constraints on transformer overloading given in Equation (6.13).

The weighting terms in the cost function J are as follows. $\mathbf{R} > 0$ is a scalar that penalizes deviations of the total vehicle power from the desired signal $S(k)$, and $\mathbf{Q}$ is an $N \times N$ diagonal matrix with elements $Q_1, Q_2, ..., Q_N > 0$ that penalizes deviations of the vehicle battery SoC from the desired final value.

6.3.3 Replacing transformer constraint

In practice, the limitation on distribution transformer overloading given in Equation (6.13) may be overly conservative and unnecessarily restrict the feasible solution space. Transformer aging is exacerbated when excessive hot-spot temperatures are applied to a transformer's insulation [13]. However, because the copper mass of the transformer acts as a low-pass filter between instantaneous power and temperature, it is possible to overload a transformer temporarily without causing overheating, provided that the delivered power eventually drops back below the transformer capacity. Therefore, it is useful to replace the constraint given by Equation (6.13) with a term in the cost function that penalizes transformer temperature violations instead.

The thermal dynamics of a distribution transformer differ depending on the type of fluid used for cooling and the geometry of the transformer [42]. These dynamics can be approximated by a first-order differential equation in which the continuous-time temperature $T_m(t)$ of transformer m is largely driven by i^2R losses in the windings and cooled by the ambient air temperature through Newton's law of cooling.

$$\dot{T}_m(t) = \frac{1}{C}\Big(D_m(t)^2 R_c - \frac{T_m(t) - T_a}{R}\Big) \tag{6.19}$$

where T_a denotes the ambient air temperature, R and C are thermal constants associated with the transformer geometry and cooling fluid, and R_c is the pseudo-resistance of the copper windings (adjusted for the voltage level of the transformer).

These dynamics are inherently non-linear; however, for the purposes of this controller they can be linearized around an operating point in the manner suggested in [55]. Assume every transformer has a specified maximum temperature above which transformer degradation begins to occur, defined as

$$T_m^{max} := \lim_{t\to\infty,\, D_m(t)=C_m} T_m(t) \tag{6.20}$$

Then the deviation in transformer temperature $\delta T_m(k)$ above or below the maximum allowable temperature T_m^{max} is given by the following linearized and discretized equation

$$\delta T_m(k+1) = \tau \delta T_m(k) + \lambda\Big(D_m(k) - C_m\Big) \tag{6.21}$$

where the parameters τ and λ are functions of $R,\ C,\ R_c$ and Δk describing the linearized and discretized thermo-electrical dynamics of the transformer, and the load dynamics are considered with respect to their deviation above or below the transformer capacity limit C_m.

One way to express the new control objective is through a *minimax* formulation, in which the goal is to minimize the maximum temperature at any distribution transformer at timestep k.

$$\min\Big\{\quad \max\Big\{\quad \delta T_1(k), \ldots, \delta T_M(k)\Big\}\Big\} \tag{6.22}$$

Note that this formulation does not prevent transformer overheating. Instead, it encourages the controller to even out loading dynamics across the population of transformers, such that no particular transformer experiences excessive overheating. Given that transformer aging effects tend to increase exponentially as transformer temper-

ature rises [13], this approach is one way to reduce total damage to the distribution system.

Equation 6.22 is equivalent to the following optimization problem, in which the variable z_k represents the highest temperature deviation $\delta T_m(k)$ of any of the transformers at time k

$$\begin{aligned} &\min && z_k \\ &\text{such that} && \delta T_m(k) \leq z_k, \quad \forall m \end{aligned} \tag{6.23}$$

By including the vector $z = \begin{bmatrix} z_1 & z_2 & \dots & z_K \end{bmatrix}^\intercal$ with the original cost function, the updated cost function becomes

$$\begin{aligned} J = \sum_{k=1}^{K} \Bigg\{ \Big(\sum_{i \in \mathcal{I}} \pi_i u_i(k) - S(k) \Big)^\intercal \mathbf{R} \Big(\sum_{i \in \mathcal{I}} \pi_i u_i(k) - S(k) \Big) \Bigg\} \\ + \Big(x(K) - x_f \Big)^\intercal \mathbf{Q} \Big(x(K) - x_f \Big) + \mathbf{\Omega} z \end{aligned} \tag{6.24}$$

where the term $\mathbf{\Omega}$ denotes a $1 \times K$ weighting vector that penalizing transformer overloading at each timestep, with elements $\Omega_1, \Omega_2, \dots, \Omega_K > 0$. This cost function is subject to the temperature dynamics described by Equation (6.21), and must adhere to the limits on the states and inputs provided by Equation (6.1) and Equation (6.2) as well as the system dynamics described by Equation (6.4).

6.4 Constrained communication

It is important to take communication capabilities into account when designing PEV charge scheduling schemes. One way to do this is to consider the case in which the communication network that interfaces between the vehicle aggregator and the PEVs is a constrained system, such that the number of vehicles that can receive a command at any timestep k is limited by some bandwidth $0 < b < N$. In [37], the authors developed a novel control method to account for this additional constraint, in order to schedule commands on a microcontroller with a limited-bandwidth communication bus. While the timescales of control and the physical means of communication are different for the PEV reference tracking application, it is possible to use a similar approach to determine an optimal control sequence for the PEVs in a limited communication environment.

In this case, the binary variable $\delta_i(k)$ is used to denote whether vehicle i receives a new control input at time k. If $\delta_i(k) = 1$, then the vehicle receives a new power setpoint command, otherwise the vehicle charger maintains the setpoint from the

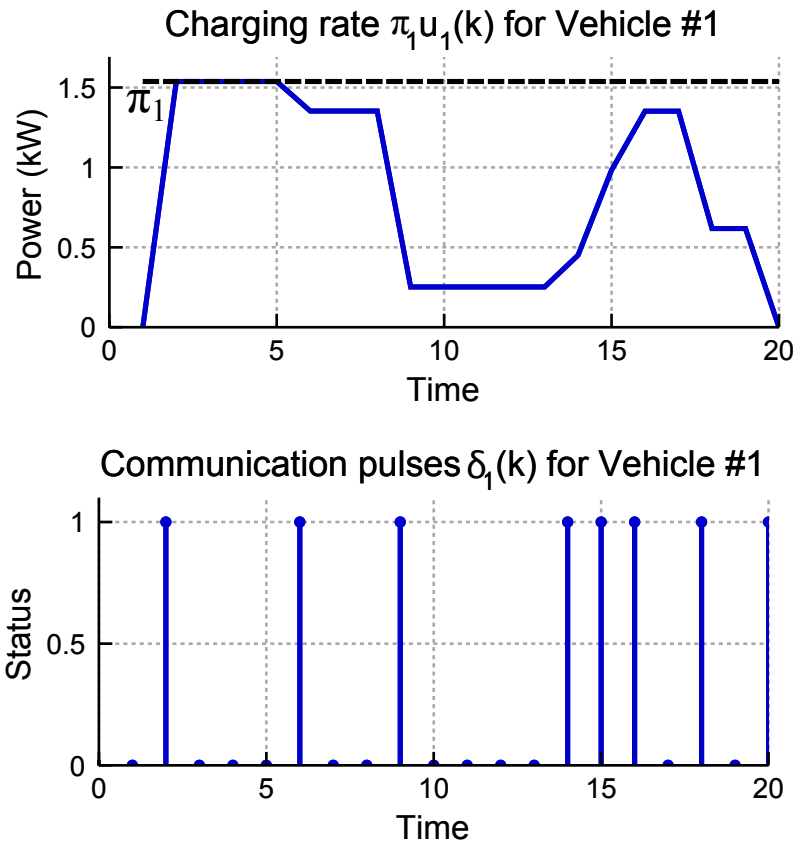

Figure 6.3: An example load profile and communication sequence associated with Vehicle #1 for a scenario with $N = 8$ vehicles and bandwidth of $b = 2$. The power setpoint $u_1(k)$ of Vehicle #1 (upper plot) is adjusted only during the timesteps when a communication pulse (bottom plot) is received; otherwise the charging rate remains at its previously set value.

previous step (see Figure 6.3).

The optimal control sequence for the constrained communication environment is determined by minimizing the cost function given in Equation (6.24) with the following additional constraints in place, using a similar formulation to the one proposed in [37].

$$\sum_{i \in \mathcal{I}} \delta_i(k) = b \tag{6.25}$$

$$\delta_i(k) \in \{0, 1\} \tag{6.26}$$

$$\delta_i(k) = 0 \implies u_i(k) = u_i(k-1) \tag{6.27}$$

Using the process developed in [8], the logical constraint in Equation (6.27) can

be converted to the following equality.

$$u_i(k) - u_i(k-1) = \delta_i(k)u_i(k) - \delta_i(k)u_i(k-1) \tag{6.28}$$

This equality constraint contains products of binary and continuous variables. The well-known technique developed in [8] can now be applied to replace these products with two corresponding variables.

$$\xi_i(k) = \delta_i(k)u_i(k) \tag{6.29}$$

$$o_i(k) = \delta_i(k)u_i(k-1) \tag{6.30}$$

Considering the constraints on the normalized input u listed in Equation (6.2), the equality constraint given by Equation (6.28) can now be rewritten as a set of inequality constraints.

$$\begin{cases} \xi_i(k) \leq L\delta_i(k) \\ \xi_i(k) \geq \ell\delta_i(k) \\ \xi_i(k) \leq u_i(k) - \ell\big(1 - \delta_i(k)\big) \\ \xi_i(k) \leq u_i(k) - L\big(1 - \delta_i(k)\big) \end{cases} \tag{6.31}$$

and

$$\begin{cases} o_i(k) \leq L\delta_i(k) \\ o_i(k) \geq \ell\delta_i(k) \\ o_i(k) \leq u_i(k-1) - \ell\big(1 - \delta_i(k)\big) \\ o_i(k) \geq u_i(k-1) - L\big(1 - \delta_i(k)\big) \end{cases} \tag{6.32}$$

where ℓ and L denote the lower and upper limits, respectively, on the normalized input $u_i(k)$. The constraint on $u_i(k)$ given by Equation (6.2) implies that these limits are as follows: $\ell = 0$, $L = 1$.

Using the notation

$$\delta(k) = \begin{bmatrix} \delta_1(k) & \delta_2(k) & \dots & \delta_N(k) \end{bmatrix}^\intercal \tag{6.33}$$

$$\Delta = \begin{bmatrix} \delta(1)^\intercal & \delta(2)^\intercal & \dots & \delta(K)^\intercal \end{bmatrix}^\intercal \tag{6.34}$$

$$\xi(k) = \begin{bmatrix} \xi_1(k) & \xi_2(k) & \dots & \xi_N(k) \end{bmatrix}^\intercal \tag{6.35}$$

$$\Xi = \begin{bmatrix} \xi(1)^\intercal & \xi(2)^\intercal & ... & \xi(K)^\intercal \end{bmatrix}^\intercal \tag{6.36}$$

$$o(k) = \begin{bmatrix} o_1(k) & o_2(k) & ... & o_N(k) \end{bmatrix}^\intercal \tag{6.37}$$

$$O = \begin{bmatrix} o(1)^\intercal & o(2)^\intercal & ... & o(K)^\intercal \end{bmatrix}^\intercal \tag{6.38}$$

$$\mathcal{V} = \begin{bmatrix} u \\ \Delta \\ \Xi \\ O \\ z \end{bmatrix} \tag{6.39}$$

the problem can be reformulated using a new objective function of the form

$$\min_{u_i(k),\delta_i(k)} \frac{1}{2}\mathcal{V}^\intercal \mathcal{H} \mathcal{V} + \mathcal{F}^\intercal \mathcal{V} \tag{6.40}$$

The PEV charge scheduling in a constrained communication environment becomes a mixed-integer quadratic programming problem of the order $(4 \times K \times N) + K$, subject to the constraints listed in Equations (6.1), (6.2), (6.4) (6.21), (6.25), (6.26), (6.31), and (6.32).

6.5 Model-predictive control formulation

The previous formulations rely on perfect prediction of the demand response signal $S(k)$ as well as the demand on each transformer $d(k)$. In practice however, the signal broadcast by the market operator is only known for the given timestep, without anticipatory knowledge of future signal data points[1]. Given this situation, a receding horizon model predictive control (MPC) formulation is proposed, in which the controller calculates the least costly trajectory over a horizon of $h = 1, \ldots, H$ timesteps based on the current information from the demand response signal, but only implements the first step of this solution before recalculating a new trajectory at the next timestep. For an overview of MPC in a constrained communication environment, see [18, 37].

[1]While future market signal values are unknown, future values for the transformer background demand may be more predictable based on historical load curves, weather patterns, etc., but a more robust controller design will not be dependent on such information. Thus it is assumed that at time k, the quantities $S(k+h)$ and $d(k+h)$ are unknown for all future timesteps $h \geq 1$.

6.5.1 Calculating desired State-of-Charge Trajectory

Since the MPC controller operates over a control horizon that is shorter than the total time horizon K, it is necessary to first calculate the desired SoC trajectory $x_{i,d}$ for each vehicle. The desired SoC for vehicle i at timestep k is given by

$$x_{i,d}(k) = x_{i,0} + \big(x_{i,f}\frac{k}{K}\big) \tag{6.41}$$

with

$$x_d(k) = \begin{bmatrix} x_{1,d}(k) & x_{2,d}(k) & \dots & x_{N,d}(k) \end{bmatrix}^\intercal \tag{6.42}$$

6.5.2 MPC Formulation

The goal of the MPC formulation is to determine at timestep k the optimal virtual control sequence $\hat{u}$ and virtual communication sequence $\hat{\delta}$ that minimize the cost function J over the time horizon from $k+1$ to $k+H$. The revised cost function is given by

$$J = \sum_{h=1}^{H} \Big\{ \Big(\sum_{i \in \mathcal{I}} \pi_i \hat{u}_i(k+h) - \hat{S}(k+h) \Big)^\intercal \mathbf{R} \Big(\sum_{i \in \mathcal{I}} \pi_i \hat{u}_i(k+h) - \hat{S}(k+h) \Big) \Big\} + \Big(\hat{x}(k+H) - x_d(k+H) \Big)^\intercal \mathbf{Q} \Big(\hat{x}(k+H) - x_d(k+H) \Big) + \mathbf{\Omega} z \tag{6.43}$$

subject to constraints on the virtual inputs and states

$$\hat{u}(k+h) \in [0,1] \tag{6.44}$$

$$\hat{x}(k+h) \in [0,1] \tag{6.45}$$

as well as binary constraints on the virtual communication sequence

$$\hat{\delta}_i(k+h) \in \{0,1\} \tag{6.46}$$

and the state-space dynamics described by

$$\hat{x}(h+1) = A\hat{x} + B\hat{u} \tag{6.47}$$

The optimization problem is further subject to the previously discussed bandwidth limitations

$$\sum_{i \in \mathcal{I}} \hat{\delta}_i(k+h) = b \tag{6.48}$$

and logical constraints that account for when a communication pulse $\hat{\delta}_i$ is zero.

$$\hat{\delta}_i(k+1) = 0 \implies \hat{u}_i(k+1) = u_i(k) \tag{6.49}$$

$$\hat{\delta}_i(k+h+1) = 0 \implies \hat{u}_i(k+h+1) = \hat{u}_i(k+h) \tag{6.50}$$

Equations (6.49) and (6.50) can be rewritten as a set of inequality constraints using the same process detailed in Section 6.4. Finally, the inequality constraint that determines the transformer temperature at time $k+h$ is included.

$$\delta\hat{T}(k+h) \leq z_{k+h} \tag{6.51}$$

Note that in the absence of predictive information regarding the demand response signal $\hat{S}(k+h)$ and transformer demand $\hat{d}_m(k+h)$, the assumption is that the current information from the demand response signal and transformer demand is sustained over the horizon H.

$$\begin{cases} \hat{S}(k+h) = S(k) \\ \hat{d}_m(k+h) = d_m(k) \end{cases} \tag{6.52}$$

Using the MPC approach, once the virtual control sequence $\hat{u}$ and virtual communication sequence $\hat{\delta}$ are calculated, only the inputs for the next timestep $k+1$ are implemented

$$u(k+1) = \hat{u}(k+1) \tag{6.53}$$

$$\delta(k+1) = \hat{\delta}(k+1) \tag{6.54}$$

The process is then repeated, and the cost function is reevaluated at time $k+1$ with updated values for the states $x_0(k+1)$ and the demand response signal $S(k+1)$.

6.6 Case Study

This section illustrates the proposed PEV charging controller using the MPC version of the communication-constrained controller detailed in the previous section.

The simulation parameters are enumerated in Table 6.2. The raw signal $\sigma(k)$ is obtained from the Pennsylvania-New Jersey-Maryland Interconnect (PJM) RegD demand response frequency regulation self-test signal [105]. This waveform is used to analyze the capability of a demand response load to respond to rapid setpoint changes, and provides a realistic reference for the PEV controller. The scaling factors $\bar{S}$ and $\widetilde{S}$ are determined by the vehicle aggregator using the calculations specified in Equations (6.16) and (6.17), respectively.

Table 6.2: Simulation parameters

N	=	20
K	=	1200
ΔK	=	.00055 hr (or 2 sec)
b	=	2
π_i	$\in$	[3,5] kW (randomized)
$x_{i,f}$	=	0.20
β_i	=	8 kWh
η_i	=	0.94
M	=	4
T_{max}	=	110°C[2]

The transformers providing power to the vehicles also service a background demand $d_m(k)$, which is sinusoidal with the demand on transformers #1 and #3 set 180° degrees out of phase of the demand on transformers #2 and #4, in order to demonstrate the controller's ability to shift load at peak times. Figure 6.4 shows the reference signal $S(k)$ and the aggregate power of all 20 vehicles. Note that, in general, the aggregate load is capable of tracking the reference signal with a high degree of accuracy. The periods when the aggregate power does not match the reference signal (such as 08:00 - 14:00) correspond to points when transformer temperatures are high, leading the controller to reduce PEV load at these times.

The charging profile of Vehicle $i = 5$ is shown in Figure 6.5. The communication pulses shown in the bottom plot of the figure illustrate that the vehicle aggregator only occasionally updates the charging setpoint of Vehicle 5. Despite this, the charger is able to keep the vehicle's SoC profile in close proximity to the desired trajectory, while simultaneously participating in reference tracking and taking into consideration the temperature dynamics of Transformer #1.

[2]IEEE Standard [13] specifies that the reference temperature for <100 MVA-rated oil-immersed transformers should be calculated as 65°C above the expected winding temperature of 45°C, hence

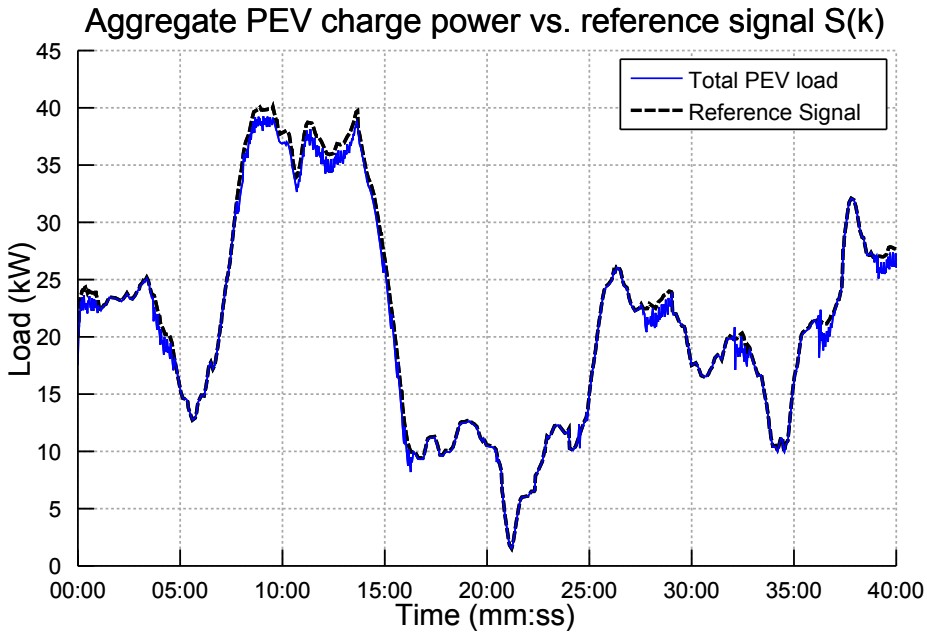

Figure 6.4: Reference tracking abilities of the PEV load

Figure 6.6 shows the total load profile and temperature dynamics of Transformers #1 and #2. Because the background demand on the two transformers is 180° out of phase, the aggregator shifts PEV load between the two transformers, depending on which one has a lower temperature. In this manner, the controller helps to prevent transformer overloading and unnecessary aging, while still accommodating the previously discussed control objectives.

6.7 Conclusion

Adding plug-in electric vehicle (PEV) load to existing power system infrastructure will necessitate new controller designs that coordinate vehicle charging, in order to prevent detrimental effects and to provide useful services to the grid. A generalized service that PEVs can provide is reference tracking, in which the vehicles' aggregate power is matched to an externally provided signal. Vehicles participating in such a regime must also consider the limitations of power system equipment, as well as vehicle owners' battery charging deadlines, when determining an appropriate charge scheduling algorithm. This chapter proposes a controller design that accomplishes all three objectives.

Furthermore, the PEV controller must take into account the limited communi-

the choice of 110°C for T_{max}.

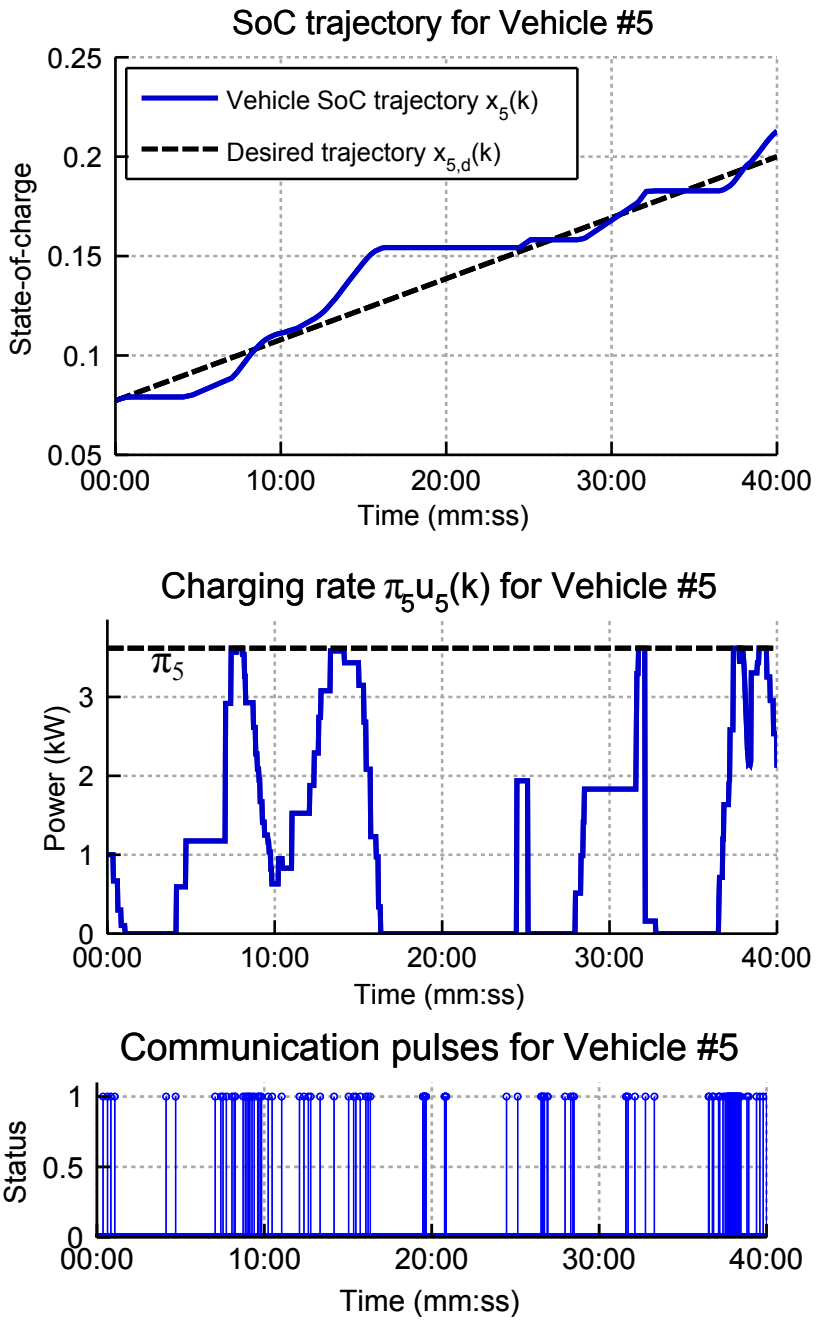

Figure 6.5: The state-of-charge, load profile, and communication sequence associated with Vehicle $i = 5$. Despite the fact that the vehicle aggregator only occasionally communicates with the vehicle to update its charging set-point $u_5(k)$ (bottom plot), the vehicle is capable of staying close to its specified SoC trajectory (top plot) while simultaneously using its load to participate in reference tracking (middle plot as well as Figure 6.4).

cation capabilities between PEVs. The proposed controller design uses additional constraints in the problem formulation to account for a bandwidth limited commu-

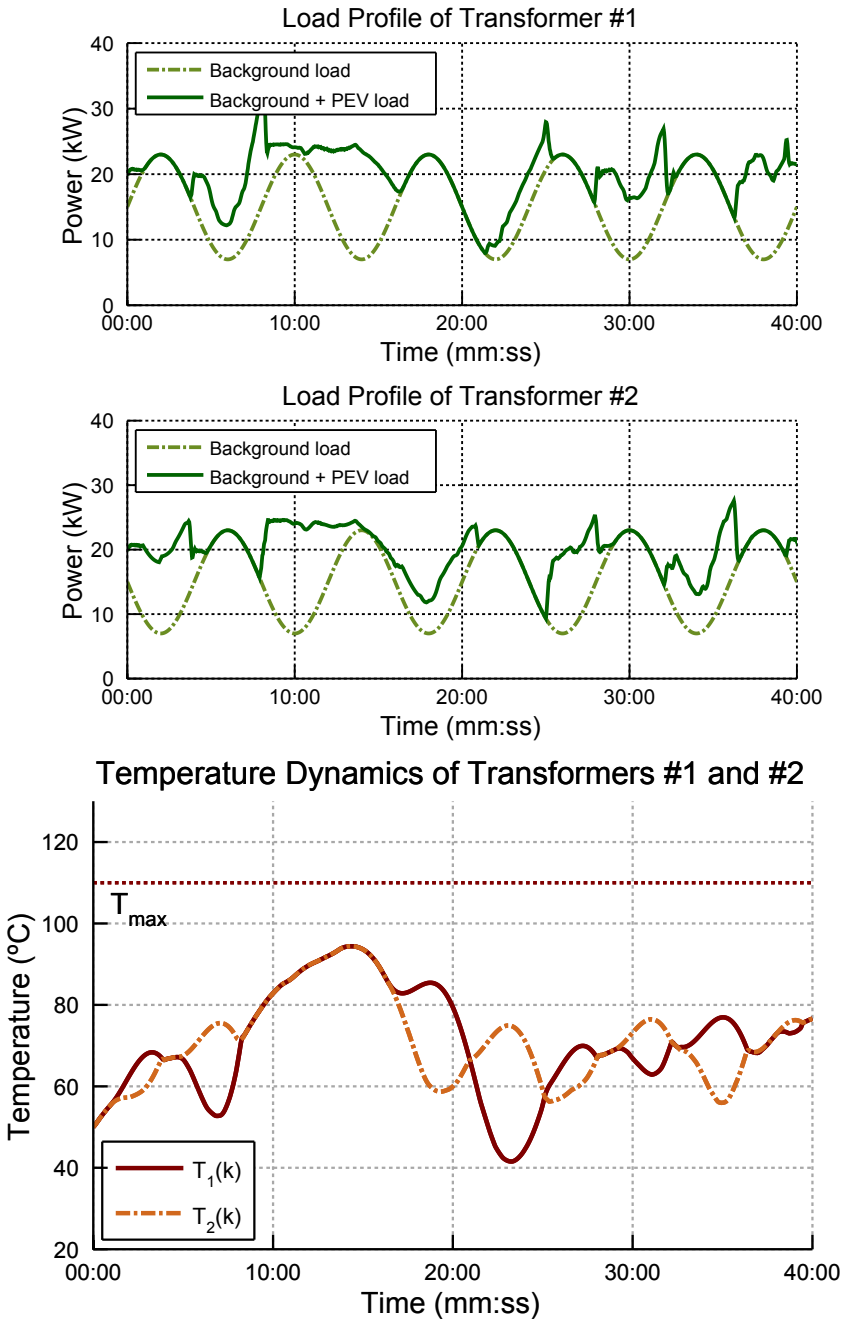

Figure 6.6: The load profile (upper and middle plots) and resulting temperature dynamics (lower plot) for two of the transformers providing power to the PEVs. The background demands of Transformers #1 and #2 (dotted green traces) are sinusoidal and 180° out of phase. Note that the controller tends to "valley fill," that is, add PEV load when a particular transformer has a low background demand, and reduce PEV load when background demand rises, thus preventing overheating of either transformer.

nication channel. The controller is then reformulated as a model-predictive control problem in order to account for unknown future values of the reference signal. Finally, a case study is presented to illustrate the controller performance during a realistic PEV charging scenario.

CHAPTER VII

Conclusion

Changes to the generation side of electrical power systems are forcing engineers to develop new and creative ways to maintain power system operability. A key technology that will help achieve this goal is demand response (DR), in which participating resources adjust their load in order to add flexibility to the system. This dissertation explores issues that occur when DR is employed at very fast (< 1 min) timescales. Broadly, it is divided into two parts - Chapters II and III examine the use of DR in a commercial building heating, ventilation, and air conditioning (HVAC) system, while Chapters IV, V, and VI develop control strategies for groups of plug-in electric vehicles (PEVs) providing DR services. While the two application vary substantially in prevalence, current energy expenditure, and speed of response, both experience challenges when attempting to adjust load at fast timescales. The main conclusions and directions of future work for each application are as follows.

7.1 Heating, Ventilation, and Air Conditioning

Commercial HVAC systems are composed of several interrelated control loops that make adjustment of the electrical load a complex process. Chapter II explains a typical commercial HVAC system layout, including the main components of the system and the supporting communication and control architecture. It then discusses the proposed ways of adjusting HVAC load in a predictable manner (fan speed offset, supply pressure or mass flow set-point offset, thermostat set-point offset), and summarizes past attempts, both in simulation and experiment, to achieve this objective. Then, utilizing an open-loop controller design and the thermostat offset approach, experimental results are presented in which a testbed building attempts to track test signals and historical data from a frequency regulation market. While it is shown that the chosen control design does not score as well as previous efforts, differences

between tests, especially the much higher magnitude of observed changes in power, suggest that the performance gap is not as stark as the numbers alone may suggest. Furthermore, the ability of the temperature offset method to enforce specific limitations on occupant comfort, a crucial operational benefit that is not provided by the other control methods, is discussed in detail.

While Chapter II focuses on the achievable performance of a commercial building employing DR, Chapter III examines the cost of control, in terms of excess energy usage, that can occur when buildings engage in DR services. The chapter first presents the energy expenditure data from the experiments in Chapter II, which show a trend of increased energy use versus comparable days when no control occurs. A battery analogy is then presented, which likens the observed energy expenditure to the losses incurred when charging and discharging a battery. Using this model, an experimental design is presented to test the effective round-trip efficiency of perturbing HVAC load around a nominal setpoint. The resulting data displays a significant energy penalty when the HVAC system is subjected to rapid changes in setpoint, even when considering errors in baseline estimation and the dynamics of chiller power consumption. These findings are corroborated by past research efforts, both simulated and experimental, which point to similar losses in efficiency. Finally, the chapter examines the economic repercussions for a building participating in HVAC driven DR.

7.1.1 Future Directions

There are many interesting and important directions for future investigations focused on using commercial HVAC systems for fast, continuously-operated DR control. Although these chapters present some general comparisons, the diversity of test platforms and protocols precludes detailed comparisons of control methods and control inputs. Current and future research would greatly benefit from access to several standard test platforms comprising real commercial buildings spanning typical commercial HVAC architectures. Furthermore, standardization of test protocols and performance metrics, e.g. a representative sample of PJM historical RegA and RegD signals combined with PJM performance metrics [36], would enable a more meaningful comparison of different control methods.

Specifically with regards to the thermostat offset method discussed in this dissertation, another way to improve this approach is to better understand the relationship between the broadcast change in conditioned space temperature, and the resulting change in HVAC power consumption. Furthermore, because it is likely that this relationship is altered as factors such as external temperature and internal heat load

change throughout the day, online model identification techniques may provide a way to account for an adjusted mapping of temperature setpoint and power.

Another area that deserves additional attention is understanding and minimizing the impact of fast-timescale DR control on HVAC energy consumption and the economics of these forms of DR. These impacts should also be explored for other resources that are being considered for these types of ancillary services; e.g., commercial refrigeration, residential HVAC, and lighting.

7.2 Plug-in Electric Vehicles

PEVs are another candidate for DR control. The existing population of PEVs represents an insignificant load on the grid; however, future changes in environmental regulation and the economics of petroleum could one day spur large increases in PEV sales. Shifting a large portion of the transportation energy burden onto the electrical grid would have significant effects if this PEV load remained uncontrolled. However, the challenge of controlling a PEV fleet is exacerbated by the paucity of communication infrastructure available in a distribution system environment.

Chapters IV, V, and VI each propose a potential method of managing PEV charging in order to accomplish a specific set of goals. It is useful to compare the main advantages and drawbacks of each controller design, in order to determine scenarios in which each one might be most useful.

7.2.1 AIMD Control

Chapter IV examines a control algorithm known as additive-increase multiplicative decrease (AIMD), which has very low communication requirements, to determine the grid level effects that occur when this algorithm is employed to prevent transformer overloading. Using simulations on a standardized distribution system model, it is shown that AIMD can effectively prevent transformer overloading without causing drastic changes to the voltage and power profiles of the network.

The main advantages of the AIMD control method are its minimal communication requirements (one way, only when a capacity event has occurred) and low computational burden (determining when the capacity limit has been reached). The lack of communication requirements also means that the algorithm scales well as the number of vehicles in the population increases.

There are several disadvantages to using AIMD. For one, the performance of the algorithm is reliant on the choices of the parameters α and β. Chapter IV identified

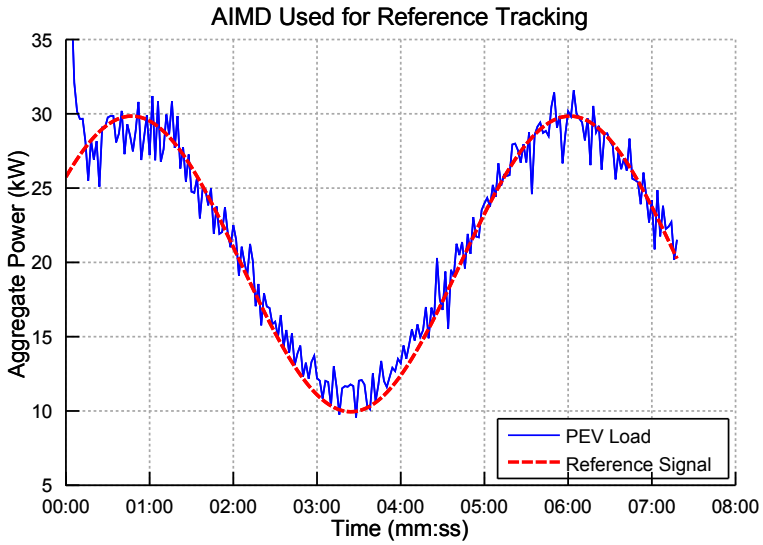

Figure 7.1: The aggregate charging profile of a fleet of vehicles attempting to track a reference signal using AIMD control. Note the sharp changes in load, which correspond to capacity events on one or more of the associated transformers.

situations in which certain values for these parameters lead to undesirable overload on the distribution transformers. While Chapter IV does not directly discuss PEV reference tracking using the AIMD algorithm, it is possible to use AIMD for this purpose. However, the large changes in power that occur when a capacity event is reached can cause a severe spiking phenomenon, as shown in Figure 7.1. This leads to an aggregate PEV load profile that has a lower accuracy than desirable when tracking a reference signal.

7.2.2 Average Consensus Algorithm

While Chapter IV examines a way to prevent detrimental equipment effects from uncontrolled PEV charging, this is only part of the challenge. A fleet of PEVs that is capable of adjusting its load in a reliable manner can be compensated in ancillary services markets such as frequency regulation. Chapter V explores the use of the average consensus approach, a distributed control algorithm, to not only prevent transformer overloading, but also attempt to track aggregate vehicle charging power to a specified reference signal. The implications of the distributed nature of the controller, especially from a communication and latency standpoint, are discussed in detail.

Unlike the AIMD algorithm, average consensus control is capable of allowing a

PEV fleet to track a reference signal with a smooth aggregate power response (see Figures 5.3 and 5.4). Similar to the AIMD algorithm, it is also capable of considering distribution transformer capacity, and dynamically assigning more PEV load to transformers that have a larger spare capacity.

The main drawback of the consensus algorithm is its sensitivity to communication network delays, a problem which is compounded as the number of nodes in the system - in this case the number of distribution transformers - increases. The distributed nature of the control algorithm means that increasing the nodes causes a corresponding increase in the convergence time of the algorithm. If the communication architecture that connects the distribution transformers is sufficiently interconnected, this problem can be avoided. However, the limited communication capabilities of a typical distribution system suggest that this would be an atypical situation.

7.2.3 Communication-Constrained Optimal Control

It is also desirable for the PEV controller to take into account vehicle owners' battery charging desires. Chapter VI develops a novel discrete-time optimal controller design that enables PEV to track a reference signal while also considering battery state-of-charge goals and transformer limitations. Additional constraints are introduced that limit the number of communication events that occur at a particular timestep, in order to model the limited communication capabilities.

Like the consensus algorithm, the proposed optimal control formulation is capable of tracking a reference signal with a high degree of accuracy. Furthermore, like the AIMD algorithm, it is not particularly susceptible to communication delays within the system. Additionally, the various weighting terms in the cost function allow the operator to prioritize specific goals - accurate reference tracking, adequate battery charging, and prevention of transformer overload - in a flexible manner. Finally, the communication-constrained formulation takes into account the limitations of the communication network, and achieves sufficient performance results despite this constraint.

The disadvantage of the proposed optimal controller is the large computational burden, and the fact that the complexity scales with the square of the number of vehicles on the system. While the simulation results presented in Section 6.6 were conducted in real time, i.e. the MPC calculation over the predicted horizon took less time to compute than the sampling rate of the reference signal, it is possible that a large vehicle population could experience large computational times and therefore enforce a lower sampling rate on the incoming signal.

7.2.4 Comparison of Controller Design

As of publication, there does not exist a standardized PEV charging scenario that could be used to test the proposed controllers. Instead, this subsection presents a test case that helps display the trends discussed above. The parameters of the test case are described in Table 7.1. Using the RegD Qualification Test from the PJM Demand Response Regulation Market [105] discussed throughout this work, the performance scores of the three controllers are compared with various amount of communication delay in the system. The results are displayed in Figure 7.2.

Table 7.1: Comparison Test Case Parameters

			Note
N	=	20	Number of PEVs
π_i	$\in$	[3,5] kW	Max charge rate of each vehicle
β_i	=	8 kWh	Battery Capacity
η_i	=	0.94	Charging Efficiency
M	=	4	Number of transformers
S		RegD	Reference signal

As expected, the consensus algorithm displays a higher sensitivity to the communication delay than the other two algorithms. Also, the performance scores displayed in Figure 7.2 for the consensus algorithm are higher that the scores listed in Table 5.1 because this test case includes fewer transformers, which increases the convergence rate of the algorithm. The sensitivity of the consensus algorithm to both the number of nodes in the system and the delay on the communication network indicates the difficulty in implementing this controller on physical hardware.

Another trend to note is that, while both the AIMD and constrained communication controllers are similarly effected by delays, the constrained communication controller consistently achieves higher scores than the AIMD algorithm. This is due to the lack of spiking phenomena, and the generally smoother aggregate PEV load, induced by the constrained communication formulation. However, this increase in performance comes at the cost of higher computational requirements. While both controllers can operate in a limited-communication environment, the cost and complexity of the constrained communication approach could make it less desirable in certain situations.

Overall, all three algorithms are capable of modulating PEV load to prevent detrimental effects on the distribution grid while simultaneously providing ancillary services to grid operators. The choice of controllers ultimately depends on the character-

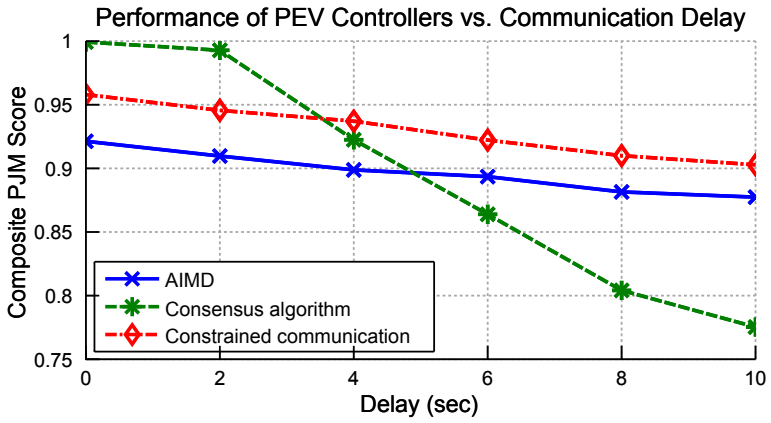

Figure 7.2: The composite PJM performance scores for the RegD Qualification Test for each of the proposed PEV controllers in the scenario described by Table 7.1, as a function of the communication delays present on the network.

istics of the PEV fleet, the topology of the associated communication infrastructure, and whether priority is given to grid-level or customer-centric concerns.

7.2.5 Future Directions

While this work adds insights into PEV controller design, there are still areas for improvement. A new version of the AIMD algorithm could be implemented that adjusts its control parameters by utilizing a feedback loop to observe current performance trends. A more advanced version of the consensus algorithm could be developed that is less suspectable to communication delays in the network. Future investigations could explore more complicated communication channel models that take into account the specific communication infrastructure available to a PEV fleet. It would also be interesting to explore the effect that varying the discrete-time timestep size has on the performance of the constrained-communication control. The effects of a bandwidth restriction become more pronounced as the time between possible successive control input updates increases. Thus, analyzing the performance of the algorithm as the timestep increases would better validate whether the computational cost is worth the reduced communication requirements. Perhaps most useful would be a comparison of the proposed algorithms on a hardware testbed to determine performance in a realistic environment.

BIBLIOGRAPHY

BIBLIOGRAPHY

[1] Abercrombie, W., Bartlett, S., and Murray, B. Load management developments in Queensland. In *Engineering Conference 1980: Engineering in the 80s; Conference Papers, The* (1980), Institution of Engineers, Australia, p. 370.

[2] Al-Anbagi, I. S., and Mouftah, H. T. QoS schemes for charging plug-in electric vehicles in a smart grid environment. In *Plug In Electric Vehicles in Smart Grids*. Springer, 2015, pp. 241–265.

[3] Allcott, H. Rethinking Real-Time Electricity Pricing. *Resource and Energy Economics 33*, 4 (2011), 820–842.

[4] Arnborg, S., Andersson, G., Hill, D. J., and Hiskens, I. A. On undervoltage load shedding in power systems. *International Journal of Electrical Power & Energy Systems 19*, 2 (1997), 141–149.

[5] Asr, N. R., and Chow, M.-Y. Network coordinated distributed demand management for optimal large-scale charging of phevs/pevs. In *Power and Energy Society General Meeting (PES), 2013 IEEE* (2013), IEEE, pp. 1–5.

[6] Barooah, P., Bušic, A., and Meyn, S. Spectral decomposition of demand-side flexibility for reliable ancillary services in a smart grid. In *48th Annual Hawaii Conference on Systems Science* (2015).

[7] Bashash, S., Moura, S. J., Forman, J. C., and Fathy, H. K. Plug-in hybrid electric vehicle charge pattern optimization for energy cost and battery longevity. *Journal of power sources 196*, 1 (2011), 541–549.

[8] Bemporad, A., and Morari, M. Control of systems integrating logic, dynamics, and constraints. *Automatica 35*, 3 (1999), 407–427.

[9] Berry, L. A review of the market penetration of us residential and commercial demand-side management programmes. *Energy Policy 21*, 1 (1993), 53–67.

[10] Beute, N., and Delport, G. An historic overview of controlling domestic water heating. In *Proceedings of the 14th Domestic Use of Energy Conference* (2006), pp. 41–46.

[11] Borenstein, S., Jaske, M., and Rosenfeld, A. Dynamic pricing, advanced metering, and demand response in electricity markets.

[12] Braun, J. E., Montgomery, K. W., and Chaturvedi, N. Evaluating the performance of building thermal mass control strategies. *HVAC&R Research 7*, 4 (2001), 403–428.

[13] C57.91-1995. IEEE guide for loading mineral-oil-immersed transformers. *IEEE Standards 57* (1995), 1–112.

[14] Cady, S. T., Domínguez-García, A., and Hadjicostis, C. N. Finite-time approximate consensus and its application to distributed frequency regulation in islanded AC microgrids. In *Proc. of the Hawaii International Conference on System Sciences, Kauai, HI* (2015).

[15] Callaway, D. S. Tapping the energy storage potential in electric loads to deliver load following and regulation, with application to wind energy. *Energy Conversion and Management 50*, 5 (2009), 1389–1400.

[16] Callaway, D. S., Hiskens, I., et al. Achieving controllability of electric loads. *Proceedings of the IEEE 99*, 1 (2011), 184–199.

[17] Cappers, P., Goldman, C., and Kathan, D. Demand response in us electricity markets: Empirical evidence. *Energy 35*, 4 (2010), 1526–1535.

[18] Çela, A., Gaid, M. B., Li, X.-G., and Niculescu, S.-I. *Optimal Design of Distributed Control and Embedded Systems*. Springer Science & Business Media, 2013.

[19] Chen, C., Wang, J., and Kishore, S. A distributed direct load control approach for large-scale residential demand response. *Power Systems, IEEE Transactions on 29* (2014).

[20] Cheng, C. S., and Shirmohammadi, D. A three-phase power flow method for real-time distribution system analysis. *IEEE Transactions on Power Systems 10*, 2 (1995), 671–679.

[21] Chiu, D.-M., and Jain, R. Analysis of the increase and decrease algorithms for congestion avoidance in computer networks. *Computer Networks and ISDN systems 17*, 1 (1989), 1–14.

[22] Clement-Nyns, K., Haesen, E., and Driesen, J. The impact of charging plug-in hybrid electric vehicles on a residential distribution grid. *Power Systems, IEEE Transactions on 25*, 1 (2010), 371–380.

[23] Cole, W. J., Powell, K. M., Hale, E. T., and Edgar, T. F. Reduced-order residential home modeling for model predictive control. *Energy and Buildings 74*, 0 (2014), 69 – 77.

[24] Cole, W. J., Powell, K. M., Hale, E. T., and Edgar, T. F. Reduced-order residential home modeling for model predictive control. *Energy and Buildings 74* (2014), 69–77.

[25] Deilami, S., Masoum, A. S., Moses, P. S., and Masoum, M. A. Real-time coordination of plug-in electric vehicle charging in smart grids to minimize power losses and improve voltage profile. *IEEE Transactions on Smart Grid 2*, 3 (2011), 456–467.

[26] Domínguez-García, A. D., Cady, S. T., and Hadjicostis, C. N. Decentralized optimal dispatch of distributed energy resources. In *CDC* (2012), pp. 3688–3693.

[27] Dominguez-Garcia, A. D., and Hadjicostis, C. N. Coordination and control of distributed energy resources for provision of ancillary services. In *Smart Grid Communications (SmartGridComm), 2010 First IEEE International Conference on* (2010), IEEE, pp. 537–542.

[28] Duvall, M., Knipping, E., Alexander, M., Tonachel, L., and Clark, C. Environmental assessment of plug-in hybrid electric vehicles. *EPRI, July* (2007).

[29] Electric Drive Transportation Association. *Cumulative U.S. Plug-In Vehicle Sales*, 2015.

[30] EPA. *Standards of Performance for Greenhouse Gas Emissions From New Stationary Sources: Electric Utility Generating Units*, January 2014. EPA-HQ-OAR-2013-0495.

[31] Farhangi, H. The path of the smart grid. *Power and Energy Magazine, IEEE 8*, 1 (2010), 18–28.

[32] Faria, P., and Vale, Z. Demand response in electrical energy supply: An optimal real time pricing approach. *Energy 36*, 8 (2011), 5374–5384.

[33] FERC. Order 745: Demand response compensation in organized wholesale energy markets. Tech. rep., Federal Energy Regulatory Commission, March 2011.

[34] FERC. Order 755: Frequency regulation compensation in the organized wholesale power markets. Tech. rep., Federal Energy Regulatory Commission, October 2011.

[35] Forward Market Operations. PJM manual 11: Energy and ancillary markets operations. Tech. rep., PJM Regional Transmission Operator, June 2014.

[36] Forward Market Operations. PJM Manual 12: Balancing operations. Tech. rep., PJM Regional Transmission Operator, August 2014. Revision 31.

[37] Gaid, M. M. B., Cela, A., and Hamam, Y. Optimal integrated control and scheduling of networked control systems with communication constraints: application to a car suspension system. *Control Systems Technology, IEEE Transactions on 14*, 4 (2006), 776–787.

[38] Galus, M. D., Art, S., and Andersson, G. A hierarchical, distributed pev charging control in low voltage distribution grids to ensure network security. In *Proceedings of the IEEE PES General Meeting* (July 2012).

[39] Gan, L., Topcu, U., and Low, S. Optimal decentralized protocol for electric vehicle charging. *IEEE Transactions on Power Systems 28*, 2 (2013), 940–951.

[40] Gharesifard, B., Basar, T., and Dominguez-Garcia, A. Price-based distributed control for networked plug-in electric vehicles. In *American Control Conference (ACC), 2013* (2013), IEEE, pp. 5086–5091.

[41] Ghatikar, G., and Bienert, R. Smart grid standards and systems interoperability: a precedent with OpenADR. In *Proceedings of the Grid Interop Forum* (2011).

[42] Gibbs, J. B. *Transformer principles and practice*. McGraw-Hill, 1950.

[43] Goddard, G., Klose, J., and Backhaus, S. Model development and identification for fast demand response in commercial hvac systems. *Smart Grid, IEEE Transactions on 5*, 4 (2014), 2084–2092.

[44] Gong, Q., Midlam-Mohler, S., Marano, V., and Rizzoni, G. Study of PEV charging on residential distribution transformer life. *IEEE Transactions on Smart Grid 3*, 1 (2012), 404–412.

[45] González Vayá, M., and Andersson, G. Combined smart-charging and frequency regulation for fleets of plug-in electric vehicles. In *IEEE Power and Energy Society General Meeting* (2013), vol. 2013.

[46] Gonzalez Vaya, M., Andersson, G., and Boyd, S. Decentralized control of plug-in electric vehicles under driving uncertainty. In *Innovative Smart Grid Technologies Conference Europe (ISGT-Europe), 2014 IEEE PES* (2014), IEEE, pp. 1–6.

[47] Grainger, J. J., and Stevenson, W. D. *Power system analysis*, vol. 31. McGraw-Hill New York, 1994.

[48] Güngör, V. C., Sahin, D., Kocak, T., Ergüt, S., Buccella, C., Cecati, C., and Hancke, G. P. Smart grid technologies: communication technologies and standards. *Industrial informatics, IEEE transactions on 7*, 4 (2011), 529–539.

[49] Gustafson, M., Baylor, J., and Epstein, G. Direct water heater load control-estimating program effectiveness using an engineering model. *Power Systems, IEEE Transactions on 8*, 1 (1993), 137–143.

[50] Hammerstrom, D. J. Pacific Northwest GridWise Testbed Demonstration Projects. Part I. Olympic Peninsula Project. Tech. Rep. PNNL-17167, Pacific Northwest National Laboratory, 2007.

[51] Hanke, S. H., and Davis, R. K. Demand management through responsive pricing. *Journal (American Water Works Association)* (1971), 555–560.

[52] Hao, H., Kowli, A., Lin, Y., Barooah, P., and Meyn, S. Ancillary service for the grid via control of commercial building HVAC systems. In *American Control Conference (ACC), 2013* (2013), IEEE, pp. 467–472.

[53] Hastings, B. Ten years of operating experience with a remote controlled water heater load management system at Detroit Edison. *Power Apparatus and Systems, IEEE Transactions on*, 4 (1980), 1437–1441.

[54] Häusler, F., Crisostomi, E., Radusch, I., and Shorten, R. Smart procurement of naturally generated energy (SPONGE) for PHEV's. *arXiv preprint arXiv:1501.02931* (2015).

[55] Hermans, R., Almassalkhi, M., and Hiskens, I. Incentive-based coordinated charging control of plug-in electric vehicles at the distribution-transformer level. In *American Control Conference (ACC), 2012* (2012), IEEE, pp. 264–269.

[56] Hill, D. H. Home production and the residential electric load curve. *Resources and Energy 1*, 4 (1978), 339–358.

[57] Hilshey, A. D., Hines, P. D., and Dowds, J. R. Estimating the acceleration of transformer aging due to electric vehicle charging. In *Proceedings of the IEEE PES General Meeting* (July 2011).

[58] Hurley, J., Peterson, P., and Whited, M. Demand response as a power system resource. Tech. rep., The Regulatory Assistance Project, May 2013.

[59] Jaleeli, N., VanSlyck, L., Ewart, D., Fink, L., and Hoffmann, A. Understanding automatic generation control. *IEEE Transactions on Power Systems 7*, 3 (August 1992), 1106–1122.

[60] Kelly, L., Rowe, A., and Wild, P. Analyzing the impacts of plug-in electric vehicles on distribution networks in British Columbia. In *Electrical Power & Energy Conference (EPEC), 2009 IEEE* (2009), IEEE, pp. 1–6.

[61] Kersting, W. H. *Radial Distribution Test Feeders*. Distribution System Analysis Subcommittee, IEEE Power and Energy Society, 2000. Available: ewh.ieee.org/soc/pes/dsacom/testfeeders/index.html.

[62] Kiliccote, S., Piette, M. A., Koch, E., and Hennage, D. Utilizing automated demand response in commercial buildings as non-spinning reserve product for ancillary services markets. In *Decision and Control and European Control Conference (CDC-ECC), 2011 50th IEEE Conference on* (2011), IEEE, pp. 4354–4360.

[63] Kim, J. J., Yin, R., and Kiliccote, S. Automated demand response technologies and demonstration in New York City using OpenADR. Tech. Rep. LBNL-6470E, Lawrence Berkeley National Laboratory, 2013.

[64] Kintner-Meyer, M. Regulatory Policy and Markets for Energy Storage in North America. *Proceedings of the IEEE* (July 2014), 1065–1072.

[65] Klobasa, M. Analysis of demand response and wind integration in germany's electricity market. *IET renewable power generation 4*, 1 (2010), 55–63.

[66] Koch, S., Mathieu, J. L., and Callaway, D. S. Modeling and control of aggregated heterogeneous thermostatically controlled loads for ancillary services. In *Proc. PSCC* (2011), pp. 1–7.

[67] Kundu, S., and Hiskens, I. A. Hysteresis-based charging control of plug-in electric vehicles. In *Decision and Control (CDC), 2012 IEEE 51st Annual Conference on* (2012), IEEE, pp. 5598–5604.

[68] Kundu, S., and Hiskens, I. A. State-space modelling of hysteresis-based control schemes. In *Control Conference (ECC), 2013 European* (2013), IEEE, pp. 2535–2540.

[69] Kundu, S., Sinitsyn, N., Backhaus, S., and Hiskens, I. Modeling and control of thermostatically controlled loads. *arXiv preprint arXiv:1101.2157* (2011).

[70] Lam, J. C., Li, D. H., and Cheung, S. An analysis of electricity end-use in air-conditioned office buildings in Hong Kong. *Building and Environment 38*, 3 (2003), 493–498.

[71] Ledva, G. S., Vrettos, E., Mastellone, S., Andersson, G., and Mathieu, J. L. Applying networked estimation and control algorithms to address communication bandwidth limitations and latencies in demand response. In *System Sciences (HICSS), 2015 48th Hawaii International Conference on* (2015), IEEE, pp. 2645–2654.

[72] Li, C.-T., Ahn, C., Peng, H., and Sun, J. Integration of plug-in electric vehicle charging and wind energy scheduling on electricity grid. In *Innovative Smart Grid Technologies (ISGT), 2012 IEEE PES* (2012), IEEE, pp. 1–7.

[73] Li, Q., Negi, R., and Ilic, M. D. A queueing based scheduling approach to plug-in electric vehicle dispatch in distribution systems. *arXiv preprint arXiv:1203.5449* (2012).

[74] Lin, Y., Barooah, P., Meyn, S., and Middelkoop, T. Experimental evaluation of frequency regulation from commercial building HVAC systems. *Smart Grid, IEEE Transactions on 6*, 2 (2015), 776–783.

[75] Liu, M., and McLoone, S. Investigation of aimd based charging strategies for evs connected to a low-voltage distribution network. In *Intelligent Computing for Sustainable Energy and Environment*. Springer, 2013, pp. 433–441.

[76] Liu, R., Dow, L., and Liu, E. A survey of pev impacts on electric utilities. In *Innovative Smart Grid Technologies (ISGT), 2011 IEEE PES* (2011), IEEE, pp. 1–8.

[77] Ljung, L. *System Identification. Theory for the User*, 2nd ed. Prentice Hall, Englewood Cliffs, NJ, 1999.

[78] Lu, B.-B., Chen, X.-Y., Ding, X.-H., Liao, Y.-C., and Yu, K. A direct control of central air conditioning load considering indoor comfort. *Environment, Energy and Sustainable Development 4* (2013), 369.

[79] Lu, L., Han, X., Li, J., Hua, J., and Ouyang, M. A review on the key issues for lithium-ion battery management in electric vehicles. *Journal of power sources 226* (2013), 272–288.

[80] Lu, N. An evaluation of the hvac load potential for providing load balancing service. *Smart Grid, IEEE Transactions on 3*, 3 (2012), 1263–1270.

[81] Lu, N., Chassin, D. P., and Widergren, S. E. Modeling uncertainties in aggregated thermostatically controlled loads using a state queueing model. *Power Systems, IEEE Transactions on 20*, 2 (2005), 725–733.

[82] Ma, J., Qin, J., Salsbury, T., and Xu, P. Demand reduction in building energy systems based on economic model predictive control. *Chemical Engineering Science 67*, 1 (2012), 92–100.

[83] Ma, Z., Callaway, D., and Hiskens, I. Decentralized charging control for large populations of plug-in electric vehicles. In *Proceedings of the IEEE Conference on Decision and Control* (December 2010), pp. 206–212.

[84] MacDonald, J., Cappers, P., Callaway, D., and Kiliccote, S. Demand Response Providing Ancillary Services: A Comparison of Opportunities and Challenges in the US Wholesale Markets. Tech. Rep. LBNL-5958E, November 2012.

[85] MacDonald, J., Kiliccote, S., Boch, J., Chen, J., Nawy, R., and Pacific Grove, C. Commercial building loads providing ancillary services in pjm. *Presented at ACEEE Summer Study on Energy Efficiency in Buildings 2014* (2014).

[86] Mammoli, A., Barsun, H., Burnett, R., Hawkins, J., and Simmins, J. Using high-speed demand response of building hvac systems to smooth cloud-driven intermittency of distributed solar photovoltaic generation. In *Transmission and Distribution Conference and Exposition (T&D), 2012 IEEE PES* (2012), IEEE, pp. 1–10.

[87] Masoum, M. A., Moses, P. S., and Smedley, K. M. Distribution transformer losses and performance in smart grids with residential plug-in electric vehicles. In *Innovative Smart Grid Technologies (ISGT), 2011 IEEE PES* (2011), IEEE, pp. 1–7.

[88] Mathieu, J. L., Callaway, D. S., and Kiliccote, S. Variability in automated responses of commercial buildings and industrial facilities to dynamic electricity prices. *Energy and Buildings 43*, 12 (2011), 3322–3330.

[89] Medicherla, T., Billinton, R., and Sachdev, M. Generation rescheduling and load shedding to alleviate line overloads-analysis. *Power Apparatus and Systems, IEEE Transactions on*, 6 (1979), 1876–1884.

[90] Millikin, M., and Rosebro, J. Chevy volt delivers novel two-motor, four-mode extended range electric drive system; seamless driver experience plus efficiency. *Green Car Congress* (October 2010).

[91] Mohseni, P., and Stevie, R. G. Electric vehicles: Holy grail or fool's gold. In *Power & Energy Society General Meeting, 2009. PES'09. IEEE* (2009), IEEE, pp. 1–5.

[92] Motegi, N., Piette, M. A., Watson, D. S., Kiliccote, S., and Xu, P. Introduction to commercial building control strategies and techniques for demand response. Tech. Rep. LBNL-59975, Lawrence Berkeley National Laboratory, 2007.

[93] Murphy, J. High-performance VAV systems. *ASHRAE Journal* (October 2011), 18–28.

[94] Oldewurtel, F., Sturzenegger, D., Andersson, G., Morari, M., and Smith, R. S. Towards a standardized building assessment for demand response. In *Decision and Control (CDC), 2013 IEEE 52nd Annual Conference on* (2013), IEEE, pp. 7083–7088.

[95] Olfati-Saber, R., Fax, J. A., and Murray, R. M. Consensus and cooperation in networked multi-agent systems. *Proceedings of the IEEE 95*, 1 (2007), 215–233.

[96] Olfati-Saber, R., and Murray, R. M. Consensus problems in networks of agents with switching topology and time-delays. *Automatic Control, IEEE Transactions on 49*, 9 (2004), 1520–1533.

[97] Palensky, P., and Dietrich, D. Demand side management: Demand response, intelligent energy systems, and smart loads. *Industrial Informatics, IEEE Transactions on 7*, 3 (2011), 381–388.

[98] Parti, M., and Parti, C. The total and appliance-specific conditional demand for electricity in the household sector. *The Bell Journal of Economics* (1980), 309–321.

[99] Perfumo, C., Kofman, E., Braslavsky, J. H., and Ward, J. K. Load management: Model-based control of aggregate power for populations of thermostatically controlled loads. *Energy Conversion and Management 55* (2012), 36–48.

[100] Peterson, S. B., Whitacre, J., and Apt, J. The economics of using plug-in hybrid electric vehicle battery packs for grid storage. *Journal of Power Sources 195*, 8 (2010), 2377–2384.

[101] Pieltain Fernandez, L., Gomez San Roman, T., Cossent, R., Domingo, C. M., and Frías, P. Assessment of the impact of plug-in electric vehicles on distribution networks. *IEEE Transactions on Power Systems 26*, 1 (2011), 206–213.

[102] Piette, M. A., Sezgen, O., Watson, D. S., Motegi, N., Shockman, C., and Ten Hope, L. Development and evaluation of fully automated demand response in large facilities. Tech. Rep. CEC-500-2005-013, Lawrence Berkeley National Laboratory, 2005.

[103] PJM. Ancillary services, June 2013. http://www.pjm.com/ /media/training/core-curriculum/ip-gen-301/gen-301-ancillary-services.ashx.

[104] PJM. PJM Regulation Zone Preliminary Billing Data, April 2013. http://pjm.com/markets-and-operations/market-settlements/preliminary-billing-reports/pjm-reg-data.aspx.

[105] PJM. Regulation Self-Test Signals, August 2014. http://www.pjm.com/markets-and-operations/ancillary-services.aspx.

[106] Rabe, B. Race to the top: The expanding role of US state renewable portfolio standards. *Sustainable Dev. L. & Pol'y 7* (2006), 10.

[107] Richardson, P., Flynn, D., and Keane, A. Optimal charging of electric vehicles in low-voltage distribution systems. *IEEE Transactions on Power Systems 27*, 1 (2012), 268–279.

[108] Roozbehani, M., Dahleh, M. A., and Mitter, S. K. Volatility of power grids under real-time pricing. *Power Systems, IEEE Transactions on 27*, 4 (2012), 1926–1940.

[109] Sanghvi, A. P. Flexible strategies for load/demand management using dynamic pricing. *Power Systems, IEEE Transactions on 4*, 1 (1989), 83–93.

[110] Sheen, J.-N., Chen, C.-S., and Yang, J.-K. Time-of-use pricing for load management programs in taiwan power company. *Power Systems, IEEE Transactions on 9*, 1 (1994), 388–396.

[111] Sioshansi, R., and Short, W. Evaluating the impacts of real-time pricing on the usage of wind generation. *Power Systems, IEEE Transactions on 24*, 2 (2009), 516–524.

[112] Solomon, S. *Climate change 2007-the physical science basis: Working group I contribution to the fourth assessment report of the IPCC*, vol. 4. Cambridge University Press, 2007.

[113] Sortomme, E., Hindi, M. M., MacPherson, S. J., and Venkata, S. Coordinated charging of plug-in hybrid electric vehicles to minimize distribution system losses. *Smart Grid, IEEE Transactions on 2*, 1 (2011), 198–205.

[114] St. John, J. The future of demand response: Legal challenges could dramatically change the industry. *GreenTechMedia* (2015).

[115] Stocker, T., Qin, D., Plattner, G., Tignor, M., Allen, S., Boschung, J., Nauels, A., Xia, Y., Bex, B., and Midgley, B. Ipcc, 2013: climate change 2013: the physical science basis. contribution of working group I to the fifth assessment report of the intergovernmental panel on climate change.

[116] Stüdli, S., Crisostomi, E., Middleton, R., and Shorten, R. A flexible distributed framework for realising electric and plug-in hybrid vehicle charging policies. *International Journal of Control 85*, 8 (2012), 1130–1145.

[117] Sturzenegger, D., Gyalistras, D., Morari, M., and Smith, R. S. Model predictive climate control of a swiss office building: Implementation, results, and cost-benefit analysis.

[118] Su, S., Jiang, J., and Wang, W. An autonomous decentralized voltage control scheme in pev charging devices on the distribution network reactive power compensation for voltage decreases caused by household loads and charging devices. *International Transactions on Electrical Energy Systems* (2013).

[119] Su, W., and Chow, M.-Y. Sensitivity analysis on battery modeling to large-scale PHEV/PEV charging algorithms. In *IECON 2011-37th Annual Conference on IEEE Industrial Electronics Society* (2011), IEEE, pp. 3248–3253.

[120] Sundström, O., and Binding, C. Flexible charging optimization for electric vehicles considering distribution grid constraints. *Smart Grid, IEEE Transactions on 3*, 1 (2012), 26–37.

[121] Taylor, C. W. Concepts of undervoltage load shedding for voltage stability. *Power Delivery, IEEE Transactions on 7*, 2 (1992), 480–488.

[122] Tesla Motors. *Model S*, 2015.

[123] Toepfer, C. SAE electric vehicle conductive charge coupler, SAE J1772. *Society of Automotive Engineers* (2009).

[124] Turitsyn, K., Sinitsyn, N., Backhaus, S., and Chertkov, M. Robust broadcast-communication control of electric vehicle charging. In *Smart Grid Communications (SmartGridComm), 2010 First IEEE International Conference on* (2010), IEEE, pp. 203–207.

[125] Ungar, B. E., and Fell, K. Plug in, turn on, and load up. *Power and Energy Magazine, IEEE 8*, 3 (2010), 30–35.

[126] U.S. Energy Information Administration. *Monthly Energy Review May 2015*, 2015. Table 2.1 - Energy Consumption by Sector.

[127] Wang, L., and Xiao, F. Finite-time consensus problems for networks of dynamic agents. *Automatic Control, IEEE Transactions on 55*, 4 (2010), 950–955.

[128] Wang, Y., Yue, S., and Pedram, M. State-of-health aware optimal control of plug-in electric vehicles. In *PES General Meeting— Conference & Exposition, 2014 IEEE* (2014), IEEE, pp. 1–5.

[129] Watson, R. T., and Albritton, D. L. *Climate change 2001: Synthesis report: Third assessment report of the Intergovernmental Panel on Climate Change*. Cambridge University Press, 2001.

[130] Wen, C.-K., Chen, J.-C., Teng, J.-H., and Ting, P. Decentralized plug-in electric vehicle charging selection algorithm in power systems. *Smart Grid, IEEE Transactions on 3*, 4 (2012), 1779–1789.

[131] Wiser, R., Namovicz, C., Gielecki, M., and Smith, R. The experience with renewable portfolio standards in the united states. *The Electricity Journal 20*, 4 (2007), 8–20.

[132] Wood, A., Wollenberg, B., and Sheblé, G. *Power Generation, Operation and Control*, third ed. John Wiley and Sons, Inc., 2014.

[133] Wu, C., Mohsenian-Rad, H., Huang, J., and Jatskevich, J. PEV-based combined frequency and voltage regulation for smart grid. In *Innovative Smart Grid Technologies (ISGT), 2012 IEEE PES* (2012), IEEE, pp. 1–6.

[134] Wu, D., Aliprantis, D. C., and Ying, L. Load scheduling and dispatch for aggregators of plug-in electric vehicles. *Smart Grid, IEEE Transactions on 3*, 1 (2012), 368–376.

[135] Xiao, L., and Boyd, S. Fast linear iterations for distributed averaging. *Systems & Control Letters 53*, 1 (2004), 65–78.

[136] Yadav, V., and Salapaka, M. V. Distributed protocol for determining when averaging consensus is reached. In *45th Annual Allerton Conf* (2007), pp. 715–720.

[137] Yan, Y., Qian, Y., Sharif, H., and Tipper, D. A survey on smart grid communication infrastructures: Motivations, requirements and challenges. *Communications Surveys & Tutorials, IEEE 15*, 1 (2013), 5–20.

[138] Yang, H., Chung, C., and Zhao, J. Application of plug-in electric vehicles to frequency regulation based on distributed signal acquisition via limited communication. *Power Systems, IEEE Transactions on 28*, 2 (2013), 1017–1026.

[139] Yang, Z., Li, K., Foley, A., and Zhang, C. Optimal scheduling methods to integrate plug-in electric vehicles with the power system: a review. In *Proceedings of the 19th world congress of the International Federation of Automatic Control (IFAC14), Cape Town, South Africa* (2014), pp. 24–29.

[140] Zhang, P., Qian, K., Zhou, C., Stewart, B. G., and Hepburn, D. M. A methodology for optimization of power systems demand due to electric vehicle charging load. *Power Systems, IEEE Transactions on 27*, 3 (2012), 1628–1636.

[141] Zhang, Z., and Chow, M.-Y. Convergence analysis of the incremental cost consensus algorithm under different communication network topologies in a smart grid. *Power Systems, IEEE Transactions on 27*, 4 (2012), 1761–1768.

[142] Zhao, P., Henze, G. P., Plamp, S., and Cushing, V. J. Evaluation of commercial building HVAC systems as frequency regulation providers. *Energy and Buildings 67* (2013), 225–235.

[143] Zhou, Z., Zhao, F., and Wang, J. Agent-based electricity market simulation with demand response from commercial buildings. *IEEE Transactions on Smart Grid 2*, 4 (2011), 580–588.